Deconstructing the Gestalt: New concepts and tests of homology, as exemplified by a re-conceptualization of "microstomy" in squamates

Catherine R. C. Strong[1*], Mark D. Scherz[2], and Michael W. Caldwell[1,3]

[1]Department of Biological Sciences, University of Alberta, Edmonton, Canada
[2]Institute for Biochemistry and Biology, University of Potsdam, Karl-Liebknecht-Str. 24–25, 14476 Potsdam, Germany. ORCID: 0000-0002-4613-7761
[3]Department of Earth and Atmospheric Sciences, University of Alberta, Edmonton, Canada. ORCID: 0000-0002-2377-3925

*Correspondence to: Catherine Strong, Department of Biological Sciences, University of Alberta, CW-405 Biological Sciences Building, T6G 2E9, Edmonton, Alberta, Canada. Email: crstrong@ualberta.ca. Telephone: 01-780-492-3458. ORCID: 0000-0002-6080-9245

Running title: Jaw homology in "microstomatan" squamates

Funding information: Grant sponsors: Natural Sciences and Engineering Research Council of Canada, National Science Foundation; Grant numbers: NSERC Alexander Graham Bell Canada Graduate Scholarship to C.R.C.S., NSERC Discovery Grant #23458 to M.W.C., NSF 1541959 to Harvard CNS.

Data availability statement: Micro-CT scans performed for this study will be made available on MorphoSource.org. The phylogeny and ancestral state scorings used herein are provided in Nexus format in the Supplemental Material. All other relevant data and sources thereof are included in the manuscript and/or figures.

Conflict of interest disclosure: All authors declare that we have no competing interests.

Abstract

Snakes—a subset of lizards—have traditionally been divided into two major groups based on feeding mechanics: "macrostomy", involving the ingestion of proportionally large prey items; and "microstomy", the lack of this ability. "Microstomy"—considered present in scolecophidian and early-diverging alethinophidian snakes—is generally viewed as a symplesiomorphy shared with non-snake lizards. However, this perspective of "microstomy" as plesiomorphic and morphologically homogenous fails to recognize the complexity of this condition and its evolution across "microstomatan" squamates. To challenge this problematic paradigm, we formalize a new framework for conceptualizing and testing the homology of overall character complexes, or "morphotypes", which underlies our re-assessment of "microstomy". Using micro-computed tomography (micro-CT) scans, we analyze the morphology of the jaws and suspensorium across purported "microstomatan" squamates (scolecophidians, early-diverging alethinophidians, and non-snake lizards) and demonstrate that key components of the jaw complex are not homologous at the level of primary character state identity across these taxa. Therefore, rather than treating "microstomy" as a uniform condition, we instead propose that non-snake lizards, early-diverging alethinophidians, anomalepidids, leptotyphlopids, and typhlopoids each exhibit a unique and non-homologous jaw morphotype: "minimal-kinesis microstomy", "snout-shifting", "axle-brace maxillary raking", "mandibular raking", and "single-axle maxillary raking", respectively. The lack of synapomorphy among scolecophidians is inconsistent with the notion of scolecophidians representing an ancestral snake condition, and instead reflects a hypothesis of the independent evolution of fossoriality, miniaturization, and "microstomy" in each scolecophidian lineage. We ultimately emphasize that a rigorous approach to comparative anatomy is necessary in constructing evolutionary hypotheses that accurately reflect biological reality.

Key words: ancestral state reconstruction; functional morphology; homology; skull anatomy; snake evolution

1. Introduction

Scolecophidians ("blindsnakes") are a distinctive group of snakes, comprised of three major lineages: Anomalepididae, Leptotyphlopidae, and Typhlopoidea, the latter of which is further subdivided into three families, Typhlopidae, Gerrhopilidae, and Xenotyphlopidae (Figs. 1 and 2). However, due in part to their small size and reclusive life habits, many aspects of scolecophidian anatomy and evolution remain understudied (Kley and Brainerd, 1999; Kley, 2006). As scolecophidians have traditionally played a key role in our understanding of the origin of snakes (e.g., Bellairs and Underwood, 1951; Rieppel, 2012; Miralles et al., 2018), it is of critical importance that these knowledge gaps continue to shrink; central among these, and the focus of this study, is the role of scolecophidians in informing our understanding of the evolution of feeding mechanisms in squamates.

Most extant snakes—including booids, pythonoids, and caenophidians (Figs. 1 and 2)—exhibit macrostomy, the ability to consume prey items with a disproportionately large cross-sectional area (Rieppel, 1988, 2012; Scanferla, 2016). Other squamates—including non-snake lizards, as well as "anilioid" (uropeltoid and amerophidian) and scolecophidian snakes—lack this ability, and have thus been termed "microstomatan" (Rieppel, 1988; Miralles et al., 2018). The presence of microstomy in non-snake lizards and several phylogenetically basal snake lineages has traditionally led to the conclusion that the microstomatan condition in "anilioids" and scolecophidians is a plesiomorphic retention of the ancestral snake condition (e.g., Bellairs and Underwood, 1951; Rieppel, 2012). This hypothesis ties into a broader perspective in which scolecophidians are considered a largely "primitive" lineage, retaining several features not just of the ancestor of snakes, but of non-snake lizards more broadly (e.g., List, 1966).

However, several authors have cautioned that, because the scolecophidian skull is highly autapomorphic, it is therefore largely uninformative regarding the ancestral snake anatomy (e.g., Kley and Brainerd, 1999; Kley, 2001; Hsiang et al., 2015; Caldwell, 2019; Chretien et al., 2019). In particular, the combined influences of fossoriality, miniaturization, and heterochrony (evolutionary changes in the rate or timing of developmental events; McNamara, 1986) have greatly affected the evolution of the scolecophidian skull (Kley, 2006; Palci et al., 2016; Harrington and Reeder, 2017; Chretien et al., 2019; Strong et al., 2021).

Despite these cautions, though, recent analyses have continued to treat scolecophidian microstomy as a plesiomorphic retention of the non-ophidian squamate condition, particularly

via ancestral state reconstructions which codify "microstomy" as a single, morphologically homogenous condition (e.g., Harrington and Reeder, 2017; Miralles et al., 2018). This perspective on scolecophidian anatomy has therefore been central in formulating higher-order hypotheses of snake phylogeny and origins, including reconstructions of the ancestral morphology and ecology of snakes (e.g., Harrington and Reeder, 2017; Miralles et al., 2018). In order to fully evaluate such hypotheses, a close analysis of the validity of this characterization of scolecophidian jaw anatomy is essential.

A re-assessment of this anatomy is also important in evaluating the phylogenetic relationships among scolecophidians. Although morphology-based phylogenies generally recover scolecophidians as monophyletic (e.g., Gauthier et al., 2012; Hsiang et al., 2015; Garberoglio et al., 2019a), molecular-based phylogenies tend to recover this group as paraphyletic (e.g., Pyron et al., 2013; Figueroa et al., 2016; Zheng and Wiens, 2016; Miralles et al., 2018; Burbrink et al., 2020). Recent authors have further suggested that, based on the highly autapomorphic nature of scolecophidians relative not only to other squamates but also relative to each other, scolecophidians may even represent completely convergent lineages (Harrington and Reeder, 2017; Caldwell, 2019; Chretien et al., 2019), rendering this group potentially polyphyletic (Caldwell, 2019). This phylogenetic hypothesis derives largely from the unique jaw structure exhibited by each major scolecophidian clade, as well as a recognition of the role of fossoriality and miniaturization in giving rise to convergent morphotypes (Harrington and Reeder, 2017; Caldwell, 2019; Chretien et al., 2019). Although this hypothesis has only recently been advocated, it presents an intriguing possibility warranting further analysis.

In light of these questions surrounding scolecophidian evolution—primarily regarding whether the scolecophidian jaw anatomy is plesiomorphic and whether "microstomy" is morphologically homogenous among "microstomatan" taxa—we herein present an assessment of the jaws and suspensorium of scolecophidians in comparison to other snakes and to non-ophidian squamates (Fig. 1). We address three major questions related to the scolecophidian jaw complex. First, can this morphofunctional system be considered homologous among the three main scolecophidian clades? Second, is this jaw structure homologous to the condition in non-ophidian squamates? And ultimately, how do the answers to these questions affect higher-level evolutionary hypotheses, such as phylogenetic analyses or ancestral state reconstructions?

To examine these questions, we begin with comparative descriptions reviewing the jaw structures of various squamates. We then discuss the homology of these conditions and implications for the scolecophidian phylogeny. Finally, we use ancestral state reconstructions to illustrate the impact that different homology concepts can have on hypotheses of squamate evolution.

On a taxonomic note, all references to scolecophidians throughout this study employ the classical definition of this group—i.e., comprising all major lineages, as outlined above (Fig. 2)—rather than the restricted, clade-based definition of "Scolecophidia *sensu stricto*" as employed by some other authors (e.g., Miralles et al., 2018). References to "anilioids" similarly evoke the classical definition of this group as an informal grade of basally-diverging alethinophidians, with the recognition that this group is likely polyphyletic (e.g., Burbrink et al., 2020) and composed of at least two distinct lineages: Amerophidia (Aniliidae and Tropidophiidae) and Uropeltoidea (Cylindrophiidae, Uropeltidae, and Anomochilidae) (Figs. 1 and 2; taxonomy from Burbrink et al., 2020).

2. Materials and Methods

2.1. Institutional abbreviations

Institutional abbreviations of specimens examined in this study are provided in Table 1.

2.2. Comparative specimens

Various micro-computed tomography (micro-CT) scans of squamate skulls were observed for this study, as listed in Table 2. For consistency, nomenclature follows the Reptile Database (http://reptile-database.reptarium.cz/) as of October 2020. Among non-snake lizards, our sampling strategy focused on phylogenetic breadth rather than completeness, with an emphasis on taxa typically recovered or hypothesized as closely related to snakes. Among snakes, our sampling strategy focused on "microstomatan" taxa, including several representatives of each major "microstomatan" group.

MCZ scans were conducted by C.R.C.S (see §2.3) and will be made available on MorphoSource.org. Information regarding *Xenotyphlops grandidieri*, *Gerrhopilus persephone*, and *Cenaspis aenigma* was derived from the figures and supplementary materials of Chretien et al. (2019), Kraus (2017), and Campbell et al. (2018), respectively. Information regarding the sources of the other scans is provided in the Acknowledgments.

2.3. Scanning protocols and visualization

All MCZ specimens observed herein were scanned using a Nikon Metrology X-Tek HMXST225 micro-CT scanner at the Harvard University Center for Nanoscale Systems. Exact scanning parameters varied among specimens, though generally employed the following settings: detector dimensions, 2000 x 2000 pixels; projections, 3142; maximum voltage, 65–80 kV; maximum current output, 116–130 μA. A 0.5 mm aluminum filter was used for MCZ R-33505, R-2885, R-14782, R-92993, R-68571, and R-40099. Exact settings for all specimens are available upon request. Slices were reconstructed using the bundled vendor software CT Pro 3D and exported as VGL files, which were loaded in VG Studio Max and exported as TIFF files.

Brightness and contrast for all scans were adjusted in ImageJ. All scans were visualized in Dragonfly 4.0 (Object Research Systems, 2019), with the Threshold tool used to digitally remove soft tissues and the Manual Segmentation tool used to digitally isolate each skull element for key taxa (Figs. 3–11).

2.4. Phylogeny construction

The phylogeny used for the ancestral state reconstructions (ASR) was constructed using a "super-tree" approach, i.e., compiling dated finer-scale phylogenies into a higher-level phylogenetic framework. Other ASRs have used a similar approach in assessing a variety of other animal groups (e.g., Finarelli and Flynn, 2006; Asplen et al., 2009).

Relationships among families and higher clades are based on Burbrink et al. (2020), with the placement of Rhineuridae and Lanthanotidae derived from Pyron et al. (2013). Species-level phylogenetic relationships are derived from Burbrink et al. (2020) for Anomalepididae, Amphisbaenia, and Iguania, from Pyron et al. (2013) for Dibamidae and Leptotyphlopidae, and from Nagy et al. (2015) for Typhlopoidea. *Dibamus leucurus* was placed based on Greer (1985) and Pyron et al. (2013), *Agamodon anguliceps* was placed based on Kearney and Stuart (2004), *Amphisbaena alba* and *Typhlops titanops* were placed based on Pyron et al. (2013), *Trilepida dimidiata* and *Rena myopica* were placed based on the location of congeneric taxa in Pyron et al. (2013), and *Amerotyphlops*, *Cubatyphlops*, and *Gerrhopilus* were placed based on the location of congeneric taxa in Nagy et al. (2015). Certain taxa (*Acutotyphlops infralabialis*, *A. solomonis*, *Anomalepis aspinosus*, *A. mexicanus*, *Helminthophis praeocularis*, *Liotyphlops argaleus*, *Myriopholis tanae*, and *M. macrorhyncha*) have not been included in any prior phylogenies

based on actual character data to our knowledge, so were placed in the most exclusive clade possible based on taxonomy.

Branch lengths, representing time, are derived mainly from Burbrink et al. (2020). Key nodes within Typhlopoidea were also dated using Miralles et al. (2018), and nodes involving *Lanthanotus* and *Rhineura* were dated using Simões et al. (2018). For some branches, dated phylogenies incorporating the relevant taxa were not available (often because genetic data are not available for those taxa), so dates for these branches were derived by evenly subdividing the distance between the closest dated nodes.

2.5. Ancestral state reconstruction

Ancestral state reconstructions of squamate feeding mechanisms were performed in Mesquite v. 3.61 (Maddison and Maddison, 2019) using both maximum parsimony (MP) and maximum likelihood (ML) algorithms. For the ML reconstructions, traits were mapped using the Markov k-state 1-parameter (Mk1) model, which assumes that forward and reverse changes occur at the same rate (Lewis, 2001; Maddison and Maddison, 2006). Feeding mechanisms were examined via three scoring schemes: "basic", "detailed microstomy", and "detailed microstomy and macrostomy". The more detailed scoring methods aim to reflect morphological variability more accurately within these broad categories, as described herein or as recognized by recent authors (e.g., Palci et al., 2016; Harrington and Reeder, 2017; Chretien et al., 2019). Feeding mechanisms were scored based on personal observations of the specimens in Table 2. Nodes were considered "definitively reconstructed" when a single state was most parsimonious or when the likelihood of any state was greater than 90%. Nodes were considered "equivocal" when multiple states were equally parsimonious or when none of the states had a likelihood greater than 50%.

The "basic" character scheme scores taxa simply as "macrostomatan" or "microstomatan", reflecting a common though arguably over-simplified approach in the literature (e.g., Harrington and Reeder, 2017; Miralles et al., 2018). The "detailed microstomy" scheme divides microstomy into five morphotypes ("minimal-kinesis", "snout-shifting", "single-axle maxillary raking", "axle-brace maxillary raking", and "mandibular raking") as described below (see §3–4); however, macrostomy remains a single state following the traditional perspective that macrostomy is a synapomorphy uniting derived alethinophidians (e.g., Rieppel, 1988; Miralles et al., 2018). The "detailed microstomy and macrostomy" scheme divides

microstomy into these same five morphotypes and also divides macrostomy into two morphotypes ("booid-" and "caenophidian-type"). Because the current study is focused on microstomy, and because macrostomy is an equally complex and poorly understood condition, we do not analyze the homology of macrostomatan jaw mechanisms herein; indeed, the homology of these latter mechanisms is a topic more than expansive enough in scope to warrant a detailed treatment of its own. Instead, this latter subdivision is based on recent suggestions from ontogenetic, phylogenetic, and anatomical perspectives that "macrostomy" may have evolved independently in booid-pythonoids and caenophidians (Palci et al., 2016; Strong et al., 2019; Burbrink et al., 2020).

3. Results

We provide below a brief description of the jaw structures of select squamate taxa (Figs. 1 and 3–11). Thorough descriptions of the overall cranial anatomy of these taxa have been provided by several previous authors, and so we refer the reader throughout to the relevant literature rather than repeating those detailed efforts here. Instead, our descriptions focus on features relevant in comparing the jaw conditions among "microstomatan" squamates. These descriptions are grouped according to functional morphology, reflecting the distinct biomechanical arrangements of the jaws and suspensorium that occur in non-snake lizards, uropeltoids and amerophidians, typhlopoids, anomalepidids, and leptotyphlopids. These distinct versions of microstomy are best reflected by the anatomy and functional morphology of the palatomaxillary arch and suspensorium, though the mandible also exhibits key differences among groups. These biomechanics-based categories are discussed from an evolutionary or homology-based perspective in the Discussion.

3.1. Non-snake lizards

As discussed by several authors (e.g., Frazzetta, 1962; Cundall, 1995), some degree of cranial kinesis occurs throughout all major lizard clades. However, this kinesis is much less pronounced in non-snake lizards than the extensive mobility—especially regarding the jaws and suspensorium—present in snakes (Cundall, 1995). References herein to the non-snake lizard skull as "minimally kinetic" thus reflect this comparison to the snake condition.

3.1.1. Mandible

The non-snake lizard mandible is long and robust, typically equal in length to the skull (Figs. 3 and 4), except in some burrowing forms (e.g., dibamids and amphisbaenians; Figs. 5 and 6) in which the mandible is 60–70% of the total skull length. The dentaries are similarly long and robust, bearing multiple teeth and articulating closely with all, or almost all, other mandibular elements (Figs. 3e,f, 4e,f, 5e,f, and 6e,f). Notably, the dentaries approach each other very closely at the mental symphysis, with roughened symphyseal or articular facets for the attachment of connective tissue and cartilage (Kley, 2006). A posteroventral process is typically present on the dentary (Figs. 3e, 5e, and 6e), though it is reduced or absent in some taxa (e.g., *Lanthanotus*, some iguanians; Fig. 4e).

The splenial varies in size and shape among taxa, from large and plate-like in *Varanus* (Fig. 3e,f), to much smaller in iguanians (Fig. 4e,f), to absent in amphisbaenians (Fig. 6e,f) and absent or fused to the articular complex in dibamids (Fig. 5e,f; Evans, 2008). However, despite these differences in morphology, its overall role in the mandible is similar: integrating tightly with all or almost all other mandibular elements to bridge the intramandibular joint.

The coronoid varies in shape among taxa, though it plays a consistent functional role in the overall mandible. In *Varanus* (Fig. 3e,f), iguanians (Fig. 4e,f), and amphisbaenians (Fig. 6e,f), the coronoid sits dorsally or dorsomedially on the mandible, extending well anteriorly and posteriorly to strongly bridge the intramandibular joint. In dibamids, the anteromedial and posteroventromedial processes of the coronoid are highly reduced or absent, though the elongate posterodorsomedial process articulates extensively with the articular complex and the coronoid process articulates closely with the dentary anterolaterally (Fig. 5e,f). Therefore, despite differences in morphology among these taxa, the coronoid plays an equivalent functional role in all of them: bracing the anterior and posterior mandibular elements and bridging the intramandibular joint.

The angular is long and thin, running along the ventral or ventromedial mandible (except in dibamids and amphisbaenians; see §3.1.4). The angular exhibits extensive mediolateral overlap with the splenial in *Varanus* (Fig. 3e,f) and extensive dorsoventral articulation with this element in iguanians (Fig. 4e,f). It also articulates with the dentary in all non-snake lizards observed herein, and with the other elements of the posterior mandible (Figs. 3–6). Via these articulations, the angular thus effectively bridges the intramandibular joint.

In most non-snake lizards, the articular and prearticular are fused—referred to herein as simply the articular, following the convention of other authors such as Evans (2008) and Werneburg et al. (2015)—but the surangular remains separate. Additional fusion of the posterior mandibular elements occurs in dibamids (Fig. 5e,f), amphisbaenians (Fig. 6e,f), and some iguanians, and so these taxa are described separately in §3.1.4. The surangular articulates tightly with all or most other mandibular elements, including strong articulation with the coronoid dorsally, the angular ventrally or ventrolaterally, and the articular ventrally (Figs. 3e,f and 4e,f). Of particular note, it extends anteriorly across the intramandibular joint to articulate anterolaterally with the dentary (Figs. 3f and 4f), as well as medially with the splenial in some taxa (e.g., *Varanus*; Fig. 3f). The articular also articulates tightly with all other mandibular elements (though see §3.1.4 for an exception in *Lanthanotus*), except for the dentary in varanoids and some iguanians. The lower jaw bears a moderate retroarticular process, comprising approximately 25–30% of the total length of the articular (Figs. 3e,f and 4e,f). This process is shorter in dibamids (comprising about 10–15% of articular complex length; Fig. 5e,f), amphisbaenians (process either essentially absent or barely extending beyond mandibular condyle; Fig. 6e,f), and *Lanthanotus* (comprising about 15–20% of articular length; see e.g., Evans, 2008:fig. 1.91).

Altogether, the intramandibular joint is typically quite tightly integrated and well braced by the mandibular elements. Almost all mandibular elements articulate closely across this joint in most non-snake lizards observed herein (Figs. 3–6). Though some mandibular kinesis is possible (Frazzetta, 1962; Cundall, 1995), this is to a lesser extent and via a different configuration than in snakes, including "anilioids" (Cundall, 1995; see also §3.2). This, combined with the upper jaw structure (see below), represents a very different configuration of the jaw and suspensorium than in scolecophidians, thus justifying a different category for non-snake lizards from a functional perspective.

3.1.2. Suspensorium

The non-snake lizard quadrate is stout and robust (Figs. 3–6). It is typically oriented roughly vertically (Figs. 3 and 4), though dibamids and amphisbaenians are exceptions to this (Figs. 5 and 6; §3.1.4). The quadrate mainly articulates with the articular ventrally and the supratemporal and squamosal dorsally (Figs. 3 and 4), with the paroccipital process of the otoccipital occasionally also contributing to this dorsal articulation (e.g., *Lanthanotus*).

The supratemporal forms a flattened rod, articulating with the squamosal laterally, the quadrate ventrally, and the postparietal process of the parietal—and paroccipital process of the otoccipital, in some taxa (e.g., *Lanthanotus*, *Sauromalus*)—medially (Figs. 3 and 4). It is absent in dibamids and most amphisbaenians (Figs. 5 and 6; §3.1.4).

The squamosal varies in shape among taxa, though typically consistently contributes to the jaw suspension via a ventral articulation with the quadrate (Figs. 3 and 4). Its anterior terminus articulates dorsomedially with the elements bordering the posterior margin of the orbit (e.g., postorbitofrontal in *Varanus*, Fig. 3; postorbital, and sometimes jugal, in iguanians, Fig. 4) to form the upper temporal bar and enclose the supratemporal fenestra. The posterior terminus of the squamosal articulates medially with the supratemporal (Figs. 3 and 4). The supratemporal and squamosal are somewhat reduced in *Sauromalus* and *Lanthanotus*, and absent in dibamids and most amphisbaenians (Figs. 5 and 6; §3.1.4).

3.1.3. Palatomaxillary arch

The key features of the palatomaxillary arch in non-snake lizards are its degree of robustness and extensive articulation among elements, resulting in minimal palatomaxillary mobility.

The non-snake lizard maxilla is generally large, robust, and toothed (Figs. 3–6). The maxilla typically bears a distinct facial process, which is posteriorly angled in dibamids (Fig. 5b) and amphisbaenians (Fig. 6b) as a result of the "telescoping" (*sensu* Rieppel, 1984) of the skull as an adaptation for fossoriality. The facial process is generally tall (Figs. 3–5), though it is shorter in a few taxa (e.g., *Amphisbaena* and *Anelytropsis*; Fig. 6), particularly *Lanthanotus*, in which the facial process is low and broad, similar to the condition in "anilioid" snakes (e.g., see Evans, 2008:fig. 1.91). The maxilla articulates very closely with all or almost all surrounding elements, including the snout (premaxilla, septomaxilla, vomer, and nasal, the latter contact absent in varanoids), palatine, ectopterygoid, jugal, lacrimal, frontal (in dibamids and amphisbaenians), and prefrontal, when these elements are present (Figs. 3–6).

The pterygoid is large, robust, and often edentulous (Figs. 3–6), though it does bear teeth in some taxa (e.g., *Lanthanotus*). It is gracile in dibamids (Fig. 5), but still well-developed, like other non-snake lizards (Figs. 3, 4, and 6) and unlike scolecophidians (Figs. 9–11; §3.4–3.6). The pterygoid articulates extensively with surrounding elements, primarily the palatine and

ectopterygoid, and is further braced by the basipterygoid processes of the parabasisphenoid medially and by the quadrate posterolaterally (Figs. 3–6).

The palatine is robust and edentulous, with well-developed pterygoid, maxillary, and vomerine processes (Figs. 3b,d, 4b,d, 5b,d, and 6b,d). These processes articulate tightly with: the pterygoid posteriorly; the maxilla, ectopterygoid, and often the lacrimal and/or jugal laterally; and the vomer anteriorly, respectively. An additional process is present in dibamids, arching over the ventral or main shelf of the palatine in a manner analogous to the choanal process of snakes (Fig. 5d).

The ectopterygoid is short and robust (Figs. 3–6). Although its specific form and articulations vary slightly across taxa, it plays a consistent functional role in tightly bracing the palatopterygoid bar medially against the maxilla and certain orbital elements (e.g., jugal, prefrontal) laterally, thus supporting and helping immobilize the tightly integrated palatomaxillary arch.

The prefrontal is closely integrated with the skull (Figs. 3–6), though in a manner quite different to typhlopoids and leptotyphlopids (Figs. 1, 9, and 11; §3.4 and 3.6). The prefrontal typically exhibits minimal to no contact with the snout, instead mainly articulating with the frontal medially and the maxilla laterally (Figs. 3a,c, 4a,c, 5a,c, and 6a,c). In some taxa (e.g., many iguanians; Fig. 4a), contact with the nasal can be fairly extensive, though this is of a very different nature than in any scolecophidian (Figs. 9–11). The prefrontal may also articulate with other surrounding elements (e.g., the lacrimal laterally in varanoids and iguanians, the palpebral dorsolaterally in *Varanus*, and the palatine ventrally in iguanians; Figs. 3 and 4).

The premaxilla is tightly integrated with the other snout elements and the maxilla, thus playing an important role in "locking together" the left and right palatomaxillary arches (Figs. 3a–c, 4a–c, 5a–c, and 6a–c). The palatomaxillary arch is often additionally braced by: the lacrimal anteriorly, at the junction between the maxilla, prefrontal, and palatine (Figs. 3c and 4c); the jugal laterally, between the maxilla, ectopterygoid, and sometimes palatine (Figs. 3c and 4c); the vomer anteriorly (Figs. 3b, 4b, 5b, and 6b); the basipterygoid processes of the parabasisphenoid posteromedially (Figs. 3b, 4b, 5b, and 6b); and the quadrate posterolaterally (Figs. 3–6). In many taxa, the prefrontal also either braces the palatine dorsally (e.g., many iguanians; Fig. 4) or very closely approaches this element (e.g., amphisbaenians, *Lanthanotus*, some iguanians).

Overall, the tight integration of the upper jaw elements in non-snake lizards therefore reflects an essentially akinetic palatomaxillary arch. This occurs via a completely different anatomical configuration than in leptotyphlopids (Figs. 1 and 11; §3.6).

3.1.4. Exceptions and variations

Given the phylogenetic, ecological, and functional diversity of non-snake lizards, it is inevitable that certain taxa present variations to the general condition described above. However, despite this variation, all taxa exhibit key features justifying their grouping with other non-snake lizards.

A particularly notable exception among non-snake lizards is *Lanthanotus* (e.g., see Evans, 2008:fig. 1.91). In this taxon, the integration between the anterior and posterior mandibular elements is reduced such that a distinct and flexible intramandibular joint occurs (Evans, 2008). This condition involves: reduced integration of the splenial with the posterior mandible (Evans, 2008); less extensive articulation of the angular with the anterior mandible and the articular with the splenial; and reduction of the anterior terminus of the coronoid and thus less distinct bracing of the intramandibular joint, including the presence of a facet anteriorly to accommodate the dentary, somewhat similar to the condition in *Cylindrophis* (Fig. 7; §3.2). Furthermore, the palatine-pterygoid articulation in *Lanthanotus* is looser than is typical of non-snake lizards (e.g., compare Evans, 2008:fig. 1.91a to Figs. 4–6 herein). Regarding these features, *Lanthanotus* could therefore be considered intermediate between typical non-snake lizards (Figs. 3–6) and early-diverging alethinophidians (Figs. 7 and 8).

Importantly, though, despite this looser palatine-pterygoid articulation, the overall structure of the jaws and suspensorium—especially the suspensorium and palatomaxillary arch—is otherwise consistent with the typical non-snake lizard condition. For example, the palatomaxillary arch of *Lanthanotus* lacks several other key "anilioid" features, such as a loosened maxilla-premaxilla articulation, "ball-and-socket"-like maxilla-palatine articulation, simplified ectopterygoid articulations, and the ability for unilateral movement, and the mandible lacks features such as an abutting splenial-angular contact (see Fig. 7 and §3.2). In light of the absence of these features, and due to the otherwise similar condition of *Lanthanotus* compared to other non-snake lizards, it is therefore most reasonable to consider *Lanthanotus* as a variation of the general non-snake lizard condition.

Dibamids and amphisbaenians represent another apparent exception among non-snake lizards. As mentioned above, the lower jaw differs in these taxa compared to other non-snake lizards due to additional fusion of the posterior mandibular elements (Figs. 5e,f and 6e,f). In dibamids, bipedids, and trogonophiids, this involves fusion of the articular, angular, surangular, and possibly splenial (in dibamids) to form a single articular complex (Fig. 5e,f; Evans, 2008; Gans and Montero, 2008). A similar condition occurs in amphisbaenids and rhineurids, although the angular remains separate, resulting in a compound bone comparable to that of snakes (Fig. 6e,f). Some iguanians also exhibit fusion of the angular and/or articular and/or surangular, again forming a "compound bone" or articular complex (Evans, 2008). These fused complexes articulate closely with the other mandibular elements, suturing dorsally or dorsomedially with the coronoid and articulating ventrally and laterally with the dentary (Figs. 5e,f and 6e,f). In dibamids, this latter articulation involves a long prearticular process (*sensu* Evans, 2008) extending anteriorly along the medial surface of the dentary, thus bridging the intramandibular joint and bracing the dentary (Fig. 5e,f).

Dibamids and amphisbaenians also differ quite distinctly from the typical condition of the non-snake lizard suspensorium. The supratemporal is highly reduced in *Trogonophis* and completely absent in *Dibamus* and most amphisbaenians (Figs. 5 and 6; Evans, 2008; Gans and Montero, 2008). The squamosal is similarly absent in *Dibamus* and most amphisbaenians, though it is present but quite reduced in *Bipes* (Figs. 5 and 6; Gans and Montero, 2008). *Anelytropsis* bears a small temporal element representing either a highly reduced squamosal or supratemporal (Evans, 2008). Due to this extreme reduction, the dorsal articulation of the quadrate with the skull is therefore quite different than in other non-snake lizards (e.g., Figs. 3 and 4). Ventrally, the quadrate articulates with the articular complex or compound bone (Figs. 5 and 6). In amphisbaenids and rhineurids, the quadrate also articulates extensively with the pterygoid medially via a broad articulatory facet on the medial surface of the quadrate shaft (Fig. 6). Finally, the quadrate itself is notable in being anteriorly displaced and angled distinctly anteroventrally (Figs. 5c and 6c).

The structure of the prefrontal in dibamids further differs from other non-snake lizards. In dibamids, the prefrontal is greatly simplified and essentially plate-like (Fig. 5a,c), similar to the form in leptotyphlopids (Fig. 11a,c; §3.6). The ectopterygoid also exhibits a simpler structure

and simpler articulations with the maxilla and pterygoid than in other non-snake lizards, similar to the condition in *Cylindrophis* (Fig. 7; §3.2.3).

Finally, the lacrimal and jugal are absent in dibamids and most amphisbaenians (Figs. 5 and 6), with the jugal being present but highly reduced in *Rhineura* (Gans and Montero, 2008). The lacrimal is also reduced in *Lanthanotus* and *Uranoscodon*. The palatomaxillary arch in these taxa therefore lacks these additional bracing structures as present in other non-snake lizards.

However, despite these differences, the functionality of the complexes in question remains consistent with other non-snake lizards. For example, the fused mandibular structures articulate closely with the other mandibular elements, therefore playing the same functional role as their constituent components in other non-snake lizards, i.e., bracing the intramandibular joint (Figs. 5e,f and 6e,f). Similarly, although the lacrimal and jugal are often absent, the palatomaxillary arch still articulates quite strongly among its constituent elements and is still braced by the vomers, premaxilla, and basipterygoid processes (Figs. 5a–d and 6a–d), a configuration consistent with the general non-snake lizard condition (Figs. 3 and 4). Finally, although the dibamid prefrontal is similar in form to that of leptotyphlopids, major differences include a lack of contact with the snout elements and much greater contact with the maxilla (Figs. 5 and 11; see also §3.6 for comparison), as well as the completely different configuration of the upper jaw complex compared to any scolecophidian (Fig. 1). Therefore, because the skulls of these taxa—particularly the structure and biomechanics of the palatomaxillary arch (e.g., robust, tightly interlocking, and immobile)—are otherwise consistent with the condition in other non-snake lizards, we find it reasonable to consider dibamids and amphisbaenians as variations of this general non-snake lizard condition, and the similarities between their anatomical arrangements and those of the blindsnakes as having arisen convergently (see also §4.4).

3.2. "Anilioids" – Uropeltoidea

The description of this morphotype is based on *Cylindrophis* (Fig. 7). Minor variations in other uropeltoid taxa are noted where relevant, with major variations being described at the end of this section. This description of uropeltoids is largely applicable to Amerophidia (Fig. 8)—the other major lineage of "anilioid" snakes—but, because Amerophidia forms a distinct phylogenetic lineage, rendering "anilioids" polyphyletic (Figs. 1 and 2; Burbrink et al., 2020), this latter clade is presented separately in the next section. Previous treatments of the uropeltoid skull supplement the descriptions provided herein. Primary among these are Cundall (1995),

Cundall and Irish (2008), Cundall and Rossman (1993), Olori and Bell (2012), Rieppel (1977), and Rieppel and Maisano (2007).

3.2.1. Mandible

The uropeltoid mandible is robust and approximately equal in length to the skull (Fig. 7). The dentary is large and robust (Fig. 7e,f), similar to the form in non-snake lizards (Figs. 1 and 3–6) and quite distinct from the reduced form in scolecophidians (Figs. 1 and 9–11). The dentary tooth row is oriented anteroposteriorly (Fig. 7e,f). The mandibles approach each other medially, much more so than in "macrostomatans", but slightly less so than in scolecophidians and especially non-snake lizards. A fibrocartilaginous interramal pad and collagenous intergular pad (*sensu* Cundall, 1995) occur at the mandibular symphysis in *Cylindrophis*, preventing lateral separation of the dentary tips (Cundall, 1995). The dentary distinctly articulates with surrounding elements, but its articulations with the compound bone and coronoid are typically quite loose compared to the tight junctions in non-snake lizards (Figs. 3–6), resulting in a greater capacity for kinesis at the intramandibular joint (Fig. 7e,f; Cundall, 1995). The posteroventral process of the dentary is present (Fig. 7e,f).

The splenial and angular are typically well-developed (Fig. 7f). These elements form low, anteriorly- and posteriorly-tapering triangles, respectively, as is typical of snakes (Fig. 7f). Laterally, they articulate closely with the dentary and compound bone, respectively (Fig.7f). The splenial and angular articulate with each other via a simple abutting contact, with their articulating surfaces exhibiting slight concavo-convexity, thus enabling intramandibular kinesis (Fig. 7f; Cundall, 1995).

The coronoid is robust in *Cylindrophis* (Fig. 7e,f). It bears a tall coronoid process (Fig. 7f), though proportionally this is not quite as tall as in scolecophidians (Figs. 1 and 9–11; §3.4–3.6). The coronoid articulates closely with the compound bone laterally and ventrally (Fig. 7e,f). The anteromedial process of the coronoid is long and extends under the posterior extent of the dentary tooth row (Fig. 7f). The coronoid-dentary articulation is relatively loose, with the coronoid being dorsoventrally flattened anteriorly with a distinct dorsal facet to accommodate the dentary, which permits intramandibular kinesis (Fig. 7e,f; Cundall, 1995).

The compound bone is typically elongate and robust, comprising about 60–70% of the total skull length (Fig. 7). The retroarticular process is very short, typically barely extending

beyond the mandibular condyle (Fig. 7e,f), though is slightly longer in *Anomochilus* (see Rieppel and Maisano, 2007).

Overall, the intramandibular joint is relatively mobile in *Cylindrophis*, particularly via lateral flexion near the angular-splenial, dentary-compound bone, and dentary-coronoid joints (Fig. 7e,f; Cundall, 1995). This is presumably also the case for *Anomochilus* and *Uropeltis*, both of which exhibit similar angular-splenial and dentary-compound bone articulations. This mobility is much more extensive than the limited mandibular kinesis present in scleroglossans (Cundall, 1995).

3.2.2. Suspensorium

The quadrate is stout and robust (Fig. 7). It is oriented roughly vertically, with a large suprastapedial process posterodorsally (Fig. 7c). This process is particularly elongate in *Anomochilus* and especially *Uropeltis*, to an extent unique among snakes (Olori and Bell, 2012). Dorsally, the quadrate typically articulates mainly with the prootic and supratemporal and minimally with the otoccipital (Fig. 7a,c). The supratemporal is present and well-developed (Fig. 7a,c). As in all snakes, the squamosal is absent.

3.2.3. Palatomaxillary arch

The maxilla is large and robust (Fig. 7a–d), similar to the robust condition in non-snake lizards (Figs. 1 and 3–6), though it differs from that of non-snake lizards in the nature of its articulations with surrounding elements. The maxilla articulates posteriorly with the ectopterygoid, medially with the palatine via a "ball-and-socket"-like joint enabling rotation and minor anteroposterior movement of the maxilla (Fig. 7b,d; Cundall, 1995), and dorsally with the prefrontal via a low facial process (Fig. 7a–d). The maxilla approaches the septomaxilla and premaxilla medially and is attached to these elements via septomaxillo-maxillary and premaxillo-maxillary ligaments, respectively (Cundall, 1995), but does not directly contact them (Fig. 7b). As such, although the maxilla articulates closely with surrounding elements, this articulation is not as tight as in non-snake lizards (Figs. 3–6), resulting in less restricted palatomaxillary mobility. The maxillary tooth row is oriented anteroposteriorly (Fig. 7).

The pterygoid is large, robust, and well-developed (Fig. 7a–d). In this manner it is similar to non-snake lizards (Figs. 3–6), but differs in bearing a more pronounced tooth row anteriorly. The pterygoid interlocks with the palatine anteriorly (Fig. 7b,d), though in a slightly more flexible manner than in non-snake lizards (Figs. 3–6; except *Lanthanotus*: see §3.1.4). As in non-

snake lizards, the pterygoids are braced medially by the basipterygoid processes of the parabasisphenoid (Figs. 3b, 4b, 5b, 6b, and 7b), a junction further strengthened by the basipterygoid ligaments (Cundall, 1995). The pterygoids are also braced by the ectopterygoid laterally (Fig. 7a–d), though via a less complex and less extensive articulation than is typical of non-snake lizards (Figs 3–6).

The palatine is similarly large and robust (Fig. 7b,d). It differs from the non-snake lizard palatine primarily in bearing teeth along the length of its main body and in bearing a distinct choanal process (Fig. 7b,d). As noted above, its posterior articulation with the pterygoid is not as tight as in most non-snake lizards. The choanal processes very closely approach the palatine processes of the vomers, with these elements being linked by the vomero-palatine ligaments, such that movements of the palatine are transferred to the corresponding vomer (Cundall, 1995). Although this is superficially similar to the close palatine-vomer articulation in non-snake lizards, it lacks the extensive direct osseous contact between these elements that occurs in non-snake lizards (Figs. 3–7). The palatine articulates with the maxilla via a "ball-and-socket"-like joint (Fig. 7b,d).

The ectopterygoid is short and robust, articulating with the ectopterygoid process of the pterygoid posteriorly and the posterior terminus of the maxilla anteriorly (Fig. 7a–d). Both articulations are less extensive and/or less complexly integrated than in non-snake lizards (e.g., compared to the broadly abutting contacts in *Physignathus* or the complexly interlocking articulations in *Varanus*; Figs. 3–6).

The uropeltoid prefrontal is very similar to non-snake lizards (except *Dibamus*; see Fig. 5 and §3.1.4) in its articulations with other skull elements. For example, as in non-snake lizards (Figs. 3–6), the prefrontal exhibits minimal contact with the snout, instead articulating mainly with the frontal medially and the maxilla laterally (Fig. 7a,c). It also articulates ventrally with the palatine, and is further connected to the maxilla via the lateral prefronto-maxillary ligament and to the palatine via the prefronto-palatine ligament (Cundall, 1995). According to Cundall (1995), though, the integration with the maxilla and palatine is looser in alethinophidians—including "anilioids"—than in non-snake lizards. Of note, typhlopoids and leptotyphlopids also exhibit tight integration of the prefrontal with the skull roof (Figs. 9 and 11; §3.4 and 3.6), though this condition differs quite distinctly from that in non-snake lizards (Figs. 3–6) or "anilioids" (Figs. 7 and 8).

The premaxilla is integrated into the snout more loosely than in non-snake lizards (Figs. 3–6) and scolecophidians (Figs. 9–11), though more tightly than in more derived alethinophidians. The prefrontal is connected to the maxilla via the premaxillo-maxillary ligament (Cundall, 1995), though, unlike non-snake lizards, it lacks direct osseous contact with the maxilla (Fig. 7a,b). This configuration enables slightly more unilateral movement of the left and right palatomaxillary arches, compared to the tightly braced condition in non-snake lizards.

Overall, the palatomaxillary arch is generally similar to the condition in non-snake lizards (e.g., large, robust, interlocking elements; Figs. 3–6), though its components are less tightly articulated with each other and with surrounding elements than in non-snake lizards (Fig. 7a–d). The palatomaxillary arch therefore has somewhat greater kinesis than in non-snake lizards, including the ability for unilateral movement of the left and right palatomaxillary arches, albeit limited compared to more "derived" alethinophidians (Cundall, 1995). This movement is largely enabled by minor decoupling of the ventral (vomer and septomaxilla) and dorsal (nasal and premaxilla) snout elements, and the ventral snout elements from their contralaterals (Cundall, 1995). This decoupling enables slight unilateral movement within the ventral snout, which extends to the rest of the palatomaxillary arch due largely to the integration of the palatine-vomer and maxilla-septomaxilla (Fig. 7; Cundall, 1995). The "ball-and-socket"-like joint between the maxilla and palatine is also essential in enabling this kinesis.

3.2.4. Exceptions and variations

As noted above for non-snake lizards, the phylogenetic diversity among uropeltoids inevitably causes variation within this group. Much of this variation arises from miniaturization, paedomorphosis, and adaptations related to fossoriality, as explained further in the Discussion.

Representing key exceptions to the general uropeltoid condition as described above, both *Anomochilus* and *Uropeltis* (and indeed other members of the Uropeltidae such as *Plectrurus* and *Melanophidium*; Cundall and Irish, 2008) exhibit reduction of certain elements compared to *Cylindrophis*. For example: the mandible is shorter (about 70–80% of total skull length); the splenial and angular are smaller or lost altogether (*Plectrurus*; Cundall and Irish, 2008); the dentary and maxilla are robust but anteroposteriorly shorter in *Anomochilus*, and of typical length but more gracile in uropeltids; the posteroventral process of the dentary is absent in uropeltids; the coronoid is highly reduced and articulates only with the compound bone; and the compound bone is shorter in *Uropeltis* (comprising about 40–50% of the total skull length), and

582 somewhat less robust in both taxa (see also Rieppel and Maisano, 2007; Olori and Bell, 2012).
583 The compound bone's length varies dramatically within the Uropeltidae (Cundall and Irish,
584 2008). Presumably as a consequence of the drastic reduction of its posterior extent, the maxillary
585 tooth row is angled somewhat anteromedially in *Anomochilus* (see also Rieppel and Maisano,
586 2007). The jaw suspension is anteriorly displaced in both *Anomochilus* and uropeltids compared
587 to *Cylindrophis* and *Anilius*, more closely resembling the placement in scolecophidians, and the
588 supratemporal is absent in uropeltids and *Anomochilus leonardi*, causing the quadrate to
589 articulate dorsally with the prootic and otoccipital in *Anomochilus* and with the fused braincase
590 in *Uropeltis* (see also Rieppel and Maisano, 2007; Olori and Bell, 2012). The pterygoid and
591 palatine are both edentulous in these taxa, and the ectopterygoid is also reduced, to the extent
592 that it is entirely suspended within the pterygomaxillary ligament in *Anomochilus* (see also
593 Cundall and Rossman, 1993; Rieppel and Maisano, 2007).
594 Other differences involve increased robustness of the skull, such as the lateral expansion
595 of the nasals, causing tighter integration of the prefrontal with the snout (see also Rieppel and
596 Maisano, 2007). The premaxilla is also more tightly integrated with surrounding elements,
597 limiting the capacity for unilateral movement of the palatomaxillary arches (see also Rieppel and
598 Maisano, 2007; Olori and Bell, 2012). Finally, the maxilla more closely approaches the
599 septomaxilla and premaxilla in *Anomochilus* and makes extensive contact with these elements,
600 especially the premaxilla, in *Uropeltis*.
601 Despite these differences, however, *Anomochilus* and *Uropeltis* still exhibit many
602 similarities to *Cylindrophis*. For instance, although the prefrontal is more tightly integrated into
603 the skull, it is otherwise consistent in form with the typical uropeltoid condition as described
604 above (see also Rieppel and Maisano, 2007; Olori and Bell, 2012). Similarly, although the
605 palatine is edentulous, the rest of its anatomy is quite similar to other uropeltoids (see also
606 Rieppel and Maisano, 2007; Olori and Bell, 2012). Most importantly, both *Anomochilus* and
607 *Uropeltis* appear capable of moving the ventral snout elements independently of the dorsal snout
608 elements (Cundall and Rossman, 1993; Cundall, 1995), a key component of the functional
609 morphology of *Cylindrophis*. Taking these similarities into account—and also recognizing that
610 *Anomochilus* and *Uropeltis* lack the hallmark features of any of the scolecophidian morphotypes,
611 especially regarding palatomaxillary suspension and biomechanics (see Figs. 9–11 and §3.4–
612 3.6)—we ultimately consider it reasonable to classify these taxa as miniaturized variants of the

general uropeltoid condition, rather than creating a different morphotype or referring them to any of the scolecophidian conditions (see also §4.4 for further discussion).

3.3. "Anilioids" – Amerophidia

The clade Amerophidia is herein represented by *Anilius* (Figs. 1, 2, and 8). The cranial morphology of this clade is largely consistent with the Uropeltoidea (Fig. 7), as described above, especially regarding the suspensorium and palatomaxillary arch. However, amerophidians form a lineage that is phylogenetically separate from uropeltoids, creating a polyphyletic "anilioid" assemblage (Figs. 1 and 2; Burbrink et al., 2020), and also exhibit a mandibular structure different from that of uropeltoids. For these reasons, these clades of early-diverging alethinophidians are treated separately. To avoid repetition, however, we here describe only the mandible of Amerophidia in detail, and refer readers to §3.2.2 and §3.2.3 for a general impression of the suspensorium and palatomaxillary arch, respectively.

3.3.1. Mandible

Anilius is notable in that the structure of its mandible differs somewhat compared to *Cylindrophis* (Fig. 7 and 8). In *Anilius*, the splenial and angular may be absent or extremely reduced (Fig. 8; Rieppel, 1977; Cundall and Irish, 2008). The anterior terminus of the compound bone articulates rather extensively with the medial surface of the dentary (Fig. 8f), in contrast to the interlocking configuration in *Cylindrophis* (Fig. 7e,f), and the coronoid overlaps this articulation dorsally (Fig. 8e,f). Altogether, this suggests a potentially lower degree of intramandibular kinesis in *Anilius* compared to *Cylindrophis*.

However, the dentary-compound bone articulation appears to still enable some degree of lateral flexion at the intramandibular joint, as the coronoid is reduced and so does not act as a medial "buttress" preventing this flexion (Fig. 8e,f). This is unlike the typhlopoid mandible, for instance, in which the coronoid would prevent this movement (see Fig. 9 and §3.4.1). Furthermore, although the intramandibular joint of *Anilius* does differ somewhat from *Cylindrophis*, the articulations and apparent mobility of this condition are much more functionally and anatomically similar to *Cylindrophis* (Fig. 7) than to the tightly and pervasively interlocking condition of the non-snake lizard mandible (Figs. 3–6). Combined with the consistent nature of the palatomaxillary arch in these taxa, including the suggestion that *Anilius* is also capable of unilateral movement of the palatomaxillary arches (Cundall, 1995), it is therefore reasonable to include *Anilius* under the same biomechanical category as *Cylindrophis*.

3.4. Typhlopoidea

The clade Typhlopoidea contains three families: Gerrhopilidae, Typhlopidae, and Xenotyphlopidae (Figs. 1 and 2). Our scans of gerrhopilids were not of sufficient resolution to digitally segment or figure these specimens in the same detail as the other scolecophidian families, but did allow us to assess key aspects of their anatomy. Iordansky (1997), Kley (2001), and Chretien et al. (2019) present detailed descriptions of typhlopoid jaw anatomy, with Iordansky (1997) and Kley (2001) also discussing the functional morphology of the typhlopid jaw complex. Classical studies such as Haas (1930), Mahendra (1936), Evans (1955), and List (1966) also provide descriptions of the typhlopid skull; much of the historical literature was summarized by Cundall and Irish (2008).

3.4.1. Mandible

The typhlopoid mandible is long and slender, measuring approximately 60–75% of the total skull length (Fig. 9). The dentaries are highly reduced, each typically forming a flat crescent or slightly rod-like form curved medially toward the mandibular symphysis (Fig. 9e,f), though the dentary is more straight and rod-like in some (e.g., *Acutotyphlops kunuaensis*, *A. subocularis*). The dentaries closely approach each other medially, linked by a cartilaginous nodule as in leptotyphlopids (Kley, 2001). The dentary exhibits broad contact ventrally with the splenial, also overlapping the coronoid and compound bone posteroventrally (Fig. 9e,f). The interramal surface is smooth, lacking articulatory or symphyseal facets, unlike the condition in non-snake lizards (see also Kley, 2006). The posteroventral process of the dentary is absent (Fig. 9e,f); Rieppel et al. (2009) described this absence as uniting all scolecophidians, though see §3.5.1 for our interpretation in anomalepidids. The dentary is edentulous (Fig. 9e,f), a condition unique to typhlopoids among snakes (Kley, 2001).

The typhlopoid splenial is proportionally quite large compared to other squamates, ranging from approximately equal in length to the dentary (e.g., *Acutotyphlops infralabialis*, among others) to approximately twice the length of the dentary (e.g., *Afrotyphlops*, *Amerotyphlops*, *Anilios*, among others; Fig. 9e,f). The gerrhopilid splenial is somewhat more gracile, being slightly shorter and thinner than the dentary in *Gerrhopilus persephone*, of typical length but thin and rod-like in *G. beddomii*, and of typical length but not extending as far anteriorly in *G. ater*. The splenial typically extends anteriorly almost to the anterior terminus of the mandible in most typhlopoids (Fig. 9e,f), though it terminates farther posteriorly in a few

taxa (*Acutotyphlops infralabialis*, *A. kunuaensis*, *Gerrhopilus persephone*, *G. ater*). The splenial articulates extensively with all other mandibular elements, fully spanning the intramandibular joint (Fig. 9e,f).

The angular is quite reduced, forming a thin splint lying between the dorsal margin of the splenial and the ventral margins of the compound bone and coronoid (Fig. 9e,f). The angular directly contacts the coronoid in some taxa (e.g., *Acutotyphlops*, *Afrotyphlops*, *Typhlops*; Fig. 9f) and closely approaches but does not directly contact it in others (e.g., *Antillotyphlops*, *Xenotyphlops*). The angular is absent in some typhlopoids (e.g., *Anilios*, *Indotyphlops*, *Ramphotyphlops*, *Xerotyphlops*, and potentially *Gerrhopilus*).

The coronoid is large, flat, and triangular, with a tall coronoid process (dorsal process *sensu* Kley, 2006; Fig. 9e,f). The base of the coronoid extends well anteriorly and posteriorly, articulating closely with the dentary, splenial, and compound bone in all typhlopoids (Fig. 9e,f), though it does not extend as far anteriorly in *Gerrhopilus ater* and *G. persephone* as in other typhlopoids. Contact with the angular varies among taxa (see above).

The typhlopoid compound bone is long, measuring approximately 50–65% of the total skull length, and is distinctly anteriorly downcurved (Fig. 9). This curvature is especially pronounced in xenotyphlopids, in conjunction with the distinctive ventral inflection of the anterior skull (see Chretien et al., 2019). The compound bone bears a moderate retroarticular process, typically comprising about 20–25% of the total length of the compound bone (Fig. 9e,f), though this process is shorter in some taxa (about 7–10% in *Acutotyphlops*, and 16–18% in *Antillotyphlops*, *Cubatyphlops*, and *Gerrhopilus*). The retroarticular process terminates well anterior to the level of the occipital condyle (Fig. 9). The compound bone articulates with all other mandibular elements (Fig. 9e,f).

Altogether, the intramandibular hinge is essentially immobile, with the mandibular elements articulating tightly with each other, especially the broadly overlapping splenial, coronoid, and compound bone (see also Kley, 2001). Additionally, although the mandibles are rather fixed with respect to one another, some longitudinally rotational intermandibular mobility is possible, as indicated by the muscular attachments of the compound bone and suspensorium and the jugomandibular ligament, which permit a deeper intermandibular oral trough than would be possible were the mandibles medially linked by more tightly interlocking articulatory or symphyseal facets (Iordansky, 1997).

706 **3.4.2. Suspensorium**

707 As is typical of scolecophidians, the quadrate is elongate and strongly anteroventrally
708 angled (Fig. 9c). However, it is not as elongate as in leptotyphlopids, with the long axis of the
709 quadrate equivalent to approximately 25–30% of the total skull length in typhlopoids (Fig. 9;
710 though it is longer in some taxa, e.g., 37–40% in *Indotyphlops*, *Typhlops*, and *Xerotyphlops*),
711 compared to approximately 40–45% in leptotyphlopids (Fig. 11). In typhlopids and gerrhopilids,
712 the quadrate bears a pronounced anterior process (*sensu* Palci et al., 2020) slightly posterior to
713 the mandibular condyle (Fig. 9c). This process is somewhat smaller and more posteriorly
714 positioned in *Xenotyphlops* (see Chretien et al., 2019). The quadrate articulates dorsally with the
715 prootic and otoccipital in most typhlopoids (Fig. 9; e.g., *Afrotyphlops*, *Amerotyphlops*, *Anilios*,
716 *Antillotyphlops*, *Cubatyphlops*, *Typhlops*, *Xerotyphlops*), though these elements are fused in
717 xenotyphlopids, gerrhopilids, and some typhlopids (e.g., *Acutotyphlops*, *Indotyphlops*,
718 *Ramphotyphlops*, and *Madatyphlops*; see also Hawlitschek et al., this volume). The
719 supratemporal is absent in all typhlopoids. As is typical of snakes, the squamosal is also absent.

720 **3.4.3. Palatomaxillary arch**

721 The typhlopoid maxilla is highly mobile and is unique among squamates in rotating
722 around the maxillary process of the palatine via a large foramen (in most typhlopoids; Fig. 9) or
723 deep medial excavation (e.g., *Acutotyphlops infralabialis*, *A. kunuaensis*, *A. solomonis*,
724 *Afrotyphlops schlegelii*). The maxillary tooth row is directed roughly transversely, with the
725 maxilla angled posteroventrally at rest (Fig. 9a–d). A pronounced facial process articulates
726 loosely alongside the lateral surface of the prefrontal (Fig. 9a–d).

727 As is typical of scolecophidians, the pterygoid is long, rod-like, and edentulous (Fig. 9a–
728 d). Its anterior terminus, or palatine process, is forked to articulate with the palatine (Fig. 9b,d).
729 The pterygoid and palatine underlie the skull more broadly than in leptotyphlopids (Fig. 11;
730 §3.6.3). The parabasisphenoid lacks basipterygoid processes in most typhlopoids (Fig. 9b),
731 though rudimentary processes are present in *Xenotyphlops* (Chretien et al., 2019). However,
732 these processes are much less prominent than in non-snake lizards and do not approach the
733 pterygoids as closely, and the pterygoids lack corresponding articulatory facets (see Chretien et
734 al., 2019).

735 The palatine is edentulous and highly reduced, essentially consisting only of its maxillary
736 and choanal processes (Fig. 9b,d). The palatine also bears a highly reduced pterygoid process

and distinct ventral process (the latter of which may reflect a uniquely forked condition of the former) which articulate with the forked anterior terminus of the pterygoid (Fig. 9b,d). The choanal process forms a thin and narrow arch very closely approaching the corresponding vomer (Fig. 9b), though—like snakes (Figs. 7–11) and unlike non-snake lizards (Figs. 3–6)—there is no direct osseous contact between these elements. Most distinctively, the maxillary process of the palatine is unique among squamates in forming an elongate rod projecting laterally to articulate with a foramen and/or medial depression in the maxilla (Fig. 9a–d).

The ectopterygoid is absent in all typhlopoids (see also Chretien et al., 2019). The prefrontals are expanded and immobile, being tightly integrated into the snout and skull roof via extensive articulation with the nasals, septomaxillae, and frontals in all typhlopoids (Fig. 9a–d), as well as the premaxilla in xenotyphlopids (see also Chretien et al., 2019). The premaxilla is tightly integrated with the other snout elements, but does not contact the palatomaxillary arches and therefore does not affect palatomaxillary mobility (Fig. 9a–c).

Altogether, the palatomaxillary arch is highly mobile, with its functionality reliant upon a unique maxilla-palatine articulation (see also Iordansky, 1997; Kley, 2001; Chretien et al., 2019). Drastic reduction of the ligamentous connection between the pterygoid and quadrate further reflects decoupling of the upper (palatomaxillary arch) and lower (mandible and suspensorium) jaws, as in leptotyphlopids (Kley, 2001).

3.5. Anomalepididae

Like typhlopoids, anomalepidid jaw biomechanics rely heavily on movements of the palatomaxillary arches; however, this occurs via a totally different anatomical configuration than in typhlopoids (Figs. 9 and 10; Chretien et al., 2019). Unfortunately, although typhlopoid jaw anatomy has been described in detail from a functional morphological perspective (Iordansky, 1997; Kley, 2001), this system has yet to be examined in similar morphofunctional detail in anomalepidids. Rieppel et al. (2009) recently provided a detailed description of the anomalepidid skull, focusing on *Liotyphlops* and *Typhlophis*, with Santos and Reis (2019) providing detailed imaging of *Anomalepis*. Classical work was summarized by Cundall and Irish (2008). Important among historical works are those by Haas (1964, 1968) describing anomalepidid skull anatomy, although it is worth noting that these studies were based on serial sectioning and suffered greatly from the small size of these animals, leading to almost comically wavy bone shapes in Haas' illustrations. This issue has been completely overcome by micro-CT approaches.

768 ### 3.5.1. Mandible

769 The anomalepidid mandible is extremely long and slender, measuring approximately 85–
770 90% of the total skull length in most anomalepidids and 100% of the total skull length in
771 *Typhlophis* (Fig. 10). The dentary is highly reduced (Fig. 10e,f), with a rod-like form—rather
772 than the more crescentic form of typhlopoids (Fig. 9e,f)—and a flattened and expanded anterior
773 terminus. The dentary is typically toothed, like leptotyphlopids (Fig. 11e,f) and unlike
774 typhlopoids (Fig. 9e,f). However, the anomalepidid dentary bears only a few tooth positions at its
775 anterior terminus (List, 1966; Haas, 1968; Rieppel et al., 2009), and so is not as extensively or
776 robustly toothed as in leptotyphlopids (see Fig. 11e,f and §3.6.1). Furthermore, we found several
777 specimens to have edentulous mandibles (a condition which Chretien et al., 2019 mistakenly
778 generalized to all anomalepidids); among our examined specimens, teeth are only distinctly
779 visible on specimens of *Anomalepis mexicanus*, *Liotyphlops beui*, and *Typhlophis*, though this
780 may be an artifact of scan resolution. List (1966) and Haas (1964) found teeth on the dentary of
781 *Liotyphlops albirostris*, Haas (1968) in *Anomalepis aspinosus*, and McDowell and Bogert (1954)
782 in *Helminthophis flavoterminatus* and *Typhlophis squamosus*. As in other snakes, the interramal
783 surface lacks articulatory or symphyseal facets (see also Kley, 2006). Finally, although Rieppel
784 et al. (2009) described the posteroventral process of the dentary as being absent in all
785 scolecophidians, we consider it present in anomalepidids: in other squamates (Figs. 3 and 5–8),
786 this process constitutes an extension of the dentary ventral to the surangular or compound bone,
787 which is also the condition in anomalepidids (Fig. 10e). In contrast, the dentary in other
788 scolecophidians (Figs. 9 and 11) extends posterodorsal to the compound bone, reflecting an
789 absence of the posteroventral process and presence of the posterodorsal process of other
790 squamates (Figs. 3 and 5–8).

791 The angular is present in anomalepidids, though the splenial is absent (Fig. 10e,f; see
792 Rieppel et al., 2009 regarding the homology of this element). The angular is elongate and rod-
793 like, extending ventrally across the intramandibular joint (Fig. 10e,f), but does not bridge this
794 joint as extensively as the splenial does in typhlopoids (see Fig. 9e,f and §3.4.1). It is similar in
795 overall shape and position to the typhlopoid angular (Fig. 9e,f), though is typically larger and
796 longer, extending anteriorly to around the midpoint of the dentary in most anomalepidids (Fig.
797 10e,f; *Liotyphlops albirostris*, *L. argaleus*, *Typhlophis*, and, to a lesser extent, *Anomalepis*
798 *mexicanus* and *Helminthophis*).

799 The coronoid is flat and boomerang-shaped, with a tall coronoid process as in
800 typhlopoids (Figs. 9e,f and 10e,f). Because the base of the anomalepidid coronoid (Fig. 10e,f)
801 typically does not project anteriorly as in typhlopoids (Fig. 9e,f), this element does not bridge the
802 intramandibular joint as extensively as in typhlopoids. However, *Anomalepis* is an exception to
803 this, as the anteroposterior extent of the coronoid in this genus is similar to the condition in
804 typhlopoids. The anomalepidid coronoid articulates with the dentary and compound bone, but
805 does not articulate to an appreciable extent with the angular (Fig. 10e,f).
806 The compound bone is elongate, measuring about 70–75% of the total skull length in
807 most anomalepidids (Fig. 10e,f) and about 80% in *Typhlophis*, and as such is longer than in
808 typhlopoids (Fig. 9e,f) and especially leptotyphlopids (Fig. 11e,f). The compound bone shows
809 shallow sinusoidal curvature in anomalepidids (Fig. 10e,f), rather than the distinct downward
810 curvature of the typhlopoid compound bone (Fig. 9e,f). The retroarticular process is typically
811 extremely long, comprising approximately 35–40% of the total length of the compound bone
812 (Fig. 10e,f), though it is slightly shorter in *Anomalepis mexicanus*. It extends posteriorly to—or
813 just beyond, in the case of *A. aspinosus* and *Typhlophis*—the level of the occiput (Fig. 10). Near
814 the anterior terminus of the compound bone, the prearticular and surangular laminae briefly
815 separate medially and laterally, respectively, before re-fusing at the anterior terminus (Fig. 10f;
816 Rieppel et al., 2009). Rieppel et al. (2009) note this separation in anomalepidids and describe it
817 as uniquely shared with leptotyphlopids among snakes; however, leptotyphlopids differ in that
818 these laminae remain completely separate, rather than re-fusing anteriorly as occurs in
819 anomalepidids (see Fig. 11e,f and §3.6.1).
820 Although functional studies of the anomalepidid mandible are lacking, the structure and
821 articulations of the mandibular elements suggest that the intramandibular joint is relatively
822 immobile, with the angular and coronoid both bridging this gap via their articulations with the
823 dentary and compound bone (Fig. 10e,f). This condition is therefore more similar to the akinetic
824 typhlopoid mandible (Fig. 9e,f; §3.4.1) than to the highly mobile intramandibular joint of
825 leptotyphlopids (Fig. 11e,f; §3.6.1). However, the integration between the anterior—dentary and
826 splenial—and posterior—compound bone and angular—mandibular subunits is less extensive
827 than in typhlopoids (Fig. 9e,f), suggesting a less rigid condition in anomalepidids (Fig. 10e,f).
828 **3.5.2. Suspensorium**

829 The quadrate is elongate and anteroventrally oriented so as to be nearly horizontal (Fig.
830 10), as is typical of scolecophidians (Figs. 9–11). The quadrate is similar in length to typhlopoids
831 (i.e., long axis equivalent to approximately 20–30% of the total skull length; Figs. 9c and 10c)
832 and shorter than in leptotyphlopids (in which the long axis of the quadrate is equivalent to
833 approximately 40–45% of the total skull length; Fig. 11c). The anterior process of the quadrate
834 typically occurs near the same location as in typhlopids and gerrhopilids (Figs. 9c and 10c)—i.e.,
835 between the mandibular condyle and the midpoint of the quadrate shaft—but is similar to or
836 smaller than the size in xenotyphlopids (see §3.4.2). The dorsal terminus of the quadrate is
837 broadly forked in most anomalepidids—except *Anomalepis*—where it meets the supratemporal
838 (Fig. 10a,c). The quadrate articulates dorsally with the fused prootic-otoccipital and the
839 extremely reduced supratemporal in *Helminthophis*, *Liotyphlops*, and *Typhlophis* (Fig. 10a,c); in
840 *Anomalepis*, it articulates only with the fused prootic-otoccipital as the supratemporal is absent
841 (see also Haas, 1968; Rieppel et al., 2009). The former taxa are unique among scolecophidians in
842 retaining a supratemporal, albeit as a highly reduced splint of bone (see also Haas, 1968; Rieppel
843 et al., 2009). As is typical of snakes, the squamosal is absent.
844 The overall mandibular and suspensorial structure of anomalepidids is therefore similar
845 to that of typhlopoids (e.g., elongate mandible, immobile intramandibular joint, and similar
846 length of the quadrate), but with several key differences (e.g., intramandibular structure and
847 articulation, compound bone structure, presence of the supratemporal, absence of the splenial,
848 specific structure of the quadrate, and general presence of teeth on the dentary).
849 **3.5.3. Palatomaxillary arch**
850 The anomalepidid maxilla is similar to that of typhlopoids (Fig. 9a–d) in being toothed
851 and highly mobile, bearing a pronounced facial process and transversely-to-anteromedially
852 directed tooth row, and being angled posteroventrally at rest (Fig. 10a–d). However, the
853 suspension of the maxilla is fundamentally different from typhlopoids: in anomalepidids, the
854 maxilla articulates posteriorly with the ectopterygoid and anterodorsally with the highly reduced
855 prefrontal (Fig. 10a–d), rather than pivoting around the palatine as in typhlopoids (Fig. 9a–d).
856 This configuration is unique to anomalepidids among squamates.
857 The pterygoid is elongate and edentulous (Fig. 10a–d), as is typical of scolecophidians
858 (Figs. 9–11). Unlike typhlopoids (Fig. 9), the anterior terminus of the pterygoid is not forked,
859 instead tapering to a simple point as in leptotyphlopids (Fig. 11), ventromedial to the pterygoid

process of the palatine (Fig. 10). The pterygoid does not articulate with the ventral surface of the skull (Fig. 10a–d), as in typhlopoids (Fig. 9a–d) and unlike leptotyphlopids (Fig. 11a–d; §3.6.3).

As in typhlopoids (Fig. 9b,d), the palatine is highly reduced, with the choanal process forming a spindly arch closely approaching the corresponding vomer (Fig. 10b,d). However, unlike typhlopoids, the maxillary process in anomalepidids is quite stubby, extending toward but still quite broadly distant from the maxilla (Fig. 10a–d; see also Rieppel et al., 2009). The palatine instead bears an elongate pterygoid process deflected posterolaterally toward the space between the pterygoid and ectopterygoid (Fig. 10b–d). The palatine is therefore not in distinct contact with any other element; this differs greatly from the typhlopoid condition, in which the palatine is an integral component of palatomaxillary biomechanics (Fig. 9a–d; §3.4.3). A variation of this condition occurs in *Anomalepis*, in which the maxillary process is absent.

The ectopterygoid is present in anomalepidids (Fig. 10b–d), a condition unique among scolecophidians (as also noted by e.g., Rieppel et al., 2009). The ectopterygoid articulates with the pterygoid posteriorly and braces the maxilla anteriorly (Fig. 10b–d). It has the same general shape as in other snakes—i.e., comprising a forked maxillary process anteriorly and rod-like pterygoid process posteriorly (Fig. 10b–d)—but is markedly reduced compared to other squamates (Fig. 1).

The anomalepidid prefrontal is quite distinct from other squamates, including other scolecophidians. It is heavily reduced, forming a thin arch connecting the frontal posteriorly to the maxilla anteroventrally (Fig. 10a–c). Its posterior terminus is forked to articulate loosely with the frontal (Fig. 10a,b). The prefrontal is thus highly mobile, playing a key role in upper jaw mobility; this is notably distinct from the condition in other scolecophidians, in which the prefrontal is firmly integrated into the lateral snout and skull roof (Figs. 9 and 11). The premaxilla is tightly integrated with the rest of the snout, but does not contact the palatomaxillary arches and therefore does not affect palatomaxillary mobility (Fig. 10a–c).

Altogether, the palatomaxillary arch is distinctly mobile, as in typhlopoids (Fig. 9a–d). However, the configuration and connectivity of the palatomaxillary arch is quite different than in typhlopoids, particularly regarding the presence of the ectopterygoid, the suspension of the maxilla, and the structure, role, and articulation of the prefrontal (Figs. 9 and 10). Therefore, although both groups rely on upper jaw mobility and maxillary rotation, the unique

palatomaxillary configuration of anomalepidids justifies the classification of this system as a biomechanically distinct version of microstomy.

3.6. Leptotyphlopidae

A thorough description of the leptotyphlopid mandible is provided by Kley (2006), who describes in detail many of the unique features noted in this section. Detailed analyses of the functional morphology of the leptotyphlopid jaws are provided by Kley and Brainerd (1999) and Kley (2001). Earlier studies such as Brock (1932) and List (1966) also describe leptotyphlopid skull anatomy (work summarized in Cundall and Irish, 2008), with micro-CT imagery of various leptotyphlopids available in Rieppel et al. (2009), Pinto et al. (2015), and Martins et al. (2019).

3.6.1. Mandible

The leptotyphlopid mandible is short and robust, typically measuring approximately 45% of the total skull length (Fig. 11), although it measures approximately 35% in *Myriopholis tanae* and 40% in *M. macrorhyncha* and *Namibiana*. The dentary is large and robust relative to other scolecophidians (Fig. 11e,f), with the tooth row angled roughly transversely and the teeth sitting on an expanded dental concha (*sensu* Kley, 2006). Each dentary also bears a prominent symphyseal process (*sensu* Kley, 2006) anteromedially, extending toward the mental symphysis (Fig. 11e,f). As in other snakes, the interramal surface lacks symphyseal facets (see also Kley, 2006). As in typhlopoids—but not anomalepidids, *contra* Rieppel et al. (2009)—the dentary does not bear a posteroventral process (Fig. 11e,f).

The splenial and angular are both quite reduced, but are similar in shape to those of other snakes, forming low, anteriorly- and posteriorly-tapering triangles, respectively (Fig. 11e,f). The angular and splenial abut against each other; the angular is slightly concave and the splenial slightly convex in the specimens observed herein (Fig. 11f), though Kley (2001, 2006) notes the splenial-angular articulation in *Leptotyphlops* (= *Rena*) as being strongly concavoconvex.

The coronoid is smaller than in typhlopoids and anomalepidids (Figs. 9–11). Primarily, it is anteroposteriorly shorter, such that it closely approaches the dentary anteroventrally but only directly contacts the compound bone (Fig. 11e,f), thus lacking the more extensive articulation with other mandibular elements as present in other scolecophidians (Figs. 9e,f and 10e,f). However, it is also much more robust and complex in structure than in other scolecophidians, bearing distinct coronoid, surangular (= posterodorsomedial), and prearticular (= posteroventromedial; present in *Leptotyphlops*) processes (Fig. 11e,f; Kley, 2006).

Similarly, the compound bone is greatly shortened relative to other scolecophidians, measuring only 20–25% of the total skull length in most leptotyphlopids and only approximately 15% in *Myriopholis tanae*, though is more robust and complex (Fig. 11e,f). The compound bone articulates posteriorly with the quadrate, dorsally with the coronoid, ventrolaterally with the angular, and anteriorly with the dentary via a loosely overlapping intramandibular hinge (Fig. 11e,f). The retroarticular process barely extends beyond the mandibular condyle (Fig. 11e,f). Uniquely among snakes, the prearticular and surangular laminae are separate anteriorly (Fig. 11f); this condition was noted by Rieppel et al. (2009) as being uniquely shared with anomalepidids among snakes, though see §3.5.1 for a comparison of these conditions. Kley (2006) also notes the leptotyphlopid compound bone as being unique among snakes in the presence of a supracotylar process and a horizontal shelf extending along the surangular lamina from this process toward the anterior surangular foramen (Fig. 11e,f).

Overall, the intramandibular joint is loosely articulated and quite flexible (Kley and Brainerd, 1999; Kley, 2001, 2006): the splenial abuts against the angular, the dentary and compound bone overlap loosely, and the coronoid approaches but does not directly contact the dentary anteriorly (Fig. 11e,f). In contrast, the mandibles of typhlopoids (Fig. 9e,f) and anomalepidids (Fig. 10e,f) show more extensive integration between the anterior and posterior mandibular elements. This looser articulation in leptotyphlopids is essential in enabling retraction and flexion of the mandible during feeding (Kley and Brainerd, 1999; Kley, 2006).

3.6.2. Suspensorium

The leptotyphlopid quadrate is oriented at the same anteroventral angle as other scolecophidians, but is comparatively much longer, with its long axis typically equivalent to about 40–45% of the total skull length (Fig. 11c), compared to 20–30% in typhlopoids (Fig. 9c) and anomalepidids (Fig. 10c). Dorsally, the quadrate typically bears a broad, paddle-like cephalic condyle, which is confluent with the quadrate shaft and pierced by a large foramen (Fig. 11c; see also Palci et al., 2020), though in some leptotyphlopids the cephalic condyle is simpler and not as expanded (e.g., *Myriopholis tanae*, *Namibiana*, *Rena*, *Tricheilostoma*). The supratemporal and squamosal are both absent, so the quadrate articulates with the braincase: typically the prootic and otoccipital (Fig. 11b,c), though the braincase elements may be fused in some taxa (e.g., *Tricheilostoma*).

Altogether, leptotyphlopids therefore exhibit an overall mandibular and suspensorial structure that is quite distinct from other scolecophidians (Figs. 9 and 10), consisting of short, robust, and complex mandibular elements (especially the dentary and compound bone), bearing a flexible intramandibular joint, and being suspended from the skull via an extremely elongate quadrate (Fig. 11).

3.6.3. Palatomaxillary arch

Most distinctively, the palatomaxillary arch is completely edentulous in leptotyphlopids, a condition unique to leptotyphlopids among snakes (see also Kley, 2001). The maxilla is immobile, articulating broadly with the premaxilla, septomaxilla, and prefrontal and closely approaching the palatine (Fig. 11a–d), with contact occurring with the latter in some taxa (e.g., *Trilepida*). Extensive ligamentous connections between the maxilla and snout further impede movement of the maxilla, and thus the palatomaxillary arch (Kley, 2001).

The pterygoid is elongate, rod-like, and edentulous (Fig. 11b–d), like other scolecophidians (Figs. 9 and 10), but underlies the skull much more closely than in other scolecophidians. Uniquely among squamates, the frontal bears a shallow ventral facet posteriorly to accommodate the palatine and the anterior terminus of the pterygoid (Fig. 11b). This palatine process of the pterygoid lies alongside the pterygoid process of the palatine in a structurally quite simple articulation (Fig. 11b–d).

The palatine is rather robust relative to other scolecophidians (Figs. 9 and 10; §3.4.3 and 3.5.3), though is still quite reduced compared to other squamates (Figs. 3–7). Similar to the pterygoid, the palatine is more integrated into the skull than in other scolecophidians (Figs. 9 and 10), articulating extensively with the frontal dorsally—which bears a corresponding ventral facet—and vomer ventromedially, and very closely approaching the prefrontal, septomaxilla, and maxilla anteriorly (Fig. 11b,c). The choanal process is particularly well-developed, articulating broadly with the vomer and frontal (Fig. 11b–d).

The ectopterygoid is absent in all leptotyphlopids (see also Chretien et al., 2019). The prefrontal is broad and plate-like (Fig. 11a,c), superficially similar in structure to that of dibamids (Fig. 5a,c), though see §3.1.4 for a comparison to the dibamid condition. The prefrontal is closely integrated with several elements—including the nasal, septomaxilla, maxilla, frontal, and palatine (Fig. 11a–c)—though this integration is not as extensive and the prefrontal not as expanded as in typhlopoids (Fig. 10a–c). The premaxilla is tightly integrated with the rest of the

snout (Fig. 11b,c). It briefly contacts the maxilla, but to a much lesser extent and in a different configuration than in non-snake lizards (Figs. 3–6). Therefore, whereas the non-snake lizard premaxilla plays a direct role in bracing the palatomaxillary arches and preventing unilateral movement (see §3.1.3), this condition is quite different in leptotyphlopids.

Altogether, the palatomaxillary arches are essentially immobile in leptotyphlopids, with feeding being performed entirely by the mandibles (Kley and Brainerd, 1999; Kley, 2001, 2006). Decoupling of the upper and lower jaws is also evident from the extensive reduction of the ligamentous connection between the pterygoid and quadrate, as in typhlopoids (Kley, 2001). However, in typhlopoids, the palatomaxillary arch is highly mobile and the mandible is relatively rigid (Fig. 9; §3.4), whereas the opposite is true of leptotyphlopids (Fig. 11).

3.7. Ancestral state reconstruction

The "basic", "detailed microstomy", and "detailed microstomy and macrostomy" scoring methods produced different ancestral state reconstructions, especially at key nodes representing the origins of major clades.

Under the "basic" scoring method (Fig. 12), microstomy is the most parsimonious state for the origin of snakes and of alethinophidians, though the evolution of macrostomy was reconstructed equivocally, with microstomy and macrostomy being equally parsimonious in the nodes separating booid-pythonoids and caenophidians (Fig. 12a). In contrast, under the "detailed microstomy" scoring method (Fig. 13), all states are equally parsimonious for the origins of snakes and of alethinophidians, as well as the origins of Scolecophidia *sensu stricto* (i.e., Typhlopoidea and Leptotyphlopidae; *sensu* Miralles et al., 2018) and of all other snakes (i.e., Anomalepididae and Alethinophidia). As in the "basic" scoring method, the reconstruction of macrostomy is equivocal (Fig. 13a). Finally, under the "detailed microstomy and macrostomy" scoring method (Fig. 14), all versions of microstomy are again equally parsimonious for the origin of snakes, the origin of Scolecophidia *sensu stricto*, and the origin of all other snakes. However, in contrast to previous scoring methods, the reconstruction of macrostomy is definitive: booid-type and caenophidian-type macrostomy are reconstructed as evolving independently, with "snout-shifting" being most parsimonious for the intervening nodes (Fig. 14a).

A similar trend of increasing complexity and decreasing certainty occurs in the ML reconstructions (Figs. 12b, 13b, and 14b). Under the "basic" scoring method (Fig. 12),

microstomy is definitively reconstructed at the origin of snakes (99.996%) and is also the most likely state for the origin of alethinophidians (77.459%), consistent with the MP reconstruction. Unlike the MP reconstruction, however, macrostomy is definitively reconstructed (90.059–90.121%) for the nodes connecting booid-pythonoids and caenophidians (Fig. 12b). Microstomy is thus reconstructed as having evolved independently in Uropeltoidea compared to Amerophidia (Fig. 12b). Under the "detailed microstomy" scoring method (Fig. 13), reconstructions at the origin of snakes, of Scolecophidia *sensu stricto*, and of the ancestor of Anomalepididae and Alethinophidia become equivocal (Fig. 13b), as in the MP reconstruction (Fig. 13a). In contrast to the MP analysis, though, macrostomy is reconstructed as by far the most likely ancestral alethinophidian state (88.466%; Fig. 13b), again reflecting an independent evolution of microstomy in Uropeltoidea and Amerophidia as in the "basic" ML scoring method (Fig. 12b). Finally, under the "detailed microstomy and macrostomy" scoring method (Fig. 14), the ancestral nodes for snakes, for Scolecophidia *sensu stricto*, and for all other snakes (Anomalepididae + Alethinophidia) are again equivocal (Fig. 14b). "Snout-shifting" is reconstructed as the most likely ancestral state for alethinophidians (58.225%) and at the nodes connecting booid-pythonoids and caenophidians (just over 57% at both nodes). Thus, as in the MP reconstruction for this scoring method (Fig. 14a), booid- and caenophidian-type macrostomy are reconstructed as evolving independently from an ancestral "snout-shifting" condition (Fig. 14b).

4. Discussion

4.1. Homology

As this discussion centres around homology, a complex topic accompanied by a vast literature, it is important to first define our approach to homology and homology assessment.

Homology can be divided into two sequential concepts: primary homology followed by secondary homology (de Pinna, 1991; Brower and Schawaroch, 1996; Hawkins et al., 1997). Primary homology is essentially a conjecture of homology, in which an anatomical or molecular feature in a taxon is proposed—based on various criteria but prior to any test of phylogenetic congruence—to be homologous to a similar feature in different taxa (de Pinna, 1991; Brower and Schawaroch, 1996; Rieppel and Kearney, 2002; Simões et al., 2017). Principal among these criteria is "topological equivalence", i.e., articulations with the same surrounding elements,

1044 which allow morphological structures in different taxa to be recognized as evolutionarily
1045 equivalent (Rieppel and Kearney, 2002; Simões et al., 2017). Ancillary to topological
1046 correspondence are the criteria of "special similarity or quality" of structures and "intermediate
1047 forms" (Rieppel and Kearney, 2002). The former refers to specific anatomical similarities among
1048 the structures in question, whereas the latter encapsulates ontogeny, fossils, and morphoclines as
1049 evidence for "intermediacy" and thus anatomical correspondence of a structure across taxa
1050 (Rieppel and Kearney, 2002). These criteria together constitute the "test of similarity" by which
1051 a hypothesis of primary homology is either refuted or supported (Patterson, 1982; Rieppel and
1052 Kearney, 2002).
1053 Secondary homology is the corroboration of this hypothesis via recovery of the feature in
1054 question as synapomorphic across the relevant taxa (Patterson, 1982; de Pinna, 1991; Rieppel,
1055 1994; Rieppel and Kearney, 2002). Just as the "test of similarity" forms the basis for primary
1056 homology, this "test of congruence" constitutes the test of secondary homology, and it is only by
1057 passing these tests of similarity and congruence that features can be considered homologous or
1058 synapomorphic (Patterson, 1982; de Pinna, 1991; Rieppel, 1994; Rieppel and Kearney, 2002).
1059 Because a feature must pass this test of secondary homology to be homologous, and because it
1060 can only reach this stage by first being accepted as a primary homolog, it is therefore clear that a
1061 hypothesis of primary homology is the most fundamental step in the recognition of homology
1062 among taxa and their traits (de Pinna, 1991; Rieppel and Kearney, 2002; Simões et al., 2017).
1063 Beyond the "test of congruence", a final test of homology in extant taxa can also be
1064 performed in the form of genetic and/or developmental confirmation, i.e., determining whether
1065 secondary homologs are consistent at an underlying genetic or developmental level. However,
1066 this, too, requires primary homology to even be considered, and then requires substantial
1067 resources, not least of which are financial. Furthermore, ontogeny has been debated as a
1068 sufficient indicator of homology (e.g., Rieppel, 1994; Simões et al., 2017; Mabee et al., 2020),
1069 and this approach would also require far greater knowledge of the connection between genotype
1070 and phenotype than generally currently exists. Thus, for now, such assessment of absolute
1071 homology is of tertiary relevance from the perspective of researchers interested in trait evolution;
1072 assessments of primary and secondary homology remain paramount.
1073 However, an important distinction must be drawn between the homology of characters
1074 and the homology of character states. Although Patterson (1982, 1988) considered characters and

character states to both be "characters", just at more or less inclusive levels, we agree with several other authors (e.g., Brower and Schawaroch, 1996; Hawkins et al., 1997; Sereno, 2007; Simões et al., 2017) that this distinction is not trivial. Characters and character states are indeed similar in that they are both a type of homolog, but differ in that characters are comparable categories which must first be established and tested before character states can be assessed (Brower and Schawaroch, 1996; Hawkins et al., 1997). For example, a modern bird and an extinct non-avian theropod may both bear feathers on the forelimb. However, before attempting to create states reflecting the conditions of these feathers, we must first determine whether the feathers themselves are homologous across these taxa. Only once we have established the homology of these feathers—i.e., the existence of the "feather" as a character—can we parse this anatomical structure into meaningful states. In other words, character states are conditioned on the fundamental existence of the character itself, in this example the feather. Thus, just as primary and secondary homology are inherently sequential subdivisions of homology as a whole, character and character state homology are inherently sequential subdivisions of primary homology.

Brower and Schawaroch (1996) addressed this distinction by considering primary homology at two levels: "topographical identity" (i.e., primary homology of characters) and "character state identity" (i.e., primary homology of character states). Essentially, topographical identity concerns the homology of structures, whereas character state identity concerns the homology of conditions of those structures. Sereno (2007) presented a similar argument for distinguishing between characters as independent variables and character states as mutually exclusive conditions of that character, though specifically eschewed the subject of homology in his treatment of this logical distinction. Unfortunately, despite the significant attention directed toward the identification and testing of topographical identity or character homology (Patterson, 1982, 1988; Rieppel, 1994), the concept of character state identity or homology has been comparatively neglected (Brower and Schawaroch, 1996; Hawkins et al., 1997). Yet, it is this latter concept which is central to answering the questions at the core of this study, as it is character states which ultimately reflect synapomorphies.

Most importantly, the question of how to test proposed character state homologs has not been explicitly addressed. Previous discussions of the "test of similarity" have focused on primary homology at the level of topographical identity, with this test's major criterion—

topological correspondence—being particularly well-suited for testing the homology of characters (e.g., whether two bones are homologous). However, as an organism's anatomy becomes more and more atomized—i.e., considered at finer and finer levels of constituent elements, as is necessary to identify homology (Rieppel, 1994; Wilkinson, 1995)—this criterion eventually becomes inadequate. Consider, for example, the squamate quadrate. The observation that this element consistently connects the mandible ventrally with the skull dorsally allows this element to be considered a primary character homolog across squamates. When considering how to test the homology of its character states (e.g., quadrate orientation), though, this criterion is not useful, as the proposed states often differ in some manner unrelated to topology. Indeed, apart from character states dealing with presence/absence of an element or structure or dealing specifically with how a structure articulates with surrounding components, the criterion of topology is often entirely uninformative. How, then, can character state homology be effectively tested?

Given the uninformative nature of the criterion of connectivity, the subsidiary criteria of "special similarity or quality" and "intermediate forms" must be employed (Rieppel and Kearney, 2002). Herein lies another important difference between the primary homology of characters and character states: for characters, anatomical topology is the main arbiter of primary homology, with the specific shape and function of structures being largely disregarded (Rieppel, 1994; Rieppel and Kearney, 2002; Zaher and Rieppel, 2002); in contrast, testing the primary homology of character states requires the consideration almost exclusively of "special quality" of the shape and size of the character in question, with topological relations serving only to identify the structure in question. This approach is often employed operationally, such as Simões et al.'s (2017) proposal that states for continuous characters should only be delimited when there are breaks in the distribution of that character, i.e., distinct subdivisions of size and shape that justify consideration of these subdivisions as distinct conditions. Admittedly, "special similarity" may seem rather nebulous compared to the more concrete process of testing character homology by assessing topological relations and connectivity. However, by comparing characters using a combination of shape, size, and function, and by employing operational criteria such as that described above, it is possible to establish and test hypotheses of character state homology in a manner that is replicable and logically consistent, as exemplified below and as is necessary to establish a "meaningful" character (Rieppel and Kearney, 2002; Simões et al., 2017).

Assessing the homology or identity of character states is in turn necessary to assess the homology of overall character complexes, such as microstomy. This concept of “character complex homology” differs from, and is essentially an expansion upon, the concept of secondary homology. Whereas secondary homology focuses on identifying a single character and its states as synapomorphic, the identification of an integrated set of characters as “homologous” is an inherently more holistic process, requiring the simultaneous consideration of several characters so as to compare entire morphofunctional systems across taxa. Although such an undertaking may seem quite subjective, this is exactly the implication of hypotheses such as whether scolecophidians retain and share an ancestral “microstomatan” feeding mechanism (e.g., Bellairs and Underwood, 1951; Miralles et al., 2018). Such hypotheses of entire morphofunctional systems as homologous are common, yet typically not explicitly assessed or justified. Thus, through this discussion of squamate feeding mechanisms, we aim to explain and enact a more transparent, replicable, and theoretically consistent approach to this broader conceptualization of homology. This more explicit approach is essential in rendering subsequent hypotheses of character evolution replicable, testable, and falsifiable (Rieppel and Kearney, 2002), as well as in avoiding the pitfalls of either under- or over-atomizing complex anatomies (e.g., as discussed by Wilkinson, 1995 for "composite" versus "reductive" character construction).

Despite the differences between the homology of individual characters and of overall character complexes, the fundamental question underlying the search for homology remains the same: did these structures (or complexes) evolve once, thus uniting these taxa as a monophyletic group bearing a synapomorphic condition, or did these structures (or complexes) evolve independently? Of course, for character complexes there is no single “test of congruence” which can instantly characterize the entire complex as synapomorphic. Rather, a different benchmark for considering such conditions as “homologous” or “synapomorphic” is necessary.

Most critically, such an approach must be able to recognize shared common ancestry while also allowing for variation among taxa. To this end, we propose a guideline based on Patterson’s (1982:35) definition of a morphotype as “a list of the homologies (synapomorphies) of a group”. We herein use the term “morphotype” to refer to homologous character complexes, defined by the possession of key synapomorphies (i.e., secondarily homologous character states). Similar to a taxonomic diagnosis, a character complex can be considered homologous among taxa—i.e., considered to belong to the same morphotype—if it possesses the key

synapomorphies of that morphotype and does not possess the features "diagnosing" other morphotypes. Character complexes can only be considered homologous if their constituent characters and character states pass the tests of primary and secondary homology, as well as the guideline described above; as such, this approach to morphotype homology allows such a hypothesis to be tested and falsified. This rigorous assessment is essential for proper identification of homology (Rieppel and Kearney, 2002), which is in turn critical for higher-level evolutionary analyses, such as ancestral state reconstructions (see below) or recent computational advances related to homology (e.g., Mabee et al., 2020 and the Phenoscape project).

4.2. Is the jaw complex homologous among scolecophidians?

An intriguing hypothesis proposed in recent works suggests that the jaw structures in anomalepidids, leptotyphlopids, and typhlopoids may have evolved independently (Harrington and Reeder, 2017; Caldwell, 2019; Chretien et al., 2019). This is of course in distinct contrast to characterizations of the scolecophidian condition as more-or-less homogenous and as reflecting the ancestral snake condition (e.g., Miralles et al., 2018). Even in previous acknowledgments of the autapomorphic nature of the scolecophidian skull (e.g., Rieppel, 1988; Kley and Brainerd, 1999; Hsiang et al., 2015), the uniqueness of this morphology is typically emphasized for scolecophidians as a whole in comparison to other squamates, rather than scolecophidians in comparison to each other (though see Bellairs and Underwood, 1951; List, 1966; Kley, 2001; Cundall and Irish, 2008 for preliminary discussions of this hypothesis).

The results of this study provide strong support for the independent evolution of microstomy in each major scolecophidian clade. We propose that each clade exhibits a unique morphotype of microstomy (Fig. 1)—"single-axle maxillary raking" in typhlopoids, "axle-brace maxillary raking" in anomalepidids, and "mandibular raking" (*sensu* Kley and Brainerd, 1999) in leptotyphlopids—each of which is distinguished by several features that are universal within and entirely unique to each morphotype (Tables 3 and 4; see also Kley, 2001; Caldwell, 2019; Chretien et al., 2019).

In the "single-axle maxillary raking" morphotype (Fig. 9; Tables 3 and 4), prey ingestion and transport occurs exclusively via asynchronous unilateral movements of the maxillae, which rotate about the elongate maxillary process of the palatine (Kley, 2001; Chretien et al., 2019). The palatines and pterygoids are highly reduced; these elements contribute to rotation of the maxillae, but only the maxillae bear teeth and thus only the maxillae are directly responsible for

prey transport (Fig. 9a–d; Kley, 2001; Caldwell, 2019; Chretien et al., 2019). The mandibles are highly reduced and rigidly integrated, so as to also not contribute to prey transport (Fig. 9e–f; Kley, 2001; Caldwell, 2019).

In the "axle-brace maxillary raking" morphotype (Fig. 10; Tables 3 and 4), the maxilla is suspended from the reduced and mobile prefrontal and braced posteriorly by the ectopterygoid (Chretien et al., 2019). The pterygoids and palatines are highly reduced, similar to "single-axle maxillary raking", and the mandibles are reduced and immobile, though to a lesser extent than in the "single-axle" morphotype (Figs. 9 and 10). The highly reduced teeth on the mandible at most help to hold the prey in the mouth during maxillary raking.

In the "mandibular raking" morphotype (Fig. 11; Tables 3 and 4), the palatomaxillary arch is immobile and edentulous, thus not contributing at all to prey transport (Kley and Brainerd, 1999; Kley, 2001, 2006; Chretien et al., 2019). Rather, it is the highly mobile mandible—including a flexible intramandibular joint—that drives feeding, bearing a quite robust and complex structure in comparison to the conditions in "single-axle" and "axle-brace" microstomy (Figs. 1 and 9–11; List, 1966; Kley and Brainerd, 1999; Kley, 2001, 2006; Caldwell, 2019; Chretien et al., 2019). The mandibles move in a bilaterally synchronous manner, being joined at the symphysis via a cartilaginous nodule (Kley, 2006) which enables rotation between the left and right mandibles, but prevents lateral and anteroposterior separation of the mandibular tips (Kley, 2001, 2006).

These morphotypes are distinct and non-homologous because they each comprise key features that are not homologous with the corresponding conditions in other taxa (Figs. 9–11; Tables 3 and 4). Consider, for example, the maxillary process of the palatine as a character, and its degree of elongation as the character states in question. At the level of topographical identity, the maxillary process passes the "test of similarity" among squamates, as it occurs in a consistent topographic location and so can be considered a primary homolog. However, when considering its character states, the elongate condition of the maxillary process is consistent among typhlopoids (Fig. 9), but is both anatomically and functionally unique compared to the condition of this process in any other squamate (Figs. 3–8, 10, and 11). Thus, this character state passes the "test of similarity" among typhlopoids but fails this test in comparison to other squamates, and so cannot be considered synapomorphic between typhlopoids and other squamates.

1229 This same process of rejecting homology at the level of character state identity also
1230 applies to other key typhlopoid features, such as the medially excavated maxilla, the downcurved
1231 compound bone, and the enlarged splenial, among many other features (Fig. 9; §3.4; Tables 3
1232 and 4). These unique primary homologs, alongside a unique combination of other distinct
1233 features, ultimately result in a feeding mechanism that is fundamentally different from the
1234 condition in any other squamate—including other scolecophidians—and so represents a
1235 morphotype functionally and evolutionarily unique to typhlopoids: “single-axle maxillary
1236 raking”.
1237 This process can also be applied to the key features of anomalepidids (Fig. 10; Tables 3
1238 and 4; §3.5), such as the structure of the prefrontal and ectopterygoid, and those of
1239 leptotyphlopids (Fig. 11; Tables 3 and 4; §3.6), such as the edentulous maxilla, fixed palatine
1240 and pterygoid, uniquely structured dentary, and extremely elongate quadrate. Again, because the
1241 character states in question are anatomically consistent within each clade but distinct from the
1242 condition in any other taxon, each state passes the “test of similarity” within each clade but fails
1243 across clades. Thus, “axle-brace maxillary raking” and “mandibular raking” each comprise their
1244 own set of unique character states that cannot be synapomorphic with any other squamate, just as
1245 in “single-axle maxillary raking”, and so are also distinct morphotypes not representative of an
1246 ancestral snake condition (see also Kley and Brainerd, 1999; Kley, 2001, 2006).
1247 Of course, there are certain features of the jaws and suspensorium that are consistent
1248 across scolecophidians, such as the anteriorly oriented quadrate, absent or heavily reduced
1249 supratemporal and ectopterygoid, tall coronoid, and, at least in typhlopoids and leptotyphlopids,
1250 the cartilaginous interramal nodule (Figs. 9–11; Kley, 2001, 2006; Rieppel et al., 2009). The
1251 presence of these shared conditions would appear to undermine our hypothesis of the
1252 independent evolution of microstomy: each of these conditions passes the “test of similarity”
1253 across scolecophidians and, according to morphology-based phylogenies in which
1254 scolecophidians are monophyletic (e.g., Gauthier et al., 2012; Hsiang et al., 2015; Garberoglio et
1255 al., 2019a), also passes the “test of congruence”. Thus, based on these criteria, these character
1256 states can be accepted as synapomorphic for scolecophidians.
1257 However, an important counterpoint to this “undermining” is the extensive
1258 paedomorphosis exhibited by scolecophidians relative to other squamates (Kley, 2006; Palci et
1259 al., 2016; Da Silva et al., 2018; Caldwell, 2019; Strong et al., 2021). Paedomorphosis is the

retention of features typical of embryonic or juvenile individuals of an ancestral taxon into adults of a descendant taxon (McNamara, 1986). In scolecophidians, as noted by other authors (e.g., Kley, 2006; Caldwell, 2019; Strong et al., 2021), this paedomorphosis occurs throughout the skull, but is particularly prevalent in the mandible, palatomaxillary arch, and suspensorium.

This includes the anteroventral orientation of the quadrate (Figs. 9–11), a condition typical of embryonic squamates (Kamal, 1966; Rieppel and Zaher, 2000; Kley, 2006; Scanferla, 2016; Caldwell, 2019). The cartilaginous interramal nodule is likely also paedomorphic: although Kley (2006) interpreted this feature as a fibrocartilaginous elaboration of the midline raphe in *Leptotyphlops* (= *Rena*), he also noted that the midline raphe is universally absent in other scolecophidians, causing us to consider this hypothesis unlikely. We instead agree with other interpretations of this nodule as an extension of the Meckelian cartilages anterior to the dentary tips (e.g., Kley, 2001; Caldwell, 2019), a phenomenon that is known to occur throughout the embryonic development of the mandible in snakes (e.g., Al-Mohammadi et al., 2020) and that therefore renders the scolecophidian interramal nodule paedomorphic. Features related to the reduction and simplification of elements (e.g., pterygoid, palatine, supratemporal; Figs. 9–11) are also tied to paedomorphosis, with the reduction or absence of these structures reflecting early developmental stages in other squamates (e.g., see Polachowski and Werneburg, 2013; Werneburg et al., 2015; Ollonen et al., 2018). Finally, a disproportionately tall coronoid (Figs. 9e,f, 10e,f, and 11e,f) aids in increasing mechanical advantage of the lower jaw musculature (Rieppel, 1984), an adaptation important in compensating for the re-organization of the lower jaw as occurs in miniaturized and paedomorphic vertebrates (Hanken and Wake, 1993; Olori and Bell, 2012).

Given that scolecophidians are highly miniaturized, that miniaturization often co-occurs with fossoriality (Olori and Bell, 2012), and that miniaturization has been hypothesized as being caused by—or at least strongly correlated with—paedomorphosis (Hanken, 1984; Wake, 1986; Fröbisch and Schoch, 2009), these shared features thus all relate to miniaturization. Importantly, miniaturization, fossoriality, and paedomorphosis are all strongly associated with homoplasy (Hanken and Wake, 1993; Wiens et al., 2005; Fröbisch and Schoch, 2009; Maddin et al., 2011; Olori and Bell, 2012). In other words, the only major features of the scolecophidian jaw complex which fully pass the test of primary homology—and which potentially unite scolecophidians to the exclusion of other snakes—are highly homoplastic. It is therefore quite possible that the

aforementioned conditions apparently shared among scolecophidians in fact arose independently, as the result of the independent evolution of fossoriality and miniaturization in each scolecophidian clade (Caldwell, 2019; Chretien et al., 2019).

Indeed, such a hypothesis is consistent with the separate morphotypes of "microstomy" present in scolecophidians. This proposed scenario of independent excursions into fossoriality and miniaturization presents a logical explanation for why the jaws and suspensorium reflect so many entirely unique and non-homologous conditions across the scolecophidian clades (see also Caldwell, 2019; Chretien et al., 2019). This degree of variation is consistent with the morphological novelty typical of miniaturized vertebrates (Hanken, 1984; Hanken and Wake, 1993). Occurring simultaneously along these independent paths of miniaturization and fossoriality, we propose that other elements—such as the supratemporal, pterygoid, and quadrate—converged upon conditions that are known to have frequently evolved independently throughout Squamata (e.g., dibamids: see Fig. 5 and Rieppel, 1984; amphisbaenians: see Fig. 6 and Gans and Montero, 2008; uropeltids: see Olori and Bell, 2012; colubroids: see Strong et al., 2021).

Although such a hypothesis clearly contradicts the morphology-based phylogenetic placement of scolecophidians as a single clade (e.g., Gauthier et al., 2012; Hsiang et al., 2015; Garberoglio et al., 2019a), it is important to recognize the potential role of homoplasy in biasing phylogenies, especially as associated with paedomorphosis and/or fossoriality (Hanken and Wake, 1993; Wiens et al., 2005; Struck, 2007; Pinto et al., 2015). As examined previously for paedomorphic salamanders, morphology-based phylogenies can be misled by the shared presence of paedomorphic traits, causing the affected taxa to be artificially grouped together (Wiens et al., 2005). The distinct incongruence between molecular and morphological phylogenies of scolecophidians (e.g., Gauthier et al., 2012; Hsiang et al., 2015; versus Figueroa et al., 2016; Zheng and Wiens, 2016) further supports the possibility that confounding factors may be at play. It is thus clear that, in order to resolve longstanding questions regarding scolecophidian phylogeny and further assess the evolutionary hypotheses presented herein, a robust morphological and molecular framework for scolecophidians is crucial. Although such an undertaking is beyond the scope of this study, morphological analyses similar to the present study represent a key component in laying the foundation for such a framework.

Ultimately, we definitively reject the contention that scolecophidians are "morphologically and ecologically consistent" (Miralles et al., 2018:1785). From a biomechanical perspective, the jaws of each scolecophidian clade function in a completely different manner, as outlined in the Results. This lack of consistency also occurs from an evolutionary perspective, on the basis of primary homology, as argued above. Beyond superficially similar reduction of the jaw complex in each scolecophidian clade, almost every element of the upper and lower jaws shows fundamental anatomical and functional differences (Figs. 9–11; Tables 3 and 4), and those elements that do remain consistent (e.g., pterygoid, suspensorium) are highly susceptible to homoplasy.

Importantly, because microstomy occurs via a distinct, non-homologous, and thus independently evolving morphotype in each scolecophidian clade, we can therefore logically reject the hypothesis that scolecophidians as a whole represent a morphologically homogenous remnant of the ancestral snake condition, as per Caldwell (2019), Chretien et al. (2019), and Strong et al. (2021), and *contra*, for example, Rieppel (2012) and Miralles et al. (2018). Indeed, scolecophidians are so strongly influenced by the constraints of ecology and heterochrony (see also §4.4)—and thus so highly modified relative to other squamates and to each other—that for this group to have given rise to the morphology of all other snakes is in our view highly unlikely (see also Caldwell, 2019; Chretien et al., 2019; Strong et al., 2021). Rather than a plesiomorphic condition, the various scolecophidian lineages instead reflect convergence upon a miniaturized, fossorial, and myrmecophagous ecomorph, superficially similar to each other but in reality highly autapomorphic (Harrington and Reeder, 2017; Caldwell, 2019; Chretien et al., 2019). The combination of strongly homoplastic and strikingly divergent features across scolecophidians highlights the complicated interplay between determinism and contingency in organismal evolution, especially in the context of phenomena such as fossoriality, myrmecophagy, miniaturization, and paedomorphosis.

4.3. Is the scolecophidian jaw complex homologous to the condition in non-snake lizards?

The hypothesis that scolecophidians are retaining the same version of microstomy as in non-snake lizards—i.e., that these conditions are homologous—is an implicit though inherent assumption of how these taxa are scored in ancestral state reconstructions of this feature (e.g., Harrington and Reeder, 2017; Miralles et al., 2018). This assumption of homology is more broadly reflected in the traditional division of squamates into "Macrostomata" and non-

1352 macrostomatans (reviewed in Rieppel, 1988), with the corresponding assumption that, because
1353 scolecophidians, early-diverging alethinophidians, and non-snake lizards all lack macrostomy,
1354 this lack of macrostomy—as characterized in this simplistic manner (on the complexities of
1355 macrostomy, see Palci et al., 2016; Caldwell, 2019)—is a fundamentally plesiomorphic retention
1356 from non-snake lizards (e.g., Bellairs and Underwood, 1951; Rieppel, 2012). However, we argue
1357 that these groups exhibit distinct morphotypes of microstomy (Tables 3 and 4), rendering the
1358 evolution of this feeding mechanism much more complex than the aforementioned perspective.
1359 From one line of reasoning, if we accept the hypothesis that microstomy is not
1360 homologous across scolecophidians and instead evolved independently in each clade (as argued
1361 above), then logically we must reject the hypothesis that "microstomy" as present in
1362 scolecophidians is "primitive" or homologous to that of non-snake lizards. Recent discussions
1363 arguing that the scolecophidian skull could quite reasonably be derived from an alethinophidian
1364 or even "macrostomatan" ancestor (Kley, 2006; Harrington and Reeder, 2017; Caldwell, 2019;
1365 Strong et al., 2021) further indicate that the presence of a scolecophidian morphotype—including
1366 the presence of microstomy—does not in and of itself indicate a "microstomatan" ancestral
1367 condition of snakes. Even if we accept the proposition from several authors—problematic as
1368 these hypotheses may be (Kley, 2006; Caldwell, 2019)—that scolecophidians retain certain
1369 plesiomorphic features of non-snake lizards (e.g., multipennate jaw adductor musculature, tall
1370 coronoid; Kley, 2006; Rieppel, 2012), the presence of many non-homologous features indicates
1371 that microstomy cannot be considered a homogenous or consistent condition across these taxa.
1372 A particularly important feature is the mandibular symphysis, which in non-snake lizards
1373 bears distinct symphyseal facets but which in snakes—including scolecophidians—is smooth and
1374 more widely separated (see also Kley, 2006). As discussed by Kley (2006), this observation
1375 suggests that scolecophidians in fact evolved from a more "snake-like" ancestor, in which the
1376 mandibles were already capable of independent movement and possibly macrostomy. This of
1377 course contradicts the hypothesis of scolecophidians retaining a non-snake lizard-like version of
1378 this component of "microstomy". Similarly, although the tightly-linked interramal symphysis in
1379 scolecophidians may superficially evoke the condition in non-snake lizards, the robust
1380 cartilaginous nodule in scolecophidians is entirely different from other squamates (Kley, 2006)
1381 and, as noted above, is most likely a distinctly paedomorphic—not plesiomorphic—condition.
1382 Finally, Kley (2006) also notes the *M. retractor pterygoidei* and *M. protractor pterygoidei* in

leptotyphlopids as suggesting derivation from an ancestral condition in which the palatomaxillary arch was quite mobile. This in turn implicates a possibly "macrostomatan" ancestral condition and contradicts Rieppel's (2012) conclusion that the scolecophidian jaw adductor musculature reflects a plesiomorphic non-snake lizard anatomy (see also Caldwell, 2019).

Several other key conditions of the jaws and suspensorium are also not homologous among scolecophidians, "anilioids", and non-snake lizards. The maxillary process of the palatine was discussed above in the context of "single-axle maxillary raking", though is also important when considering "anilioids" and non-snake lizards (Table 4). In non-snake lizards, this process is quite broad, articulating extensively with the maxilla (Figs. 3b,d, 4b,d, 5b,d, and 6b,d); in uropeltoids and amerophidians, however, this process is reduced and the maxilla-palatine articulation is instead a "ball-and-socket"-like joint formed mainly by the palatine process of the maxilla (Figs. 7b,d and 8b,d). Thus, although the maxillary process of the palatine passes the "test of similarity" at the level of topographical identity (i.e., primary character homology), it fails at the level of character state identity, as it exhibits anatomically and functionally distinct forms across these taxa. The condition of this character in uropeltoids and amerophidians is further notable in that, although these lineages are not closely related (Figs. 1 and 2), they exhibit primary homology or character state identity of the "ball-and-socket"-like joint. This is a key innovation of the feeding mechanism in these taxa, distinct from any other "microstomatan" squamate. The shared presence of this feature in these distinct lineages suggests it to better reflect the ancestral snake condition than any state exhibited by scolecophidians for this character.

The vomerine process of the palatine also differs among these taxa (Table 4), with non-snake lizards bearing a broad vomerine process in extensive osseous contact with the vomer (Figs. 3b,d, 4b,d, 5b,d, and 6b,d), uropeltoids and amerophidians bearing a broad choanal process lacking this sutural contact (Figs. 7b,d and 8b,d), and scolecophidians bearing a highly reduced and likely paedomorphic choanal process (Figs. 9b,d, 10b,d, and 11b,d). Other characters with states that differ across non-snake lizards, "anilioids", and scolecophidians include: the basipterygoid processes and their size and extent of articulation with the pterygoids; the presence and extent of the premaxilla-maxilla articulation; the integration and extent of mobility between

1413 the ventral and dorsal snout elements; and the suspension of the quadrate (Figs. 1 and 3–11;
1414 Tables 3 and 4).
1415 All of these characters exhibit character states which differ distinctly and consistently
1416 among the taxa in question (Tables 3 and 4; as described in the Results), which bear distinct
1417 functional consequences, and which altogether reflect a lack of primary and thus secondary
1418 homology across these taxa. As a result, because so many of these key features are non-
1419 homologous, the overall jaw complex cannot be considered consistent across these taxa. Rather,
1420 non-snake lizards, "anilioids", and the scolecophidian clades each exhibit distinct morphotypes
1421 of microstomy, characterized by their own unique sets of character states (Figs. 1 and 3–11;
1422 Tables 3 and 4).
1423 The morphotype exhibited by non-snake lizards (Figs. 3–6; Tables 3 and 4) is
1424 characterized by robust and tightly integrated jaw elements compared to the condition in snakes,
1425 particularly at the intramandibular joint and mandibular symphysis. We herein term this
1426 morphotype "minimal-kinesis microstomy", in recognition of the numerous robustness-related
1427 character states of this morphotype, as well as previous discussions of the minimally kinetic
1428 nature of the non-snake lizard skull relative to that of snakes (e.g., Cundall, 1995).
1429 The uropeltoid and amerophidian morphotype (Figs. 7 and 8; Tables 3 and 4) is similar to
1430 non-snake lizards in terms of general robustness, though it differs in certain key aspects (see also
1431 Cundall, 1995). This includes greater kinesis of the intramandibular joint and, perhaps most
1432 importantly, the capacity for unilateral movement of the palatomaxillary arches (§3.2; Cundall,
1433 1995). Because decoupling of the snout elements is integral to the jaw biomechanics of
1434 *Cylindrophis* (see §3.2.3; analyzed in greater detail by Cundall, 1995), and has further been
1435 proposed to occur throughout Uropeltoidea and Amerophidia (Cundall, 1995), we retain
1436 Cundall's (1995) use of the term "snout-shifting" to describe this biomechanical morphotype
1437 (Tables 3 and 4).
1438 However, despite its capacity for unilateral palatomaxillary movement, the "snout-
1439 shifting" jaw complex is still more closely integrated than the condition in "macrostomatan"
1440 snakes, indicating a much more limited degree of kinesis in uropeltoids and amerophidians
1441 relative to these more derived alethinophidians (Cundall, 1995). The "snout-shifting"
1442 morphotype is therefore intermediate between the "minimally-kinetic microstomatan" and

"macrostomatan" conditions in terms of both anatomy and function (Cundall and Rossman, 1993; Cundall, 1995; Kley, 2001).

Due to this intermediacy, it is tempting to hypothesize the "anilioid" skull as representing the ancestral snake condition. Indeed, the presence of a highly consistent jaw morphotype in uropeltoids and amerophidians—two basally-diverging but phylogenetically distinct alethinophidian lineages (Figs. 1 and 2)—provides compelling evidence for this morphotype as ancestral for alethinophidians, if not all snakes. However, attempts to reconstruct the ancestral condition for snakes should not rest solely on extant taxa (see also Caldwell, 2019). Given that millions of years have elapsed since the origin of snakes (e.g., 166.76 Ma; Garberoglio et al., 2019a), a more logical approach would be to give precedence to the fossil record, using morphological information from taxa temporally—and thus likely morphologically—much closer to the origin of Ophidia (Caldwell, 2019). This is especially true as extinct taxa can provide character state information not present in modern taxa, thus providing a necessary supplement to the neontological record (Finarelli and Flynn, 2006; Finarelli and Goswami, 2013; Betancur-R et al., 2015; Puttick, 2016; Caldwell, 2019; Mongiardino Koch and Parry, 2020).

This is not to say that extant taxa are altogether uninformative in hypothesizing the ancestral snake morphology. Indeed, recently discovered and exceptionally preserved specimens of the extinct *Najash* (Garberoglio et al., 2019a; Garberoglio et al., 2019b) reveal a morphology similar to "anilioids", suggesting uropeltoids and amerophidians to be the extant taxa most representative of this ancestral condition (Caldwell, 2019; Garberoglio et al., 2019b). However, an important logical distinction must be emphasized: uropeltoids and amerophidians are not representative of this ancestral morphology because they are the most "lizard-like" groups of snakes; rather, they are representative of this ancestral condition because they are the extant groups most morphologically similar to early-evolving fossil snakes (Garberoglio et al., 2019b). The primacy of the fossil record in hypothesizing ancestral conditions is paramount (Caldwell, 2019), as reflected by the key role of fossils in fuelling phylogenetic debates regarding the origin of snakes (e.g., Lee and Caldwell, 1998; Zaher, 1998; Zaher and Rieppel, 1999; Caldwell, 2000; Zaher and Rieppel, 2002; Apesteguía and Zaher, 2006; Caldwell, 2007; Harrington and Reeder, 2017).

On a similar note, this intermediate status of "anilioids" may suggest that their jaw complex ought to be considered homologous to the non-snake lizard condition, i.e., grouped

1474 under the same morphotype due to the shared presence of robust features. However, as outlined
1475 above, a number of key character states do differ between non-snake lizards and "anilioids", in
1476 turn reflecting the distinct functional nature of the uropeltoid and amerophidian jaw complex
1477 (e.g., the ability for "snout-shifting") compared to that of non-snake lizards (Figs. 3–8; Tables 3
1478 and 4). Because of these consistent homological and functional differences between the non-
1479 snake lizard and early-diverging alethinophidian jaw mechanisms, these conditions therefore
1480 cannot be considered directly homologous; although hypotheses of the "anilioid" condition as
1481 representing an evolutionarily intermediate stage between non-snake lizards and
1482 "macrostomatan" snakes are possible, any such hypothesis must recognize the distinct nature of
1483 the "anilioid" skull. Other studies have similarly cautioned against drawing direct parallels
1484 between "anilioids" and non-snake lizards (e.g., Harrington and Reeder, 2017).
1485 Finally, an important clarification to this discussion of homology is that synapomorphies
1486 can only be fully corroborated by the "test of congruence" *sensu* Patterson (1982, 1988), a test
1487 requiring rigorous phylogenetic analysis and thus falling beyond the scope of the current study.
1488 Although we do not perform this test herein, the rejection of homology at the level of character
1489 state identity for several key features means that we *can* definitively deem these conditions—
1490 and, by extension, their morphotypes of "microstomy"—as non-homologous and non-
1491 synapomorphic. Essentially, our perspective that the jaw complexes in non-snake lizards, early-
1492 diverging alethinophidians, and the scolecophidian lineages are not primary homologs by
1493 definition precludes them from being secondary homologs, i.e., synapomorphic.
1494 A related caveat applies to "snout-shifting" snakes. Amerophidians and uropeltoids both
1495 possess the character states comprising this morphotype, thus satisfying the test of primary
1496 homology. However, under the current phylogenetic framework (Figs. 1 and 2), two evolutionary
1497 scenarios for this morphotype are equally possible: either each constituent character state—and
1498 thus the overall "snout-shifting" morphotype—arose once at the base of Alethinophidia and was
1499 subsequently lost in caenophidians and booid-pythonoids, meaning that "snout-shifting" is
1500 indeed a synapomorphy of uropeltoids and amerophidians and the plesiomorphic state for
1501 Alethinophidia (e.g., Fig. 14a); or "snout-shifting" arose independently in Amerophidia and
1502 Uropeltoidea, and is in fact convergent (e.g., Fig. 13b). It is therefore currently ambiguous as to
1503 whether this morphotype would pass the test of congruence. However, the fossil evidence
1504 presented above, combined with the presence of numerous consistent character states in such

distantly-related lineages—not least of which is an unusual morphological innovation, the "ball-and-socket"-like maxilla-palatine joint—in our view favours the interpretation of this morphotype as indeed homologous across these early-diverging alethinophidian clades, reflecting an ancestral snake morphology.

4.4. Variation within morphotypes

As a final note when considering the homology of "microstomy" across squamates, the anatomical variants discussed in §3.1.4 and §3.2.4 raise the question of whether it is appropriate to include the taxa in question (dibamids and amphisbaenians, and *Anomochilus* and *Uropeltis*) under the same morphotype as other non-snake lizards and other early-diverging alethinophidians, respectively. As mentioned in §4.1, when considering the homology of entire morphofunctional complexes, it is inevitable that some variation will arise due to the taxonomic breadth of each morphotype and thus must be allowed and accounted for. For the taxa mentioned above, although certain features may vary relative to their respective morphotypes, ultimately these taxa do remain consistent with these overall morphotypes.

For all of these taxa, many of the differences they exhibit compared to other non-snake lizards or "anilioids" are paedomorphic. In this case, these paedomorphic features mainly include the absence or drastic reduction of elements (e.g., supratemporal, squamosal, ectopterygoid; Figs. 5 and 6), which can be recognized as paedomorphic by comparison to the typical, well-developed condition of these elements in other squamates (e.g., see Polachowski and Werneburg, 2013; Werneburg et al., 2015; Ollonen et al., 2018). Anterior displacement of the jaw suspension and anteroventral orientation of the quadrate (Figs. 5 and 6) are also paedomorphic traits, common among miniaturized vertebrates (Olori and Bell, 2012; Strong et al., 2021) and reflecting retention of the embryonic condition of the suspensorium in squamates (Kamal, 1966; Rieppel and Zaher, 2000; Kley, 2006; Scanferla, 2016). This paedomorphosis is likely tied to miniaturization (Rieppel, 1984; Rieppel and Maisano, 2007; Maddin et al., 2011; Olori and Bell, 2012), as dibamids, *Anomochilus*, and uropeltids have all been recognized as miniaturized (e.g., Rieppel, 1984; Olori and Bell, 2012), and developmental truncation has been hypothesized as one of the main processes by which such drastic size reduction occurs (Hanken, 1984).

Other features, such as the structure of the suspensorium (Figs. 5 and 6), are also common among miniaturized and fossorial taxa (see also Rieppel, 1984; Evans, 2008; Maddin et al., 2011). Similarly, features such as the more tightly integrated premaxilla and prefrontal in

Anomochilus and *Uropeltis*, as well as the laterally enclosed braincase in dibamids and amphisbaenians, are logical consequences of fossoriality in these taxa (Cundall and Rossman, 1993). Miniaturization may also play a role, as elements must be more compactly arranged in a smaller skull, resulting in tighter integration relative to non-miniaturized taxa.

In light of these phenomena, it is reasonable to hypothesize the derivation of the dibamid or amphisbaenian skull from a more "typical" non-snake lizard morphotype via miniaturization- and/or fossoriality-related paedomorphosis, or the derivation of the skull of *Anomochilus* or *Uropeltis* from a more "typical" uropeltoid condition in a similar manner. As in scolecophidians, features susceptible to homoplasy—such as those related to fossoriality, miniaturization, and paedomorphosis—must be taken into account and recognized as superimposing potentially misleading features upon the morphology in question. For scolecophidians, this means recognizing these potentially homoplastic features as quite weak evidence for synapomorphy or homology (see §4.2); for dibamids, amphisbaenians, and paedomorphic uropeltoids, this means recognizing this homoplasy as a likely independent superimposition overtop the core morphotype in question. After accounting for such phenomena as miniaturization and fossoriality, the dibamid and amphisbaenian skulls otherwise share several conditions with other non-snake lizards, and the same is true for *Anomochilus* and *Uropeltis* in comparison to other "anilioids" (see §3.1.4 and §3.2.4). In contrast, after taking these phenomena into account for scolecophidians, the jaw complexes are still fundamentally different, justifying separate morphotypes. Accounting for these phenomena is therefore essential in recognizing and accounting for homoplasy when evaluating the homology of character complexes.

Of these taxa, *Anomochilus* most prominently displays a unique skull structure that is not easily referable to any of the main morphotypes. As described by Cundall and Rossman (1993), the skull of *Anomochilus* is unique among snakes, having been proposed as an intermediate between scolecophidians and alethinophidians. One of the most unique features of *Anomochilus* is its palatomaxillary structure: the maxilla is reduced compared to other "anilioids", especially in anteroposterior length, and does not contact the reduced ectopterygoid (Cundall and Rossman, 1993; Rieppel and Maisano, 2007). This would suggest different palatomaxillary biomechanics, as movement of the maxilla would presumably be driven only by the palatine, with which it articulates medially (Cundall and Rossman, 1993). This is reminiscent of "maxillary raking" as occurs in some scolecophidians.

1567 However, the rest of the jaws and suspensorium differ sufficiently from
1568 scolecophidians—and molecular evidence places *Anomochilus* firmly within the Uropeltoidea,
1569 possibly as sister to Cylindrophiidae (Pyron et al., 2013)—such that we consider this similarity
1570 convergent, driven by paedomorphosis affecting the ectopterygoid and maxilla in *Anomochilus*,
1571 rather than modification from a "maxillary raking" scolecophidian ancestor. Cundall and
1572 Rossman (1993) similarly reject the possibility that *Anomochilus* and scolecophidians (in their
1573 discussion, specifically typhlopids) share a homologous feeding mechanism. Ultimately, the
1574 exact nature and phylogenetic position of *Anomochilus* requires its own detailed treatment,
1575 beyond the scope of the current paper. However, following the effects of paedomorphosis and
1576 fossoriality as discussed above, and in light of previous morphological analyses supporting the
1577 uropeltoid affinities of *Anomochilus* (e.g., Rieppel and Maisano, 2007) and genetic evidence
1578 affirming this conclusion (e.g., Pyron et al., 2013), we consider it most reasonable to classify
1579 *Anomochilus* as a modified "snout-shifting" taxon.
1580 Finally, many morphological phylogenies often recover dibamids, amphisbaenians, and
1581 snakes as part of a clade of fossorial and/or limb-reduced taxa (e.g., the Scincophidia of Conrad,
1582 2008). Indeed, certain features are consistent among these taxa; for example, the suspensorium in
1583 dibamids and amphisbaenians (Figs. 5 and 6; §3.1) is quite similar to the condition in
1584 scolecophidians (Figs. 9–11; §3.4–3.6), particularly regarding the extreme reduction of the
1585 supratemporal and anterior orientation of the quadrate. However, as noted above, these features
1586 likely result from miniaturization-driven paedomorphosis (Rieppel, 1984; Maddin et al., 2011;
1587 Olori and Bell, 2012). Given that miniaturization, paedomorphosis, and fossoriality are often
1588 associated with homoplasy (Rieppel, 1984, 1988; Hanken and Wake, 1993; Wiens et al., 2005;
1589 Fröbisch and Schoch, 2009; Maddin et al., 2011), and the fact that amphisbaenians, dibamids,
1590 and scolecophidians are not considered to be closely related in most recent phylogenies (e.g.,
1591 Wiens et al., 2010; Reeder et al., 2015; Simões et al., 2018; Burbrink et al., 2020), these
1592 similarities are therefore almost certainly driven by the independent evolution of miniaturization
1593 and fossoriality in these groups. This conclusion is consistent with previous arguments that the
1594 recovery of a "fossorial clade" is simply the result of a homoplastic fossorial ecomorph evolving
1595 convergently in these taxa (e.g., Rieppel, 1988; Lee, 1998). The numerous ways in which the
1596 amphisbaenian or dibamid skull differs from that of scolecophidians—especially regarding the
1597 robustness and degree of integration of the jaw elements (Figs. 5, 6, and 9–11)—support the

hypothesis that these similarities are convergent, rather than reflecting that the scolecophidian jaw condition is strictly homologous to, or a retention of, the dibamid or amphisbaenian condition.

4.5. Ancestral state reconstruction

The overarching outcome of our ancestral state reconstructions is that different hypotheses of homology result in very different reconstructions of key nodes (Figs. 12–14). For example, the ancestral snake node is definitively reconstructed as “microstomy” under the simplest scoring scheme (Fig. 12), but is equivocal under both other schemes (Figs. 13 and 14) under both ML and MP algorithms. Similarly, the ancestral alethinophidian node is variably reconstructed as definitively “microstomy” (Fig. 12a) or “snout-shifting” (Fig. 14a), very likely “macrostomy” (Fig. 13b), or ambiguous (Figs. 12b, 13a, and 14b).

Although it may seem a foregone conclusion that increasing the number of character states increases the uncertainty of reconstruction, such an outcome is not trivial. Simple approaches to reconstruction tend to produce correspondingly straightforward hypotheses of character evolution, such as “microstomy” as the definitive ancestral condition for snakes. However, scoring “microstomy” under a single state reflects an implicit assumption that this condition is directly comparable—i.e., homologous—across the taxa in question. Once homology is explicitly assessed and character scoring adjusted to reflect this homology (or lack thereof), ancestral state reconstructions become more complicated, more ambiguous, and therefore less apparently informative. However, most importantly, these reconstructions also become more accurate, as they more closely reflect the biological reality of the conditions in question and thus provide a more realistic reconstruction of their evolution.

Arguably, to provide the most realistic reconstruction of ancestral nodes, any semblance of morphotypes or overarching character complexes should be eliminated altogether, and each character should instead be reconstructed separately (e.g., the "reductive coding" approach of Wilkinson, 1995). Indeed, such an approach is essential in reconstructing hypothetical transitional taxa, i.e., nodes bearing novel combinations of character states (Wilkinson, 1995). However, this method is not without flaws. For example, how much atomization is enough, or is too much (Wilkinson, 1995)? Are these novel trait combinations plausible, or even biologically possible? Focusing on morphotypes—rather than individual characters—avoids these issues, as this concept involves accurately conceptualizing morphofunctional systems without sacrificing

their inherent integration and complexity. Ultimately, both approaches to ancestral state reconstruction have merit, with the morphotype concept in particular avoiding both the under-atomization (e.g., treating "microstomy" as homogenous) and over-atomization (e.g., as may occur in "reductive coding") of complex morphofunctional systems.

Conversely, one could instead argue that our more complex scoring methods essentially "over-separate" microstomy into so many states as to be uninformative. For example, what if the purpose of the analysis is simply to determine if the ancestral snake was "some kind of microstomatan" versus "some kind of macrostomatan", regardless of the specific morphology of this condition? In this case, would it not be acceptable to simply score taxa as "microstomy" versus "macrostomy"? Such an approach, however, is untenable, and would be similar to the problems created, for example, by using the term "big wing" versus "small wing" in systematizing birds using wing size. In any examination of the evolution of a character and its states, the anatomy in all of its details must take primacy (Wilkinson, 1995; Rieppel and Kearney, 2002; Simões et al., 2017). Hypotheses regarding character evolution must be constructed using a "bottom-up" approach, i.e., starting with assessments of fundamental homology and building from this starting point. "Top-down" approaches—i.e., lumping various conditions together from the outset, and only later considering non-homology—represent a theoretically "backwards" approach to the study of character evolution.

The fallacy of this approach is especially true when it results in hypotheses that taxa such as scolecophidians are plesiomorphically "retaining" ancestral conditions (e.g., Miralles et al., 2018). Of note, Harrington and Reeder (2017) also scored all taxa as simply "macrostomy" or "non-macrostomy" in their analysis of snake morphotype evolution. However, following their ancestral state reconstruction, they did critically examine the relevant morphologies in a manner similar to that recommended by Griffith et al. (2015), ultimately concluding that the scolecophidian morphotype is not representative of the ancestral snake condition and in fact may have evolved convergently (Harrington and Reeder, 2017). We commend this comparative anatomical perspective, with our results supporting these authors' conclusions. However, in order to be fully theoretically sound, this assessment of homology should be performed prior to the analysis—i.e., when delimiting character states—rather than afterwards.

Critical examination of primary homology prior to reconstructing ancestral states is indeed crucial: non-homologous conditions cannot be included under the same character or state

in a phylogenetic analysis (Rieppel and Kearney, 2002; Simões et al., 2017), a principle which logically must also apply to ancestral state reconstructions. To do otherwise is to equate conditions which are fundamentally incomparable, creating an artificial category—in this case, of uniform "microstomy"—without reflecting the morphological nuance associated with this condition. Just as Simões et al. (2017:200) caution against "naïve connectivity" in the employment of the "test of similarity", we caution against the issue of "naïve homology" when comparing character complexes across taxa. Admittedly, for certain conditions (e.g., diel activity pattern, biome, aquatic habits, prey preference: Hsiang et al., 2015; limb reduction: Harrington and Reeder, 2017), primary homology is difficult or impossible to assess; as such, it is often unavoidable to group each of these conditions under the same overarching character state. However, for a condition such as microstomy, for which homology can be thoroughly assessed, conflating non-homologous conditions introduces substantive, not to mention unnecessary, logical error into the analysis. We therefore advocate the importance of a thorough comparative anatomical approach when formulating hypotheses regarding evolution (see also Rieppel and Kearney, 2002; Simões et al., 2017). This echoes recent discussions that ancestral state reconstructions should not be an analytical endpoint, but rather should be treated as hypotheses to be rigorously assessed in their own right (Griffith et al., 2015).

Although the present study focuses on "microstomy", the concept of "macrostomy" is equally in need of re-examination. Recent authors have suggested that the versions of "macrostomy" present in booid-pythonoids and caenophidians may have evolved independently, based on both molecular (Burbrink et al., 2020) and ontogenetic (Palci et al., 2016) evidence. Furthermore, even within each of these groups, different variations of macrostomy may have arisen convergently (Caldwell, 2019; Strong et al., 2019). Similarly, although specimens of tropidophiids were not available for the present study, this family is particularly worthy of attention: recent phylogenies (e.g., Burbrink et al., 2020) have recovered these "macrostomatans" as the sister group to Aniliidae within the Amerophidia, an early-diverging placement in turn suggesting that macrostomy may have evolved earlier among snakes than is often recognized, including within our own ancestral state reconstructions (Figs. 12–14). Therefore, much like the conflation of "microstomy" as a uniform character state is inaccurate, as presented herein, the conflation of "macrostomy" in a similar manner may also be incorrect. Our scoring methods include "macrostomy" as both single and separate morphotypes in order to recognize this

uncertainty; however, a detailed re-examination of macrostomy very much requires its own treatment, so as to better understand the complexity of this feeding mechanism and its evolution.

Finally, this ancestral state reconstruction is not an attempt to definitively determine the ancestral snake morphology. Indeed, certain aspects of our analysis—particularly regarding limited sampling of "macrostomatans" (given our focus on microstomy) and no sampling of extinct taxa (given our chosen phylogenetic framework)—largely preclude such a definitive determination of such a complex problem. Rather, our aim was to assess the impact that different perspectives on homology and morphology might have in shaping higher-level hypotheses of character and taxon evolution, as examined above.

As for future studies which do aim to definitively reconstruct the "ancestral snake morphology", the inclusion of extinct taxa is a particularly crucial component. Data from fossils have consistently been shown to improve ancestral state reconstructions by providing critical information not reflected by extant taxa, such as taxonomic diversity, character state distributions, unique character states or state combinations, and impact upon the phylogeny itself on which the ancestral state reconstruction is based (Finarelli and Flynn, 2006; Finarelli and Goswami, 2013; Betancur-R et al., 2015; Puttick, 2016; Caldwell, 2019; Mongiardino Koch and Parry, 2020). Exceptionally preserved snake fossils, such as recently described specimens of *Najash* (Garberoglio et al., 2019a; Garberoglio et al., 2019b), are particularly promising in allowing the detailed anatomical analysis necessary for accurate reconstructions. We therefore encourage the inclusion of extinct taxa alongside thorough comparative anatomical analysis in future attempts at reconstructing the "ancestral snake morphology".

Acknowledgments

Funding for this research was provided via an Alexander Graham Bell Canada Graduate Scholarship awarded by the Natural Sciences and Engineering Research Council of Canada (NSERC) to C.R.C.S. and an NSERC Discovery Grant (#23458) to M.W.C. This work was also performed in part at the Center for Nanoscale Systems (CNS), a member of the National Nanotechnology Coordinated Infrastructure Network (NNCI) and part of Harvard University, which is supported by the National Science Foundation under NSF award no. 1541959.

Copyright of all MCZ scans belongs to the Museum of Comparative Zoology, Harvard University, and the associated raw digital media are © President and Fellows of Harvard College, 2020, all rights reserved. These are used herein with permission.

Several scans were obtained from DigiMorph.org, as provided by the University of Texas High-Resolution X-ray CT Facility (UTCT). Scans of YPM 14378 and YPM 14376 were originally collected under NSF grants DEB-0132227, EF-0334961, and IIS-9874781. Scans of FMNH 58299, FRIM 0026, FMNH 216257, USNM 12378, FMNH 148589, FMNH 22468, and UMMZ 190285 were collected under NSF grants IIS-0208675 and EF-0334961. Scans of USNM 204078, FMNH 60958, FMNH 62204, FMNH 63117, FMNH 117833, FMNH 104800, and FMNH 148900 were collected under NSF grant EF-0334961. Scans of TNHC 60638 and YPM 12871 were collected under NSF grants EF-0334961 and IIS-9874781. Scans of TMM M-10006, YPM 6057, and TNHC 18483 were collected under NSF grant IIS-9874781. Scans of TNHC 62769 were collected under NSF grant IIS-0208675. Scans of FMNH 167048 and UTA 50569 were also obtained from DigiMorph. Scans of FMNH 179335, FMNH 30522, FMNH 58322, FMNH 62248, FMNH 259340, FMNH 31162, and FMNH 128304 were examined using images provided online by DigiMorph.

Several other scans were downloaded from MorphoSource, Duke University. The University of Michigan Museum of Zoology provided access to the data for UMMZ 201901 (M39211-70987) and UMMZ 174763 (M45443-82778), the collection of which was funded by oVert TCN under NSF DBI-1701714 and NSF DBI-1701713. The University of Florida provided access to the data for UF 33488 (M33644-62342), the collection of which was funded by oVert TCN under NSF DBI-1701714. The University of Kansas Center for Research Inc provided access to the data for KUH 125976 (M41676-75015), the collection of which was funded by oVert TCN under NSF DBI-1701714, NSF DBI-1701713, and NSF DBI-1701932.

The Field Museum of Natural History provided access to the data for FMNH 264702 (M27566-52993), the collection of which was funded by oVert TCN under NSF DBI-1701714 and NSF DBI-1702421. oUTCT provided access to the data for FMNH 195924 (M53075-96074), FMNH 22847 (M54489-98383), FMNH 31182 (M54499-98393), TCWC 45501 (M62793-113753), CAS 126478 (M54497-98391), CAS 134753 (M54498-98392), CAS 26937 (M54605-98507), FMNH 31774 (M54687-98600), and FMNH 109462 (M54697-98610), originally appearing in Gauthier et al. (2012), with data collection funded by NSF EF-0334961 and data upload to MorphoSource funded by DBI-1902242. Mark D. Scherz provided access to the data for ZSM 2194/2007 (M43873-79510), originally appearing in Chretien et al. (2019).

Finally, scans from the AMS, QM, and SAMA collections were provided courtesy of A. Palci, and scans of UAMZ specimens were provided courtesy of lab colleagues.

Literature Cited

2019. Dragonfly 4.0. http://www.theobjects.com/dragonfly

Al-Mohammadi AGA, Khannoon ER, Evans SE. 2020. The development of the osteocranium in the snake *Psammophis sibilans* (Serpentes: Lamprophiidae). J Anat 236:117–131.

Apesteguía S, Zaher H. 2006. A Cretaceous terrestrial snake with robust hindlimbs and a sacrum. Nature 440:1037–1040.

Asplen MK, Whitfield JB, de Boer JG, Heimpel GE. 2009. Ancestral state reconstruction analysis of hymenopteran sex determination mechanisms. J Evol Biol 22:1762–1769.

Bellairs AD, Underwood G. 1951. The origin of snakes. Biol Rev 26:193–237.

Betancur-R R, Ortí G, Pyron RA. 2015. Fossil-based comparative analyses reveal ancient marine ancestry erased by extinction in ray-finned fishes. Ecol Lett 18:441–450.

Brock GT. 1932. The skull of *Leptotyphlops* (*Glauconia nigricans*). Anat Anz 73:199–204.

Brower AVZ, Schawaroch V. 1996. Three steps of homology assessment. Cladistics 12:265–272.

Burbrink FT, Grazziotin FG, Pyron RA, Cundall D, Donnellan S, Irish F, Keogh JS, Kraus F, Murphy RW, Noonan B, Raxworthy CJ, Ruane S, Lemmon AR, Lemmon EM, Zaher H. 2020. Interrogating genomic-scale data for Squamata (lizards, snakes, and amphisbaenians) shows no support for key traditional morphological relationships. Syst Biol 69:502–520.

Caldwell MW. 2000. On the phylogenetic relationships of *Pachyrhachis* within snakes: a response to Zaher (1998). J Vert Paleontol 20:187–190.

Caldwell MW. 2007. The role, impact, and importance of fossils: snake phylogeny, origins, and evolution (1869–2006). In: Anderson J, Sues H-D, editors. Major Transitions in Vertebrate Evolution. Bloomington, Indiana: Indiana University Press. p 253–302.

Caldwell MW. 2019. The Origin of Snakes: Morphology and the Fossil Record. Boca Raton: Taylor & Francis.

Campbell JA, Smith EN, Hall AS. 2018. Caudals and calyces: the curious case of a consumed Chiapan colubroid. J Herpetol 52:459–472.

Chretien J, Wang-Claypool CY, Glaw F, Scherz MD. 2019. The bizarre skull of *Xenotyphlops* sheds light on synapomorphies of Typhlopoidea. J Anat 234:637–655.

1814 Conrad JL. 2008. Phylogeny and systematics of Squamata (Reptilia) based on morphology. Bull
1815 Am Mus Nat Hist N Y 310:1–182.
1816 Cundall D. 1995. Feeding behaviour in *Cylindrophis* and its bearing on the evolution of
1817 alethinophidian snakes. J Zool 237:353–376.
1818 Cundall D, Irish F. 2008. The snake skull. In: Gans C, Gaunt AS, Adler K, editors. Biology of
1819 the Reptilia: Morphology H, The Skull of Lepidosauria. Ithaca, New York: Society for
1820 the Study of Amphibian and Reptiles. p 349–692.
1821 Cundall D, Rossman DA. 1993. Cephalic anatomy of the rare Indonesian snake *Anomochilus*
1822 *weberi*. Zool J Linn Soc 109:235–273.
1823 Da Silva FO, Fabre A-C, Savriama Y, Ollonen J, Mahlow K, Herrel A, Müller J, Di-Poï N. 2018.
1824 The ecological origins of snakes as revealed by skull evolution. Nature Communications
1825 9:376.
1826 de Pinna MGG. 1991. Concepts and tests of homology in the cladistic paradigm. Cladistics
1827 7:367–394.
1828 Evans HE. 1955. The osteology of a worm snake, *Typhlops jamaicensis* (Shaw). Anat Rec
1829 122:381–396.
1830 Evans SE. 2008. The Skull of Lizards and Tuatara. In: Gans C, Gaunt AS, Adler K, editors.
1831 Biology of the Reptilia, Vol. 20: The Skull of Lepidosauria. Ithaca: Society for the Study
1832 of Amphibians and Reptiles. p 1–347.
1833 Figueroa A, McKelvy AD, Grismer LL, Bell CD, Lailvaux SP. 2016. A species-level phylogeny
1834 of extant snakes with description of a new colubrid subfamily and genus. PLoS ONE
1835 11:e0161070.
1836 Finarelli JA, Flynn JJ. 2006. Ancestral state reconstruction of body size in the Caniformia
1837 (Carnivora, Mammalia): the effects of incorporating data from the fossil record. Syst Biol
1838 55:301–313.
1839 Finarelli JA, Goswami A. 2013. Potential pitfalls of reconstructing deep time evolutionary
1840 history with only extant data, a case study using the Canidae (Mammalia, Carnivora).
1841 Evolution 67:3678–3685.
1842 Frazzetta TH. 1962. A functional consideration of cranial kinesis in lizards. J Morphol 111:287–
1843 319.

1844 Fröbisch NB, Schoch RR. 2009. Testing the impact of miniaturization on phylogeny: Paleozoic
1845 dissorophoid amphibians. Syst Biol 58:312–327.
1846 Gans C, Montero R. 2008. An atlas of amphisbaenian skull anatomy. In: Gans C, Gaunt AS,
1847 Adler K, editors. Biology of the Reptilia. Volume 21. Morphology I. The Skull and
1848 Appendicular Locomotor Apparatus of Lepidosauria. Ithaca, New York: Society for the
1849 Study of Amphibians and Reptiles. p 621–738.
1850 Garberoglio FF, Apesteguía S, Simões TR, Palci A, Gómez RO, Nydam RL, Larsson HCE, Lee
1851 MSY, Caldwell MW. 2019a. New skulls and skeletons of the Cretaceous legged snake
1852 *Najash*, and the evolution of the modern snake body plan. Science Advances 5:eaax5833.
1853 Garberoglio FF, Gómez RO, Apesteguía S, Caldwell MW, Sánchez ML, Veiga G. 2019b. A new
1854 specimen with skull and vertebrae of *Najash rionegrina* (Lepidosauria: Ophidia) from the
1855 early Late Cretaceous of Patagonia. Journal of Systematic Palaeontology 17:1533–1550.
1856 Gauthier JA, Kearney M, Maisano JA, Rieppel O, Behlke ADB. 2012. Assembling the squamate
1857 tree of life: Perspectives from the phenotype and the fossil record. Bull Peabody Mus Nat
1858 Hist 53:3–308.
1859 Greer AE. 1985. The relationships of the lizard genera *Anelytropsis* and *Dibamus*. J Herpetol
1860 19:116–156.
1861 Griffith OW, Blackburn DG, Brandley MC, van Dyke JU, Whittington CM, Thompson MB.
1862 2015. Ancestral state reconstructions require biological evidence to test evolutionary
1863 hypotheses: a case study examining the evolution of reproductive mode in squamate
1864 reptiles. J Exp Zool B Mol Dev Evol 324B:493–503.
1865 Haas G. 1930. Über das Kopfskelett und die Kaumuskulatur der Typhlopiden und Glauconiiden.
1866 Zoologische Jahrbücher Abteilung für Anatomie 52:1–94.
1867 Haas G. 1964. Anatomical observations on the head of *Liotyphlops albirostris* (Typhlopidae,
1868 Ophidia). Acta Zool 1964:1–62.
1869 Haas G. 1968. Anatomical observations on the head of *Anomalepis aspinosus* (Typhlopidae,
1870 Ophidia). Acta Zool 48:63–139.
1871 Hanken J. 1984. Miniaturization and its effects on cranial morphology in plethodontid
1872 salamanders, genus *Thorius* (Amphibia: Plethodontidae). I. Osteological variation. Biol J
1873 Linn Soc 23:55–75.

1874 Hanken J, Wake DB. 1993. Miniaturization of body size: organismal consequences and
1875 evolutionary significance. Annu Rev Ecol Syst 24:501–519.
1876 Harrington SM, Reeder TW. 2017. Phylogenetic inference and divergence dating of snakes using
1877 molecules, morphology and fossils: new insights into convergent evolution of feeding
1878 morphology and limb reduction. Biol J Linn Soc 121:379–394.
1879 Hawkins JA, Hughes CE, Scotland RW. 1997. Primary homology assessment, characters and
1880 character States. Cladistics 13:275–283.
1881 Hawlitschek O, Scherz MD, Webster KC, Ineich I, Glaw F. 2021. Morphological, osteological,
1882 and genetic data support a new species of *Madatyphlops* (Serpentes: Typhlopidae)
1883 endemic to Mayotte Island, Comoros Archipelago. Anat Rec 2021:1–15.
1884 Hsiang AY, Field DJ, Webster TH, Behlke ADB, Davis MB, Racicot RA, Gauthier JA. 2015.
1885 The origin of snakes: revealing the ecology, behavior, and evolutionary history of early
1886 snakes using genomics, phenomics, and the fossil record. BMC Evol Biol 15:87.
1887 Iordansky NN. 1997. Jaw apparatus and feeding mechanics of *Typhlops* (Ophidia: Typhlopidae):
1888 a reconsideration. Russ J Herpetol 4:120–127.
1889 Kamal AM. 1966. On the process of rotation of the quadrate cartilage in Ophidia. Anat Anz
1890 118:87–90.
1891 Kearney M, Stuart BL. 2004. Repeated evolution of limblessness and digging heads in worm
1892 lizards revealed by DNA from old bones. Proc R Soc Lond, Ser B: Biol Sci 271:1677–
1893 1683.
1894 Kley NJ. 2001. Prey transport mechanisms in blindsnakes and the evolution of unilateral feeding
1895 systems in snakes. Am Zool 41:1321–1337.
1896 Kley NJ. 2006. Morphology of the lower jaw and suspensorium in the Texas blindsnake,
1897 *Leptotyphlops dulcis* (Scolecophidia: Leptotyphlopidae). J Morphol 267:494–515.
1898 Kley NJ, Brainerd EL. 1999. Feeding by mandibular raking in a snake. Nature 402:369–370.
1899 Kraus F. 2017. New species of blindsnakes (Squamata: Gerrhopilidae) from the offshore islands
1900 of Papua New Guinea. Zootaxa 4299:75–94.
1901 Lee MSY. 1998. Convergent evolution and character correlation in burrowing reptiles: towards a
1902 resolution of squamate relationships. Biol J Linn Soc 65:369–453.

1903 Lee MSY, Caldwell MW. 1998. Anatomy and relationships of *Pachyrhachis problematicus*, a
1904 primitive snake with hindlimbs. Philos Trans R Soc Lond, Ser B: Biol Sci 353:1521–
1905 1552.
1906 Lewis PO. 2001. A likelihood approach to estimating phylogeny from discrete morphological
1907 character data. Syst Biol 50:913–925.
1908 List JC. 1966. Comparative osteology of the snake families Typhlopidae and Leptotyphlopidae.
1909 Illinois Biological Monographs 36:1–112.
1910 Mabee PM, Balhoff JP, Dahdul WM, Lapp H, Mungall CJ, Vision TJ. 2020. A logical model of
1911 homology for comparative biology. Syst Biol 69:345–362.
1912 Maddin HC, Olori JC, Anderson JS. 2011. A redescription of *Carrolla craddocki* (Lepospondyli:
1913 Brachystelechidae) based on high-resolution CT, and the impacts of miniaturization and
1914 fossoriality on morphology. J Morphol 272:722–743.
1915 Maddison WP, Maddison DR. 2006. StochChar: a package of Mesquite modules for stochastic
1916 models of character evolution. Version 1.1.
1917 Maddison WP, Maddison DR. 2019. Mesquite: a modular system for evolutionary analysis.
1918 Version 3.61. http://mesquiteproject.org
1919 Mahendra BC. 1936. Contributions to the osteology of the Ophidia. I. The endoskeleton of the
1920 so-called 'blind-snake', *Typhlops braminus* Daud. Proceedings of the Indian Academy of
1921 Sciences 3:128–142.
1922 Martins A, Koch C, Pinto R, Folly M, Fouquet A, Passos P. 2019. From the inside out: discovery
1923 of a new genus of threadsnakes based on anatomical and molecular data, with discussion
1924 of the leptotyphlopid hemipenial morphology. J Zool Syst Evol Res 57:840–863.
1925 McDowell SB, Bogert CM. 1954. The systematic position of *Lanthanotus* and the affinities of
1926 the anguimorphan lizards. Bull Am Mus Nat Hist N Y 105:1–142.
1927 McNamara KJ. 1986. A guide to the nomenclature of heterochrony. J Paleontol 60:4–13.
1928 Miralles A, Marin J, Markus D, Herrel A, Hedges SB, Vidal N. 2018. Molecular evidence for the
1929 paraphyly of Scolecophidia and its evolutionary implications. J Evol Biol 31:1782–1793.
1930 Mongiardino Koch N, Parry LA. 2020. Death is on our side: paleontological data drastically
1931 modify phylogenetic hypotheses. Syst Biol 0:1–16.

1932 Nagy ZT, Marion AB, Glaw F, Miralles A, Nopper J, Vences M, Hedges SB. 2015. Molecular
1933 systematics and undescribed diversity of Madagascan scolecophidian snakes (Squamata:
1934 Serpentes). Zootaxa 4040:31–47.
1935 Ollonen J, Silva FOD, Mahlow K, Di-Poï N. 2018. Skull development, ossification pattern, and
1936 adult shape in the emerging lizard model organism *Pogona vitticeps*: a comparative
1937 analysis with other squamates. Front Physiol 9:278.
1938 Olori JC, Bell CJ. 2012. Comparative skull morphology of uropeltid snakes (Alethinophidia:
1939 Uropeltidae) with special reference to disarticulated elements and variation. PLoS ONE
1940 7:e32450.
1941 Palci A, Caldwell MW, Hutchinson MN, Konishi T, Lee MSY. 2020. The morphological
1942 diversity of the quadrate bone in squamate reptiles as revealed by high-resolution
1943 computed tomography and geometric morphometrics. J Anat 236:210–227.
1944 Palci A, Lee MSY, Hutchinson MN. 2016. Patterns of postnatal ontogeny of the skull and lower
1945 jaw of snakes as revealed by micro-CT scan data and three-dimensional geometric
1946 morphometrics. J Anat 229:723–754.
1947 Patterson C. 1982. Morphological characters and homology. In: Joysey KA, Friday AE, editors.
1948 Problems of Phylogenetic Reconstruction. London and New York: Academic Press. p
1949 21–74.
1950 Patterson C. 1988. Homology in classical and molecular biology. Mol Biol Evol 5:603–625.
1951 Pinto RR, Martins AR, Curcio F, Ramos LO. 2015. Osteology and cartilaginous elements of
1952 *Trilepida salgueiroi* (Amaral, 1954) (Scolecophidia: Leptotyphlopidae). Anat Rec
1953 298:1722–1747.
1954 Polachowski KM, Werneburg I. 2013. Late embryos and bony skull development in
1955 *Bothropoides jararaca* (Serpentes, Viperidae). Zoology 116:36–63.
1956 Puttick MN. 2016. Partially incorrect fossil data augment analyses of discrete trait evolution in
1957 living species. Biol Lett 12:20160392.
1958 Pyron RA, Burbrink FT, Wiens JJ. 2013. A phylogeny and revised classification of Squamata,
1959 including 4161 species of lizards and snakes. BMC Evol Biol 13:93.
1960 Reeder TW, Townsend TM, Mulcahy DG, Noonan BP, Wood PL, Sites JW, Wiens JJ. 2015.
1961 Integrated analyses resolve conflicts over squamate reptile phylogeny and reveal
1962 unexpected placements for fossil taxa. PLoS ONE 10:e0118199.

1963 Rieppel O. 1977. Studies on the skull of the Henophidia (Reptilia: Serpentes). J Zool 181:145–
1964 173.
1965 Rieppel O. 1984. The cranial morphology of the fossorial lizard genus *Dibamus* with a
1966 consideration of its phylogenetic relationships. J Zool 204:289–327.
1967 Rieppel O. 1988. A review of the origin of snakes. In: Hecht MK, Wallace B, Prance GT,
1968 editors. Evolutionary Biology. Boston, MA: Springer. p 37–130.
1969 Rieppel O. 1994. Homology, topology, and typology: the history of modern debates. In: Hall
1970 BK, editor. Homology: The Hierarchical Basis of Comparative Biology. San Diego:
1971 Academic Press. p 63–100.
1972 Rieppel O. 2012. "Regressed" macrostomatan snakes. Fieldiana Life and Earth Sciences
1973 2012:99–103.
1974 Rieppel O, Kearney M. 2002. Similarity. Biol J Linn Soc 75:59–82.
1975 Rieppel O, Kley NJ, Maisano JA. 2009. Morphology of the skull of the white-nosed blindsnake,
1976 *Liotyphlops albirostris* (Scolecophidia: Anomalepididae). J Morphol 270:536–557.
1977 Rieppel O, Maisano JA. 2007. The skull of the rare Malaysian snake *Anomochilus leonardi*
1978 Smith, based on high-resolution X-ray computed tomography. Zool J Linn Soc 149:671–
1979 685.
1980 Rieppel O, Zaher H. 2000. The intramandibular joint in squamates, and the phylogenetic
1981 relationships of the fossil snake *Pachyrhachis problematicus* Haas. Fieldiana Geology
1982 43:1–69.
1983 Santos FJM, Reis RE. 2019. Redescription of the blind snake *Anomalepis colombia* (Serpentes:
1984 Anomalepididae) using high-resolution X-ray computed tomography. Copeia 107:239–
1985 243.
1986 Scanferla A. 2016. Postnatal ontogeny and the evolution of macrostomy in snakes. R Soc Open
1987 Sci 3:160612.
1988 Sereno PC. 2007. Logical basis for morphological characters in phylogenetics. Cladistics
1989 23:565–587.
1990 Simões TR, Caldwell MW, Palci A, Nydam RL. 2017. Giant taxon-character matrices: Quality
1991 of character constructions remains critical regardless of size. Cladistics 33:198–219.

1992 Simões TR, Caldwell MW, Tałanda M, Bernardi M, Palci A, Vernygora O, Bernardini F,
1993 Mancini L, Nydam RL. 2018. The origin of squamates revealed by a Middle Triassic
1994 lizard from the Italian Alps. Nature 557:706–709.
1995 Strong CRC, Palci A, Caldwell MW. 2021. Insights into skull evolution in fossorial snakes, as
1996 revealed by the cranial morphology of *Atractaspis irregularis* (Serpentes: Colubroidea). J
1997 Anat 238:146–172.
1998 Strong CRC, Simões TR, Caldwell MW, Doschak MR. 2019. Cranial ontogeny of *Thamnophis*
1999 *radix* (Serpentes: Colubroidea) with a re-evaluation of current paradigms of snake skull
2000 evolution. R Soc Open Sci 6:182228.
2001 Struck TH. 2007. Data congruence, paedomorphosis and salamanders. Front Zool 4:22.
2002 Wake MH. 1986. The morphology of *ldiocranium russeli* (Amphibia: Gymnophiona), with
2003 comments on miniaturization through heterochrony. J Morphol 189:1–16.
2004 Werneburg I, Polachowski KM, Hutchinson MN. 2015. Bony skull development in the Argus
2005 monitor (Squamata, Varanidae, *Varanus panoptes*) with comments on developmental
2006 timing and adult anatomy. Zoology 118:255–280.
2007 Wiens JJ, Bonett RM, Chippindale PT. 2005. Ontogeny discombobulates phylogeny:
2008 Paedomorphosis and higher-level salamander relationships. Syst Biol 54:91–110.
2009 Wiens JJ, Kuczynski CA, Townsend TM, Reeder TW, Mulcahy DG, Sites JWJ. 2010.
2010 Combining phylogenomics and fossils in higher-level squamate reptile phylogeny:
2011 molecular data change the placement of fossil taxa. Syst Biol 59:674–688.
2012 Wilkinson M. 1995. A comparison of two methods of character construction. Cladistics 11:297–
2013 308.
2014 Zaher H. 1998. The phylogenetic position of *Pachyrhachis* within snakes (Squamata,
2015 Lepidosauria). J Vert Paleontol 18:1–3.
2016 Zaher H, Rieppel O. 1999. The phylogenetic relationships of *Pachyrhachis problematicus*, and
2017 the evolution of limblessness in snakes (Lepidosauria, Squamata). C R Acad Sci - Ser IIA
2018 - Sci Terre plan/Earth Plan Sci 329:831–837.
2019 Zaher H, Rieppel O. 2002. On the phylogenetic relationships of the Cretaceous snakes with legs,
2020 with special reference to *Pachyrhachis problematicus* (Squamata, Serpentes). J Vert
2021 Paleontol 22:104–109.

Zheng Y, Wiens JJ. 2016. Combining phylogenomic and supermatrix approaches, and a time-calibrated phylogeny for squamate reptiles (lizards and snakes) based on 52 genes and 4162 species. Mol Phylogen Evol 94:537–547.

Figure Legends

Figure 1. Overview of jaw evolution in squamates. Coloured branches reflect the proposed jaw morphotype for each major squamate clade (see legend, Figures 12–14, and main text). Relevant skull elements are highlighted in an exemplar specimen from each group (colouration as in Figures 3–11). See Table 2 for specimen numbers. MCZ scan data used by permission of the Museum of Comparative Zoology, Harvard University.

Figure 2. Phylogenetic context of taxa examined herein. Relationships are provided at the species level for scolecophidians and at the family level for other taxa. Relevant higher taxa are indicated in colour, with broader groups labelled in black. Branch lengths represent divergence time, with the scale bar measuring 30 million years. See Materials and Methods for phylogeny construction, including relevant literature sources.

Figure 3. Skull of *Varanus exanthematicus* (FMNH 58299), exemplifying "minimal-kinesis microstomy". Key elements related to feeding are highlighted. In this morphotype, these elements are robust and solidly braced (see text for details). (a–c) Skull, with mandibles digitally removed, in (a) dorsal, (b) ventral, and (c) lateral view. (d) Palatomaxillary arch in dorsal view. (e–f) Mandible in (e) lateral and (f) medial view. Abbreviations: am.pr, anteromedial process; bpt.pr, basipterygoid process; co.pr, coronoid process; ecp.pr, ectopterygoid process; f, frontal; f.pr, facial process; j, jugal; l, lacrimal; mx.pr, maxillary process; n, nasal; p, parietal; pal.pr, palatine process; pbs, parabasisphenoid; pd.pr, posterodorsal process; pof, postorbitofrontal; pop.pr, postparietal process; pp, palpebral; p.pr, posterior process; pt.pr, pterygoid process; pvm.pr, posteroventromedial process; pv.pr, posteroventral process; r.pr, retroarticular process; v, vomer; v.pr, vomerine process.

Figure 4. Skull of *Physignathus cocincinus* (YPM 14378), exemplifying "minimal-kinesis microstomy". Key elements related to feeding are highlighted. In this morphotype, these elements are robust and solidly braced (see text for details). (a–c) Skull, with mandibles digitally removed, in (a) dorsal, (b) ventral, and (c) lateral view. (d) Palatomaxillary arch in dorsal view. (e–f) Mandible in (e) lateral and (f) medial view. Abbreviations: am.pr, anteromedial process; bpt.pr, basipterygoid process; co.pr, coronoid process; ecp.pr, ectopterygoid process; f, frontal; f.pr, facial process; j, jugal; l, lacrimal; mx.pr, maxillary process; n, nasal; p, parietal; pal.pr, palatine process; pbs, parabasisphenoid; pdm.pr, posterodorsomedial process; pd.pr, posterodorsal process; po, postorbital; pop.pr, postparietal process; p.pr, posterior process; pt.pr,

pterygoid process; pvm.pr, posteroventromedial process; r.pr, retroarticular process; v, vomer; v.pr, vomerine process.

Figure 5. Skull of *Dibamus novaeguineae* (UF 33488), exemplifying "minimal-kinesis microstomy" in a miniaturized and fossorial non-snake lizard. Key elements related to feeding are highlighted. In this morphotype, these elements are robust and solidly braced (see text for details). (a–c) Skull, with mandibles digitally removed, in (a) dorsal, (b) ventral, and (c) lateral view. (d) Palatomaxillary arch in dorsal view. (e–f) Mandible in (e) lateral and (f) medial view. Abbreviations: b-e, basioccipital-exoccipital; bpt.pr, basipterygoid process; ch.pr, choanal process; co.pr, coronoid process; ecp.pr, ectopterygoid process; f, frontal; f.pr, facial process; mx.pr, maxillary process; n, nasal; op, opisthotic; p, parietal; pal.pr, palatine process; part.pr, prearticular process; pbs, parabasisphenoid; pdm.pr, posterodorsomedial process; pd.pr, posterodorsal process; p.pr, posterior process; pro, prootic; pt.pr, pterygoid process; pv.pr, posteroventral process; r.pr, retroarticular process; v, vomer; v.pr, vomerine process.

Figure 6. Skull of *Amphisbaena fuliginosa* (FMNH 22847), exemplifying "minimal-kinesis microstomy" in a fossorial non-snake lizard. Key elements related to feeding are highlighted. In this morphotype, these elements are robust and solidly braced (see text for details). (a–c) Skull, with mandibles digitally removed, in (a) dorsal, (b) ventral, and (c) lateral view. (d) Palatomaxillary arch in dorsal view. (e–f) Mandible in (e) lateral and (f) medial view. Abbreviations: am.pr, anteromedial process; bpt.pr, basipterygoid process; co.pr, coronoid process; ecp.pr, ectopterygoid process; f, frontal; f.pr, facial process; mx.pr, maxillary process; n, nasal; oc, occipital complex; p, parietal; pal.pr, palatine process; pdm.pr, posterodorsomedial process; pd.pr, posterodorsal process; p.pr, posterior process; pt.pr, pterygoid process; pvm.pr, posteroventromedial process; pv.pr, posteroventral process; v, vomer; v.pr, vomerine process.

Figure 7. Skull of *Cylindrophis ruffus* (UMMZ 201901), exemplifying "snout-shifting" (*sensu* Cundall, 1995) in a uropeltoid alethinophidian. Key elements related to feeding are highlighted. In this morphotype, these elements are generally robust and well-braced; however, the maxilla-palatine joint exhibits a distinct "ball-and-socket"-like form and the vomers and septomaxillae are more loosely connected to the dorsal snout elements and to their contralaterals, thus enabling a slight degree of unilateral movement of the left and right palatomaxillary arches (see text for details). (a–c) Skull, with mandibles digitally removed, in (a) dorsal, (b) ventral, and (c) lateral view. (d) Palatomaxillary arch in dorsal view. (e–f) Mandible in (e) lateral and (f) medial view.

Abbreviations: am.pr, anteromedial process; bpt.pr, basipterygoid process; ch.pr, choanal process; co.pr, coronoid process; ecp.pr, ectopterygoid process; f, frontal; f.pr, facial process; n, nasal; p, parietal; pal.pr, palatine process; pbs, parabasisphenoid; pd.pr, posterodorsal process; p.pr, posterior process; pro, prootic; pt.pr, pterygoid process; pv.pr, posteroventral process; r.pr, retroarticular process; smx, septomaxilla; ss.pr, suprastapedial process; v, vomer.

Figure 8. Skull of *Anilius scytale* (KUH 125976), exemplifying "snout-shifting" (*sensu* Cundall, 1995) in an amerophidian alethinophidian. Key elements related to feeding are highlighted. This taxon largely resembles *Cylindrophis*, though the mandibular structure differs somewhat (see Figure 7 and text for details). (a–c) Skull, with mandibles digitally removed, in (a) dorsal, (b) ventral, and (c) lateral view. (d) Palatomaxillary arch in dorsal view. (e–f) Mandible in (e) lateral and (f) medial view. Abbreviations: bpt.pr, basipterygoid process; ch.pr, choanal process; ecp.pr, ectopterygoid process; f, frontal; f.pr, facial process; mx.pr, maxillary process; n, nasal; p, parietal; pal.pr, palatine process; pbs, parabasisphenoid; pd.pr, posterodorsal process; p.pr, posterior process; pro, prootic; pv.pr, posteroventral process; r.pr, retroarticular process; smx, septomaxilla; ss.pr, suprastapedial process; v, vomer.

Figure 9. Skull of *Afrotyphlops angolensis* (MCZ R-170385), exemplifying "single-axle maxillary raking". Key elements related to feeding are highlighted. In this morphotype of microstomy, the mandible is reduced and largely akinetic, with feeding being driven by rotation of the maxilla about the elongate maxillary process of the palatine (see text for details). (a–c) Skull, with mandibles digitally removed, in (a) dorsal, (b) ventral, and (c) lateral view. (d) Palatomaxillary arch in dorsal view. (e–f) Mandible in (e) lateral and (f) medial view. Abbreviations: am.pr, anteromedial process; a.pr, anterior process; ch.pr, choanal process; co.pr, coronoid process; f, frontal; f.pr, facial process; mx.pr, maxillary process; n, nasal; p, parietal; pal.pr, palatine process; pbs, parabasisphenoid; pd.pr, posterodorsal process; p.pr, posterior process; pro, prootic; pt.pr, pterygoid process; pvm.pr, posteroventromedial process; r.pr, retroarticular process; smx, septomaxilla; v, vomer. MCZ scan data used by permission of the Museum of Comparative Zoology, Harvard University.

Figure 10. Skull of *Liotyphlops argaleus* (MCZ R-67933), exemplifying "axle-brace maxillary raking". Key elements related to feeding are highlighted. In this morphotype of microstomy, the maxilla is suspended from the mobile and highly reduced prefrontal and is braced posteriorly by the ectopterygoid. As in typhlopoids, the mandible is reduced and does not contribute to feeding

(see text for details). (a–c) Skull, with mandibles digitally removed, in (a) dorsal, (b) ventral, and (c) lateral view. (d) Palatomaxillary arch in dorsal view. (e–f) Mandible in (e) lateral and (f) medial view. Abbreviations: a.pr, anterior process; ch.pr, choanal process; co.pr, coronoid process; f, frontal; f.pr, facial process; mx.pr, maxillary process; n, nasal; p, parietal; pal.pr, palatine process; part.l, prearticular lamina; pbs, parabasisphenoid; p.pr, posterior process; pro-ot, prootic-otoccipital; pt.pr, pterygoid process; pv.pr, posteroventral process; r.pr, retroarticular process; smx, septomaxilla; sur.l, surangular lamina; v, vomer. MCZ scan data used by permission of the Museum of Comparative Zoology, Harvard University.

Figure 11. Skull of *Epictia albifrons* (MCZ R-2885), exemplifying "mandibular raking" (*sensu* Kley and Brainerd, 1999). Key elements related to feeding are highlighted. In this morphotype of microstomy, feeding is driven by rapid retraction of the mandibles, enabled by a flexible intramandibular joint, whereas the palatomaxillary arches are edentulous and do not contribute to feeding (see text for details). (a–c) Skull, with mandibles digitally removed, in (a) dorsal, (b) ventral, and (c) lateral view. (d) Palatomaxillary arch in dorsal view. (e–f) Mandible in (e) lateral and (f) medial view. Abbreviations: ch.pr, choanal process; co.pr, coronoid process; dc, dental concha; f, frontal; f.pr, facial process; mx.pr, maxillary process; n, nasal; ot, otoccipital; p, parietal; pal.pr, palatine process; part.l, prearticular lamina; pbs, parabasisphenoid; pd.pr, posterodorsal process; p.pr, posterior process; pro, prootic; pt.pr, pterygoid process; r.pr, retroarticular process; sc.pr, supracotylar process; smx, septomaxilla; sur.l, surangular lamina; sur.pr, surangular process; sym.pr, symphyseal process; v, vomer. MCZ scan data used by permission of the Museum of Comparative Zoology, Harvard University.

Figure 12. Ancestral state reconstruction (ASR) of feeding mechanisms in squamates, using a "basic" character scoring scheme with two states: microstomy and macrostomy. (a) Maximum parsimony (MP)-based ASR; (b) maximum likelihood (ML)-based ASR. Key nodes are numbered: 1, origin of snakes; 2, origin of Alethinophidia; 3, origin of "Macrostomata". See text for details regarding results, including the impact of different character scoring approaches.

Figure 13. Ancestral state reconstruction (ASR) of feeding mechanisms in squamates, using a "detailed microstomy" character scoring scheme dividing microstomy into the five morphotypes described herein: "axle-brace maxillary raking", "mandibular raking", "minimal-kinesis microstomy", "single-axle maxillary raking", and "snout-shifting". Macrostomy is scored under a single state. (a) Maximum parsimony (MP)-based ASR; (b) maximum likelihood (ML)-based

ASR. Key nodes are numbered: 1, origin of snakes; 2, origin of Alethinophidia; 3, origin of “Macrostomata”. See text for details regarding results, including anatomical descriptions and the impact of different character scoring approaches.

Figure 14. Ancestral state reconstruction (ASR) of feeding mechanisms in squamates, using a “detailed microstomy and macrostomy” character scoring scheme. This scheme divides microstomy into the five morphotypes described herein (“axle-brace maxillary raking”, “mandibular raking”, “minimal-kinesis microstomy”, “single-axle maxillary raking”, and “snout-shifting”) and divides macrostomy into separate morphotypes (“booid-type” and “caenophidian-type” macrostomy) as proposed in recent literature (e.g., Palci et al., 2016; Strong et al., 2019; Burbrink et al., 2020). (a) Maximum parsimony (MP)-based ASR; (b) maximum likelihood (ML)-based ASR. Key nodes are numbered: 1, origin of snakes; 2, origin of Alethinophidia; 3, origin of “Macrostomata”. See text for details regarding results, including anatomical descriptions and the impact of different character scoring approaches.

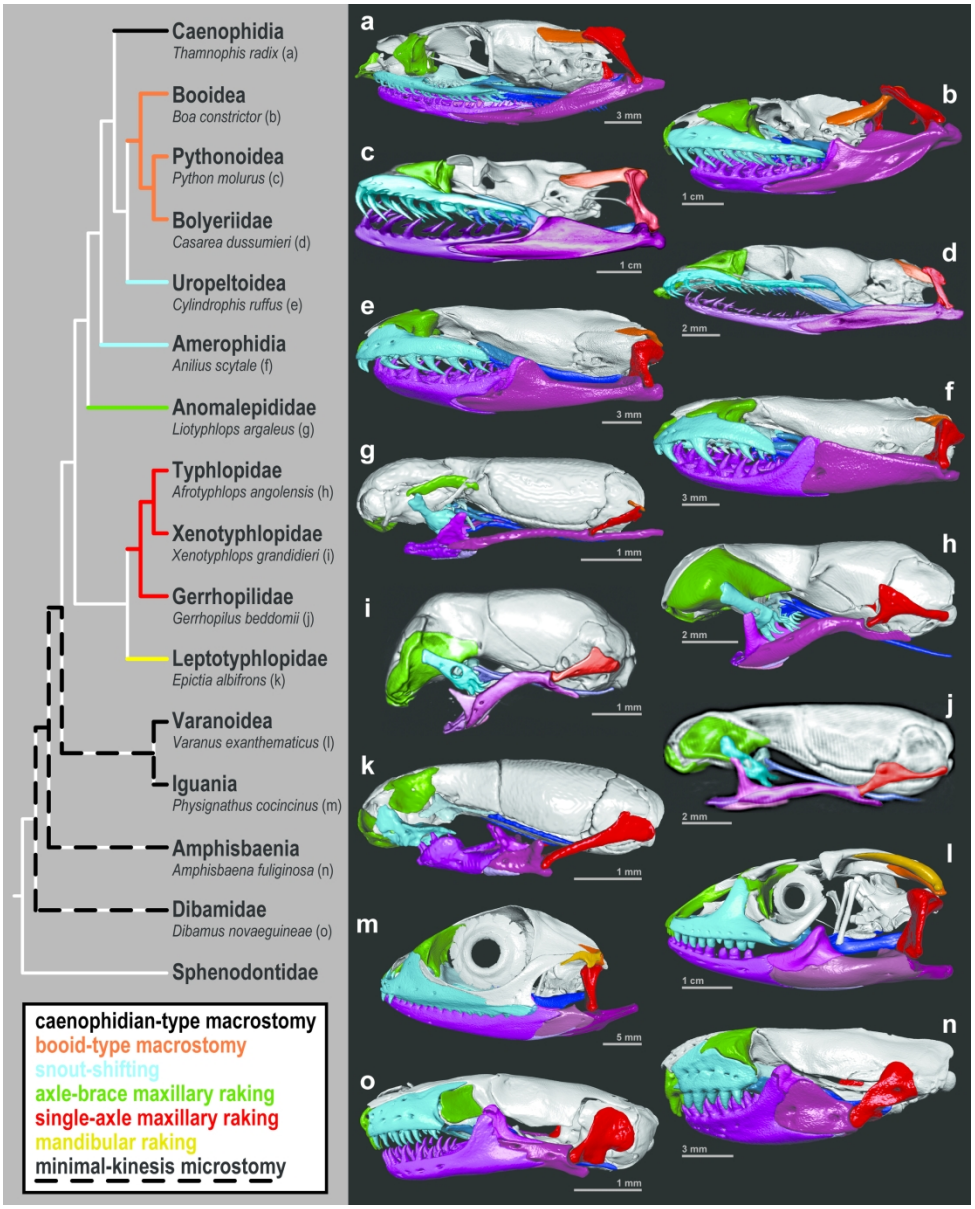

Figure 1. Overview of hypothesized jaw evolution in squamates. Coloured branches reflect the proposed jaw morphotype for each major squamate clade (see legend, Figures 12–14, and main text). Relevant skull elements are highlighted in an exemplar specimen from each group (colouration as in Figures 3–11). See Table 2 for specimen numbers. MCZ scan data used by permission of the Museum of Comparative Zoology, Harvard University.

209x259mm (300 x 300 DPI)

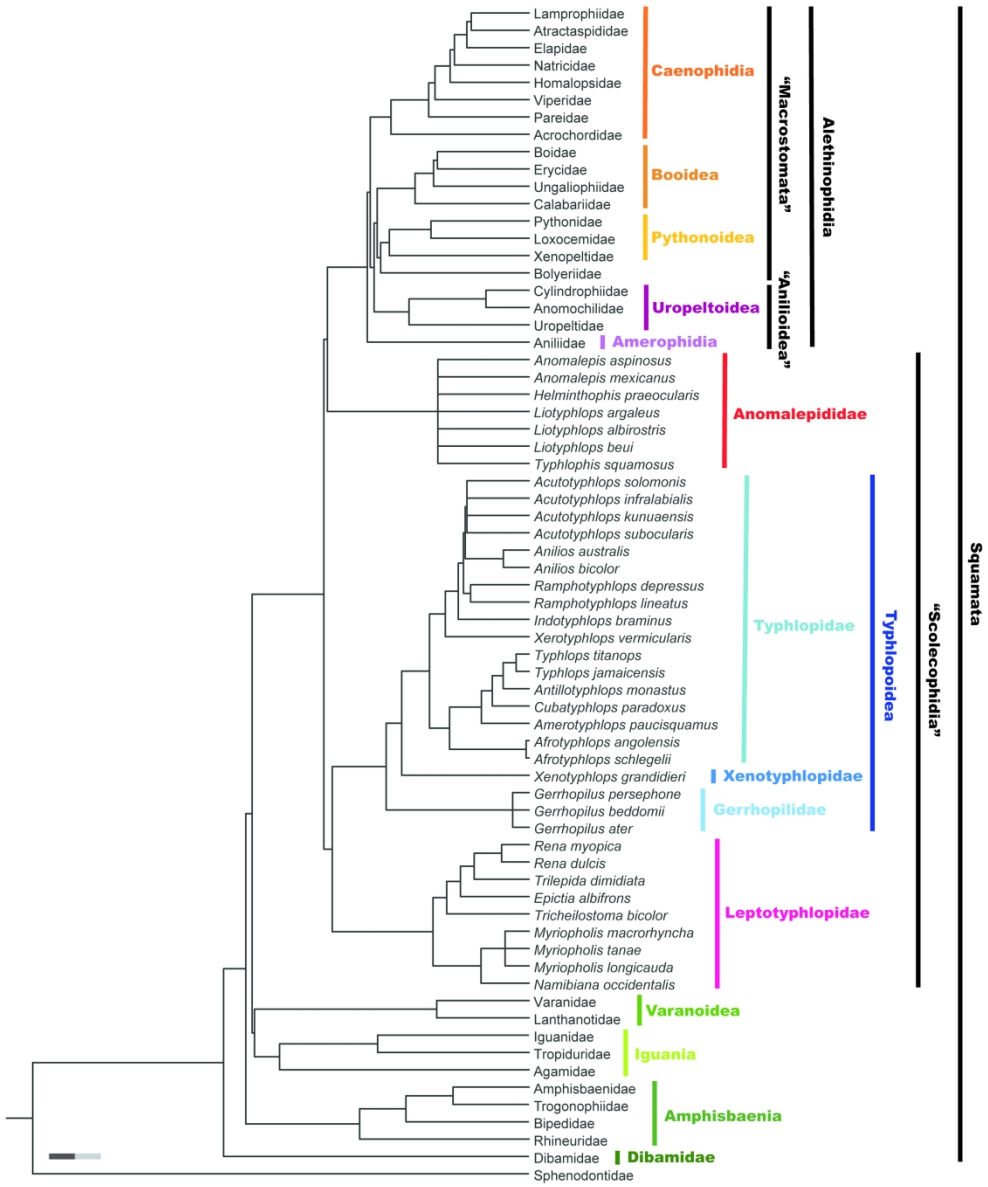

Figure 2. Phylogenetic context of taxa examined herein. Relationships are provided at the species level for scolecophidians and at the family level for other taxa. Relevant higher taxa are indicated in colour, with broader groups labelled in black. Branch lengths represent divergence time, with the scale bar measuring 30 million years. See Materials and Methods for phylogeny construction, including relevant literature sources.

231x277mm (300 x 300 DPI)

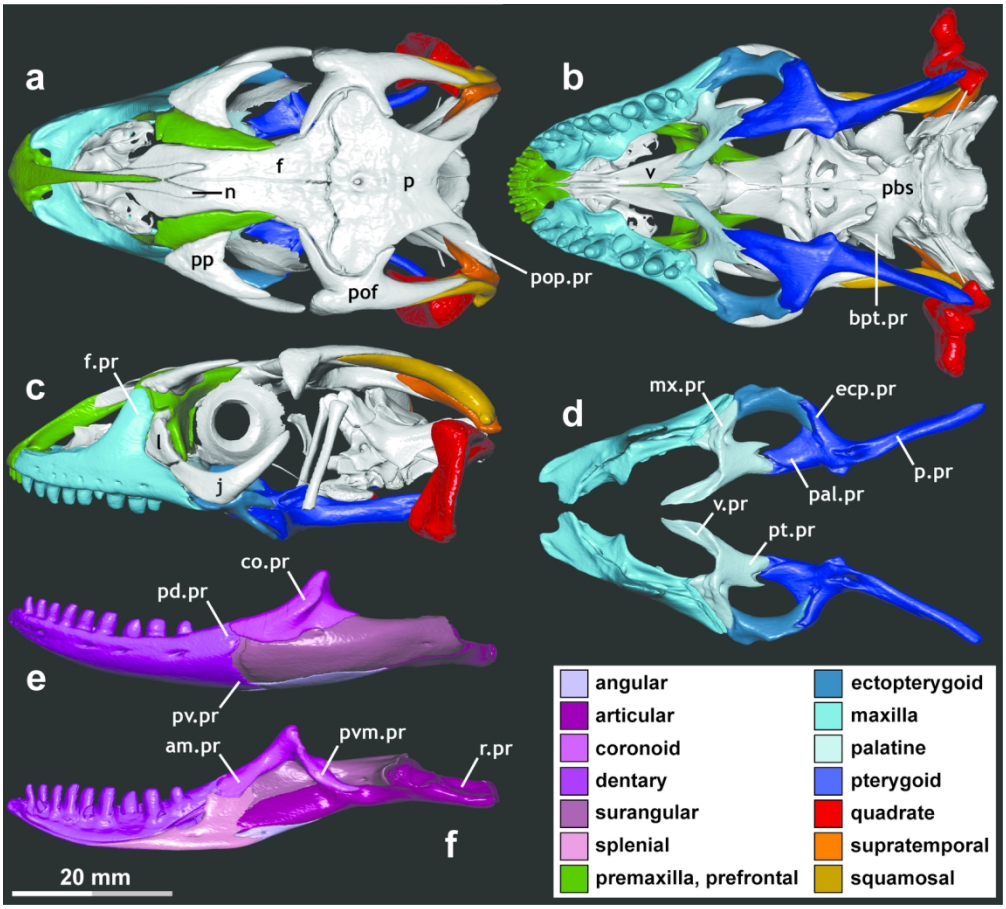

Figure 3. Skull of *Varanus exanthematicus* (FMNH 58299), exemplifying "minimal-kinesis microstomy". Key elements related to feeding are highlighted. In this morphotype, these elements are robust and solidly braced (see text for details). (**a**–**c**) Skull, with mandibles digitally removed, in (**a**) dorsal, (**b**) ventral, and (**c**) lateral view. (**d**) Palatomaxillary arch in dorsal view. (**e**–**f**) Mandible in (**e**) lateral and (**f**) medial view. Abbreviations: am.pr, anteromedial process; bpt.pr, basipterygoid process; co.pr, coronoid process; ecp.pr, ectopterygoid process; f, frontal; f.pr, facial process; j, jugal; l, lacrimal; mx.pr, maxillary process; n, nasal; p, parietal; pal.pr, palatine process; pbs, parabasisphenoid; pd.pr, posterodorsal process; pof, postorbitofrontal; pop.pr, postparietal process; pp, palpebral; p.pr, posterior process; pt.pr, pterygoid process; pvm.pr, posteroventromedial process; pv.pr, posteroventral process; r.pr, retroarticular process; v, vomer; v.pr, vomerine process.

141x127mm (300 x 300 DPI)

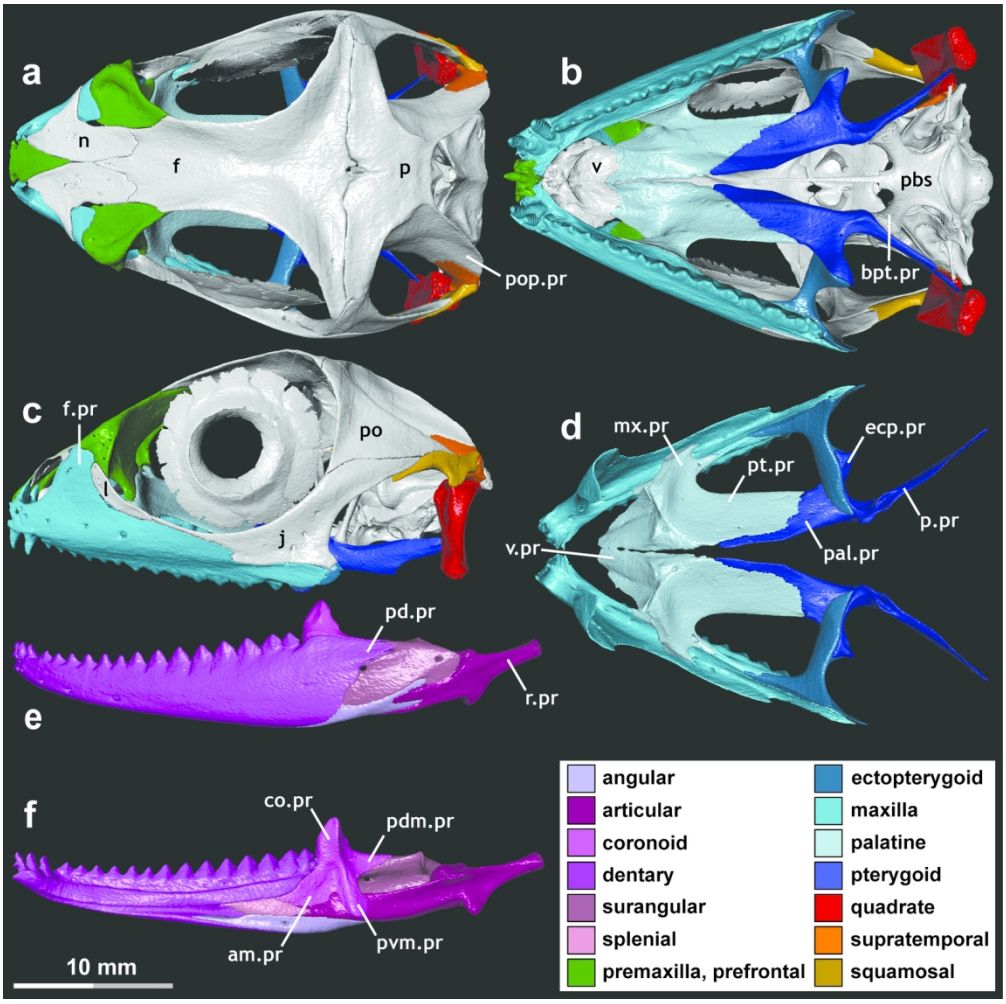

Figure 4. Skull of *Physignathus cocincinus* (YPM 14378), exemplifying "minimal-kinesis microstomy". Key elements related to feeding are highlighted. In this morphotype, these elements are robust and solidly braced (see text for details). (**a**–**c**) Skull, with mandibles digitally removed, in (**a**) dorsal, (**b** ventral, and (**c**) lateral view. (**d**) Palatomaxillary arch in dorsal view. (**e**–**f**) Mandible in (**e**) lateral and (**f**) medial view. Abbreviations: am.pr, anteromedial process; bpt.pr, basipterygoid process; co.pr, coronoid process; ecp.pr, ectopterygoid process; f, frontal; f.pr, facial process; j, jugal; l, lacrimal; mx.pr, maxillary process; n, nasal; p, parietal; pal.pr, palatine process; pbs, parabasisphenoid; pdm.pr, posterodorsomedial process; pd.pr, posterodorsal process; po, postorbital; pop.pr, postparietal process; p.pr, posterior process; pt.pr, pterygoid process; pvm.pr, posteroventromedial process; r.pr, retroarticular process; v, vomer; v.pr, vomerine process.

141x140mm (300 x 300 DPI)

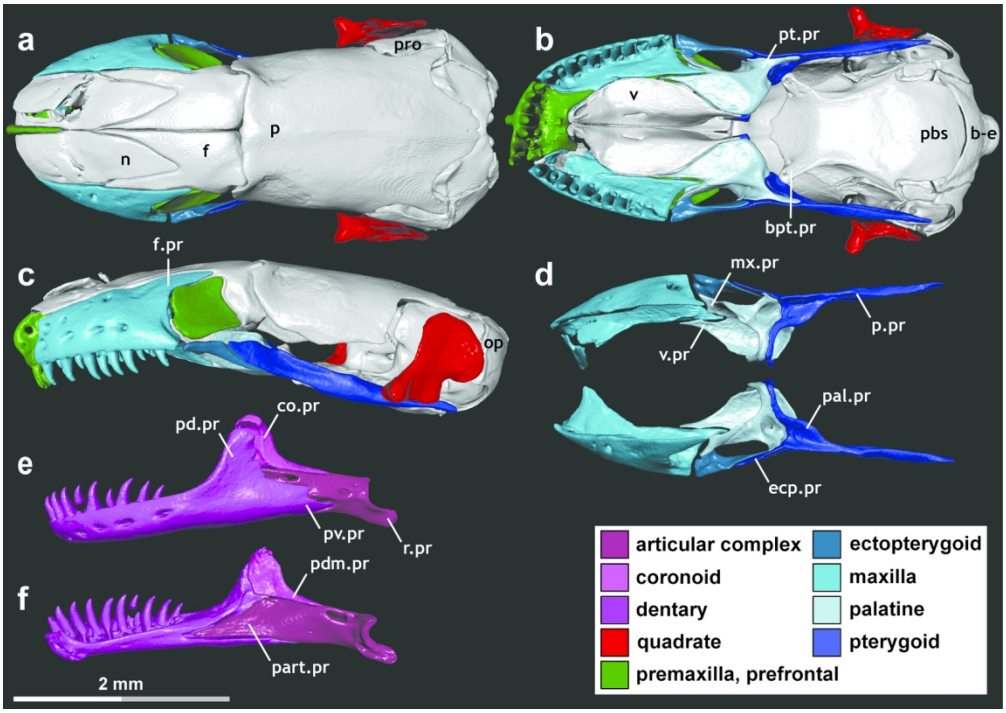

Figure 5. Skull of *Dibamus novaeguineae* (UF 33488), exemplifying "minimal-kinesis microstomy" in a miniaturized and fossorial non-snake lizard. Key elements related to feeding are highlighted. In this morphotype, these elements are robust and solidly braced (see text for details). (**a**–**c**) Skull, with mandibles digitally removed, in (**a**) dorsal, (**b**) ventral, and (**c**) lateral view. (**d**) Palatomaxillary arch in dorsal view. (**e**–**f**) Mandible in (**e**) lateral and (**f**) medial view. Abbreviations: b-e, basioccipital-exoccipital; bpt.pr, basipterygoid process; ch.pr, choanal process; co.pr, coronoid process; ecp.pr, ectopterygoid process; f, frontal; f.pr, facial process; mx.pr, maxillary process; n, nasal; op, opisthotic; p, parietal; pal.pr, palatine process; part.pr, prearticular process; pbs, parabasisphenoid; pdm.pr, posterodorsomedial process; pd.pr, posterodorsal process; p.pr, posterior process; pro, prootic; pt.pr, pterygoid process; pv.pr, posteroventral process; r.pr, retroarticular process; v, vomer; v.pr, vomerine process.

141x99mm (300 x 300 DPI)

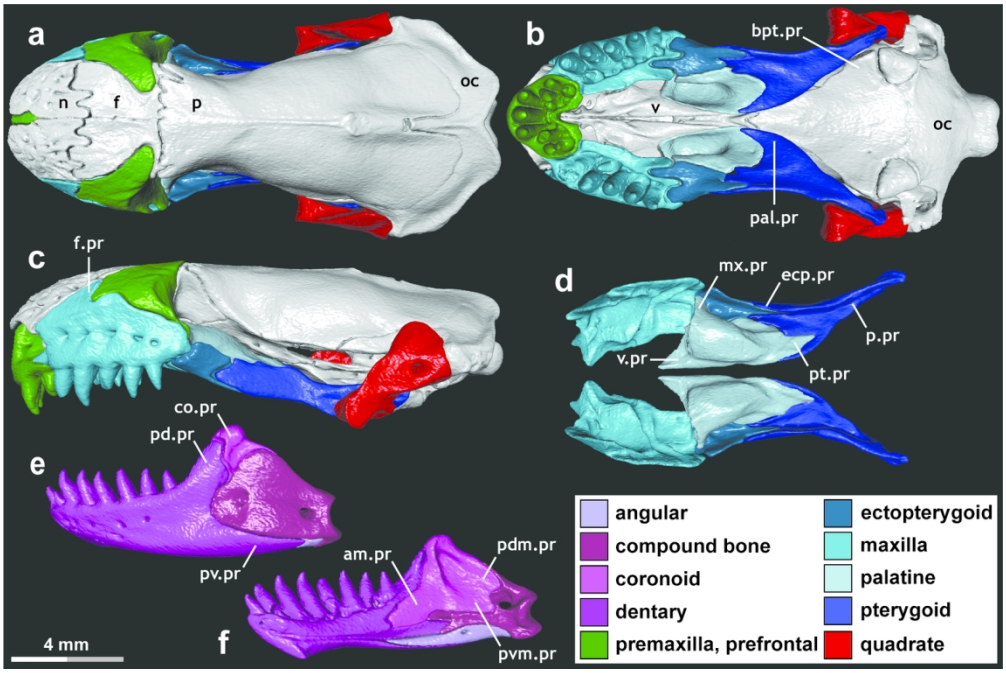

Figure 6. Skull of *Amphisbaena fuliginosa* (FMNH 22847), exemplifying "minimal-kinesis microstomy" in a fossorial non-snake lizard. Key elements related to feeding are highlighted. In this morphotype, these elements are robust and solidly braced (see text for details). (**a**–**c**) Skull, with mandibles digitally removed, in (**a**) dorsal, (**b**) ventral, and (**c**) lateral view. (**d**) Palatomaxillary arch in dorsal view. (**e**–**f**) Mandible in (**e**) lateral and (**f**) medial view. Abbreviations: am.pr, anteromedial process; bpt.pr, basipterygoid process; co.pr, coronoid process; ecp.pr, ectopterygoid process; f, frontal; f.pr, facial process; mx.pr, maxillary process; n, nasal; oc, occipital complex; p, parietal; pal.pr, palatine process; pdm.pr, posterodorsomedial process; pd.pr, posterodorsal process; p.pr, posterior process; pt.pr, pterygoid process; pvm.pr, posteroventromedial process; pv.pr, posteroventral process; v, vomer; v.pr, vomerine process.

141x93mm (300 x 300 DPI)

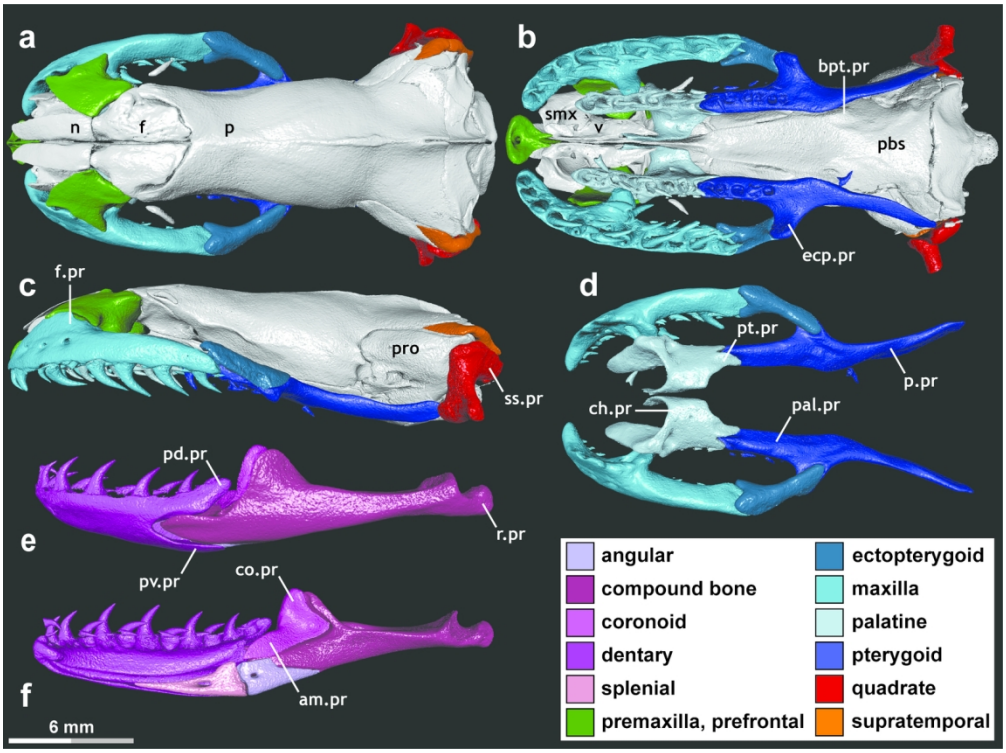

Figure 7. Skull of *Cylindrophis ruffus* (UMMZ 201901), exemplifying "snout-shifting" (*sensu* Cundall, 1995) in a uropeltoid alethinophidian. Key elements related to feeding are highlighted. In this morphotype, these elements are generally robust and well-braced; however, the maxilla-palatine joint exhibits a distinct "ball-and-socket"-like form and the vomers and septomaxillae are more loosely connected to the dorsal snout elements and to their contralaterals, thus enabling a slight degree of unilateral movement of the left and right palatomaxillary arches (see text for details). (**a**–**c**) Skull, with mandibles digitally removed, in (**a**) dorsal, (**b**) ventral, and (**c**) lateral view. (**d**) Palatomaxillary arch in dorsal view. (**e**–**f**) Mandible in (**e**) lateral and (**f**) medial view. Abbreviations: am.pr, anteromedial process; bpt.pr, basipterygoid process; ch.pr, choanal process; co.pr, coronoid process; ecp.pr, ectopterygoid process; f, frontal; f.pr, facial process; n, nasal; p, parietal; pal.pr, palatine process; pbs, parabasisphenoid; pd.pr, posterodorsal process; p.pr, posterior process; pro, prootic; pt.pr, pterygoid process; pv.pr, posteroventral process; r.pr, retroarticular process; smx, septomaxilla; ss.pr, suprastapedial process; v, vomer.

141x105mm (300 x 300 DPI)

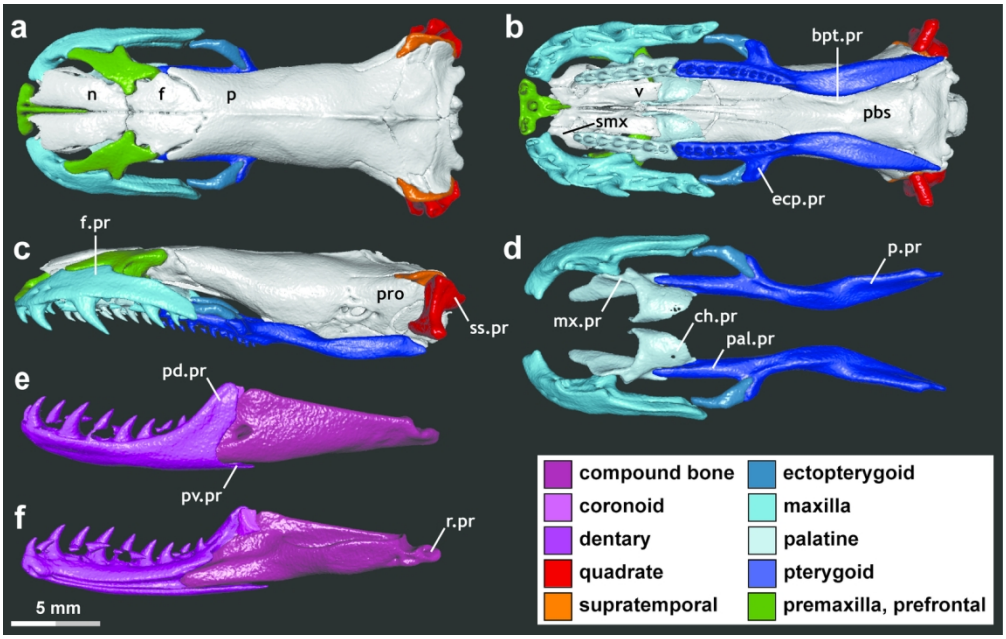

Figure 8. Skull of *Anilius scytale* (KUH 125976), exemplifying "snout-shifting" (*sensu* Cundall, 1995) in an amerophidian alethinophidian. Key elements related to feeding are highlighted. This taxon largely resembles *Cylindrophis*, though the mandibular structure differs somewhat (see Figure 7 and text for details). (**a**–**c**) Skull, with mandibles digitally removed, in (**a**) dorsal, (**b**) ventral, and (**c**) lateral view. (**d**) Palatomaxillary arch in dorsal view. (**e**–**f**) Mandible in (**e**) lateral and (**f**) medial view. Abbreviations: bpt.pr, basipterygoid process; ch.pr, choanal process; ecp.pr, ectopterygoid process; f, frontal; f.pr, facial process; mx.pr, maxillary process; n, nasal; p, parietal; pal.pr, palatine process; pbs, parabasisphenoid; pd.pr, posterodorsal process; p.pr, posterior process; pro, prootic; pv.pr, posteroventral process; r.pr, retroarticular process; smx, septomaxilla; ss.pr, suprastapedial process; v, vomer.

141x88mm (300 x 300 DPI)

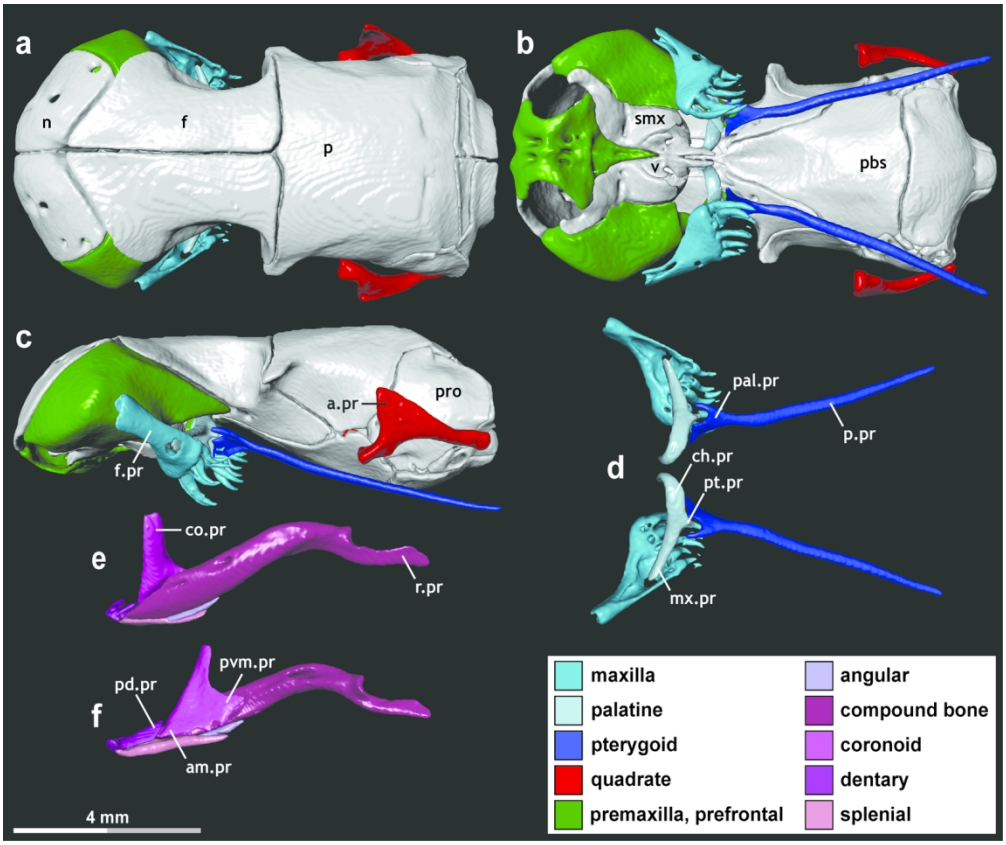

Figure 9. Skull of *Afrotyphlops angolensis* (MCZ R-170385), exemplifying "single-axle maxillary raking". Key elements related to feeding are highlighted. In this morphotype of microstomy, the mandible is reduced and largely akinetic, with feeding being driven by rotation of the maxilla about the elongate maxillary process of the palatine (see text for details). (**a**–**c**) Skull, with mandibles digitally removed, in (**a**) dorsal, (**b**) ventral, and (**c**) lateral view. (**d**) Palatomaxillary arch in dorsal view. (**e**–**f**) Mandible in (**e**) lateral and (**f**) medial view. Abbreviations: am.pr, anteromedial process; a.pr, anterior process; ch.pr, choanal process; co.pr, coronoid process; f, frontal; f.pr, facial process; mx.pr, maxillary process; n, nasal; p, parietal; pal.pr, palatine process; pbs, parabasisphenoid; pd.pr, posterodorsal process; p.pr, posterior process; pro, prootic; pt.pr, pterygoid process; pvm.pr, posteroventromedial process; r.pr, retroarticular process; smx, septomaxilla; v, vomer. MCZ scan data used by permission of the Museum of Comparative Zoology, Harvard University.

141x118mm (300 x 300 DPI)

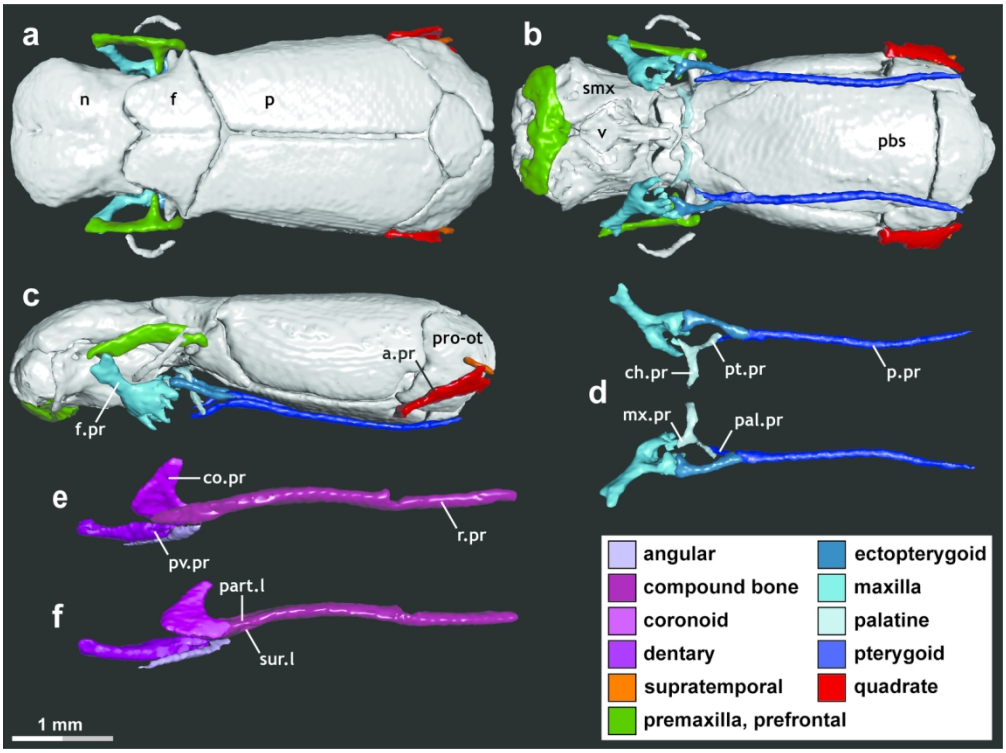

Figure 10. Skull of *Liotyphlops argaleus* (MCZ R-67933), exemplifying "axle-brace maxillary raking". Key elements related to feeding are highlighted. In this morphotype of microstomy, the maxilla is suspended from the mobile and highly reduced prefrontal and is braced posteriorly by the ectopterygoid. As in typhlopoids, the mandible is reduced and does not contribute to feeding (see text for details). (**a**–**c**) Skull, with mandibles digitally removed, in (**a**) dorsal, (**b**) ventral, and (**c**) lateral view. (**d**) Palatomaxillary arch in dorsal view. (**e**–**f**) Mandible in (**e**) lateral and (**f**) medial view. Abbreviations: a.pr, anterior process; ch.pr, choanal process; co.pr, coronoid process; f, frontal; f.pr, facial process; mx.pr, maxillary process; n, nasal; p, parietal; pal.pr, palatine process; part.l, prearticular lamina; pbs, parabasisphenoid; p.pr, posterior process; pro-ot, prootic-otoccipital; pt.pr, pterygoid process; pv.pr, posteroventral process; r.pr, retroarticular process; smx, septomaxilla; sur.l, surangular lamina; v, vomer. MCZ scan data used by permission of the Museum of Comparative Zoology, Harvard University.

141x104mm (300 x 300 DPI)

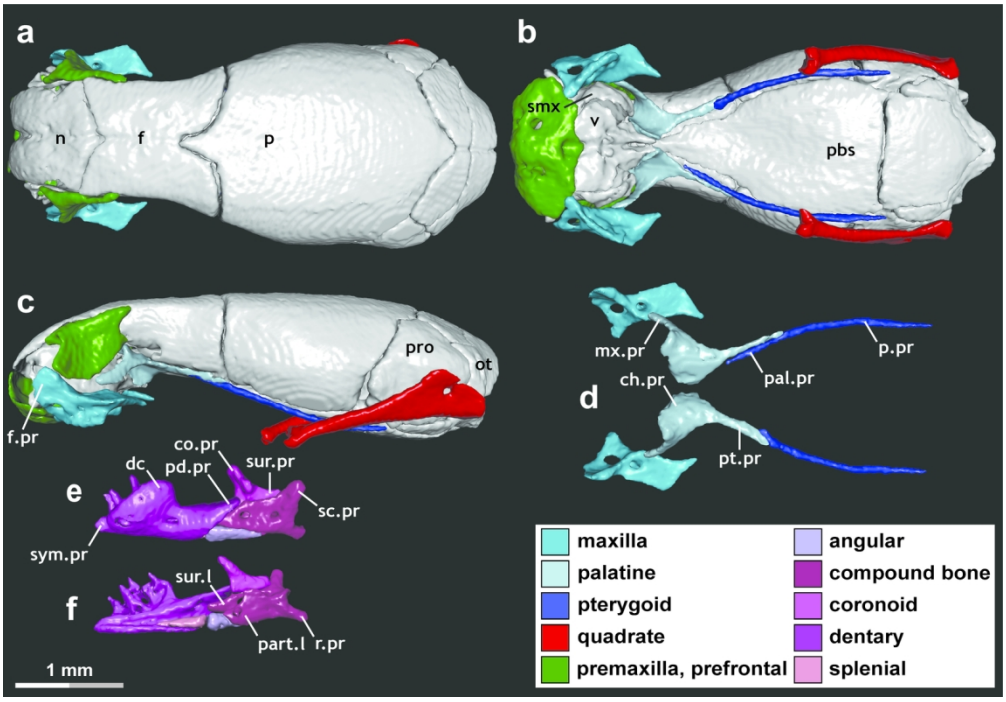

Figure 11. Skull of *Epictia albifrons* (MCZ R-2885), exemplifying "mandibular raking" (*sensu* Kley and Brainerd, 1999). Key elements related to feeding are highlighted. In this morphotype of microstomy, feeding is driven by rapid retraction of the mandibles, enabled by a flexible intramandibular joint, whereas the palatomaxillary arches are edentulous and do not contribute to feeding (see text for details). (**a**–**c**) Skull, with mandibles digitally removed, in (**a**) dorsal, (**b**) ventral, and (**c**) lateral view. (**d**) Palatomaxillary arch in dorsal view. (**e**–**f**) Mandible in (**e**) lateral and (**f**) medial view. Abbreviations: ch.pr, choanal process; co.pr, coronoid process; dc, dental concha; f, frontal; f.pr, facial process; mx.pr, maxillary process; n, nasal; ot, otoccipital; p, parietal; pal.pr, palatine process; part.l, prearticular lamina; pbs, parabasisphenoid; pd.pr, posterodorsal process; p.pr, posterior process; pro, prootic; pt.pr, pterygoid process; r.pr, retroarticular process; sc.pr, supracotylar process; smx, septomaxilla; sur.l, surangular lamina; sur.pr, surangular process; sym.pr, symphyseal process; v, vomer. MCZ scan data used by permission of the Museum of Comparative Zoology, Harvard University.

141x97mm (300 x 300 DPI)

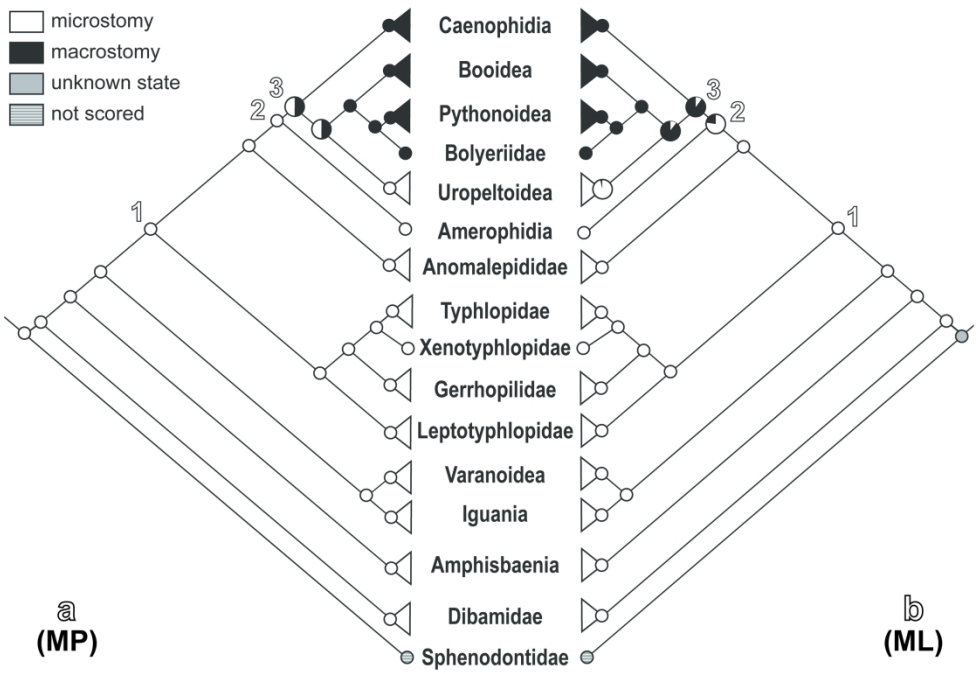

Figure 12. Ancestral state reconstruction (ASR) of feeding mechanisms in squamates, using a "basic" character scoring scheme with two states: microstomy and macrostomy. (**a**) Maximum parsimony (MP)-based ASR; (**b**) maximum likelihood (ML)-based ASR. Key nodes are numbered: **1**, origin of snakes; **2**, origin of Alethinophidia; **3**, origin of "Macrostomata". See text for details regarding results, including the impact of different character scoring approaches.

246x166mm (300 x 300 DPI)

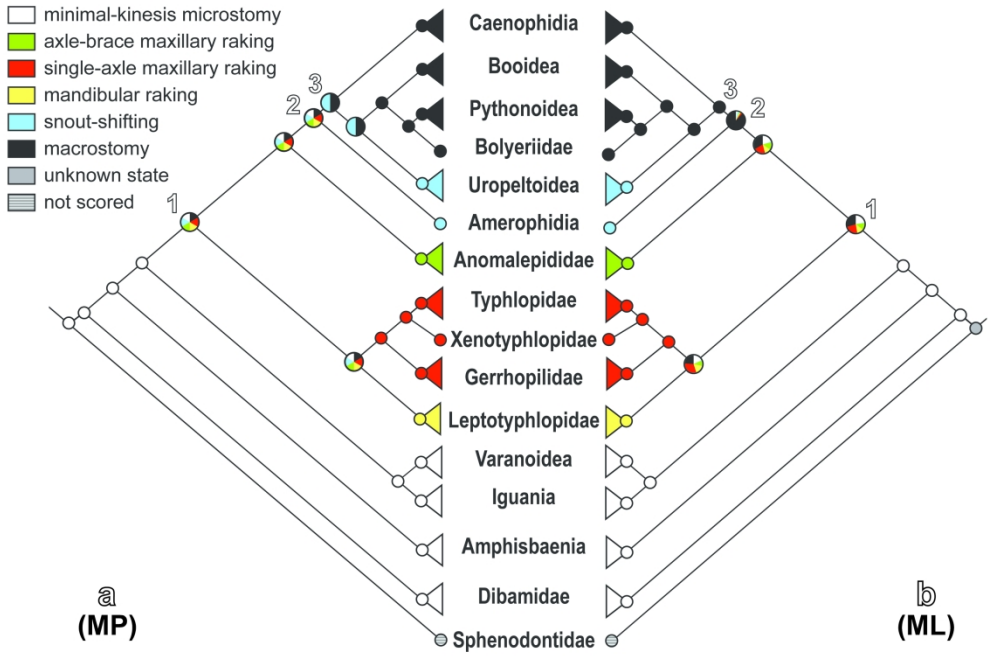

Figure 13. Ancestral state reconstruction (ASR) of feeding mechanisms in squamates, using a "detailed microstomy" character scoring scheme dividing microstomy into the five morphotypes described herein: "axle-brace maxillary raking", "mandibular raking", "minimal-kinesis microstomy", "single-axle maxillary raking", and "snout-shifting". Macrostomy is scored under a single state. (**a**) Maximum parsimony (MP)-based ASR; (**b**) maximum likelihood (ML)-based ASR. Key nodes are numbered: **1**, origin of snakes; **2**, origin of Alethinophidia; **3**, origin of "Macrostomata". See text for details regarding results, including anatomical descriptions and the impact of different character scoring approaches.

254x167mm (300 x 300 DPI)

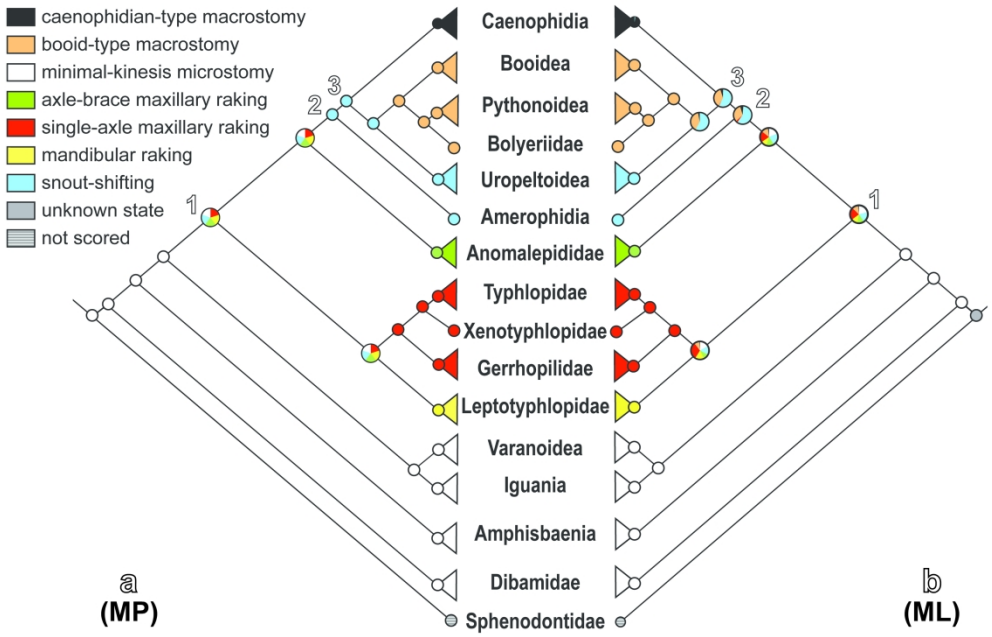

Figure 14. Ancestral state reconstruction (ASR) of feeding mechanisms in squamates, using a "detailed microstomy and macrostomy" character scoring scheme. This scheme divides microstomy into the five morphotypes described herein ("axle-brace maxillary raking", "mandibular raking", "minimal-kinesis microstomy", "single-axle maxillary raking", and "snout-shifting") and divides macrostomy into separate morphotypes ("booid-type" and "caenophidian-type" macrostomy) as proposed in recent literature (e.g., Palci et al., 2016; Strong et al., 2019; Burbrink et al., 2020). (**a**) Maximum parsimony (MP)-based ASR; (**b**) maximum likelihood (ML)-based ASR. Key nodes are numbered: **1**, origin of snakes; **2**, origin of Alethinophidia; **3**, origin of "Macrostomata". See text for details regarding results, including anatomical descriptions and the impact of different character scoring approaches.

259x167mm (300 x 300 DPI)

Table 1. Institutional abbreviations of specimens examined in this study.

Abbreviation	Institution	Location
AMS	Australian Museum	Sydney, Australia
CAS	California Academy of Sciences	San Francisco, USA
FMNH	Field Museum of Natural History	Chicago, USA
FRIM	Forest Research Institute Malaysia	Kuala Lumpur, Malaysia
KUH	University of Kansas Biodiversity Institute and Natural History Museum	Lawrence, USA
MCZ	Museum of Comparative Zoology, Harvard University	Cambridge, USA
QM	Queensland Museum	South Brisbane, Australia
SAMA	South Australian Museum	Adelaide, Australia
TCWC	Biodiversity Research and Teaching Collections, Texas A&M University	College Station, USA
TNHC	Texas Natural History Collections, Texas Memorial Museum of Science and History, University of Texas at Austin	Austin, USA
TMM	Texas Memorial Museum of Science and History, University of Texas at Austin	Austin, USA
UAMZ	University of Alberta Museum of Zoology	Edmonton, Canada
UF	Florida Museum of Natural History, University of Florida	Gainesville, USA
UMMZ	University of Michigan Museum of Zoology	Ann Arbor, USA
UTA	University of Texas at Arlington	Arlington, USA
YPM	Yale Peabody Museum	New Haven, USA
ZSM	Zoologische Staatssammlung München	Munich, Germany

Table 2. List of specimens observed for this study. See Table 1 for institutional abbreviations.

HIGHER TAXON			SPECIES	SPECIMEN NUMBER
Alethinophidia	**"Anilioidea"**	**Amerophidia**	*Anilius scytale*	USNM 204078 KUH 125976
		Uropeltoidea	*Anomochilus leonardi*	FRIM 0026
			Cylindrophis ruffus	UMMZ 201901 FMNH 60958
			Uropeltis melanogaster	FMNH 167048
			Uropeltis woodmasoni	TMM M-10006
	Bolyeriidae		*Casarea dussumieri*	UMMZ 190285
	Booidea	**Boidae**	*Boa constrictor*	FMNH 31182
		Calabariidae	*Calabaria reinhardtii*	FMNH 117833
		Erycidae	*Eryx colubrinus*	FMNH 63117
		Ungaliophiidae	*Ungaliophis continentalis*	UTA 50569
	Caenophidia	**Acrochordidae**	*Acrochordus arafurae*	QM J11033
			Acrochordus granulatus	MCZ R-146128
		Atractaspididae	*Atractaspis irregularis*	FMNH 62204
		Elapidae	*Naja naja*	FMNH 22468
		Homalopsidae	*Homalopsis buccata*	FMNH 259340
		Lamprophiidae	*Boaedon fuliginosus*	FMNH 62248
			Lycophidion capense	FMNH 58322
		Natricidae	*Afronatrix anoscopus*	FMNH 179335
			Natrix natrix	FMNH 30522
			Thamnophis radix	UAMZ R636
		Pareidae	*Pareas hamptoni*	FMNH 128304
		Viperidae	*Bothrops asper*	FMNH 31162

	Pythonoidea	**Loxocemidae**	*Loxocemus bicolor*	FMNH 104800
		Pythonidae	*Python molurus*	TNHC 62769
			Python regius	UAMZ R381
		Xenopeltidae	*Xenopeltis unicolor*	FMNH 148900
“Scolecophidia”	**Anomalepididae**		*Anomalepis aspinosus*	MCZ R-14782
			Anomalepis mexicanus	MCZ R-191201
			Helminthophis praeocularis	MCZ R-17960
			Liotyphlops albirostris	FMNH 216257
			Liotyphlops argaleus	MCZ R-67933
			Liotyphlops beui	SAMA 40142
			Typhlophis squamosus	MCZ R-145403
	Leptotyphlopidae		*Epictia albifrons*	MCZ R-2885
			Myriopholis longicauda	MCZ R-184447
			Myriopholis macrorhyncha	MCZ R-9650
			Myriopholis tanae	MCZ R-40099
			Namibiana occidentalis	MCZ R-193094
			Rena dulcis	TNHC 60638 UAMZ R335
			Rena myopica	MCZ R-45563
			Tricheilostoma bicolor	MCZ R-49718
			Trilepida dimidiata	SAMA 40143
	Typhlopoidea	**Gerrhopilidae**	*Gerrhopilus ater*	MCZ R-33505
			Gerrhopilus beddomii	MCZ R-22372
			Gerrhopilus persephone	UMMZ 242536
		Typhlopidae	*Acutotyphlops infralabialis*	AMS R.77116
			Acutotyphlops kunuaensis	AMS R.12305
			Acutotyphlops solomonis	AMS R.11452
			Acutotyphlops subocularis	SAMA R64770

			Afrotyphlops angolensis	MCZ R-170385
			Afrotyphlops schlegelii	MCZ R-190405
			Amerotyphlops paucisquamus	MCZ R-147336
			Anilios australis	SAMA R26901
			Anilios bicolor	SAMA 60626 SAMA 62252
			Antillotyphlops monastus	MCZ R-81112
			Cubatyphlops paradoxus	MCZ R-92993
			Indotyphlops braminus	UAMZ R363
			Ramphotyphlops depressus	AMS R.129537
			Ramphotyphlops lineatus	MCZ R-37751
			Typhlops jamaicensis	USNM 12378
			Typhlops titanops	MCZ R-68571
			Xerotyphlops vermicularis	MCZ R-56477
		Xenotyphlopidae	*Xenotyphlops grandidieri*	ZSM 2194/2007 ZSM 2213/2007 ZSM 2216/2007
Non-snake lizards	**Amphisbaenia**	**Amphisbaenidae**	*Amphisbaena alba*	FMNH 195924
			Amphisbaena fuliginosa	FMNH 22847
		Bipedidae	*Bipes biporus*	CAS 126478
			Bipes canaliculatus	CAS 134753
		Rhineuridae	*Rhineura floridana*	FMNH 31774
		Trogonophiidae	*Agamodon anguliceps*	FMNH 264702
			Trogonophis wiegmanni	FMNH 109462
	Dibamidae		*Anelytropsis papillosus*	TCWC 45501
			Dibamus leucurus	UMMZ 174763
			Dibamus novaeguineae	UF 33488 CAS 26937

	Iguania	**Agamidae**	*Physignathus cocincinus*	YPM 14378
		Iguanidae	*Dipsosaurus dorsalis*	YPM 14376
			Sauromalus ater	TNHC 18483
		Tropiduridae	*Uranoscodon superciliosus*	YPM 12871
	Varanoidea	**Lanthanotidae**	*Lanthanotus borneensis*	FMNH 148589 YPM 6057
		Varanidae	*Varanus exanthematicus*	FMNH 58299

Table 3. Summary of morphotypes of "microstomy", including select key synapomorphies of each morphotype. See text for details, including anatomical descriptions and additional synapomorphies. See Table 4 for key features summarized in taxon-character matrix format.

Morphotype and Taxa	Key Biomechanics	Key Synapomorphies
Axle-brace maxillary raking (Anomalepididae)	- Suspension of maxilla from prefrontal - Bracing of maxilla by ectopterygoid - No contribution of mandible to feeding	- Reduced, arch-like, and mobile prefrontal - Reduced ectopterygoid - Highly reduced palatine, including stubby maxillary process - Inflexible mandible, with elongate angular and reduced dentition - Elongate and anteroventrally oriented quadrate
Mandibular raking (Leptotyphlopidae)	- Bilaterally synchronous retraction of mandibles - No contribution of palatomaxillary arch to feeding	- Edentulous and fixed palatomaxillary arch - Reduced mandible with flexible intramandibular joint - Robust dentary, including dental concha and symphyseal process - Structurally complex coronoid and compound bone - Extremely elongate and anteroventrally oriented quadrate

Minimal-kinesis microstomy (Non-snake lizards)	- No unilateral movement of jaws - Minimal kinesis due to tight integration and strong bracing of jaw elements	- Robust and tightly integrated palatomaxillary arch elements - Tight bracing at ectopterygoid-maxilla and -pterygoid articulations - Osseous contact between premaxilla and maxilla - Well-developed basipterygoid processes - Robust mandibular elements tightly integrated, including across intramandibular joint - Symphyseal facets on mandibular symphysis - Stout and upright quadrate, with squamosal present
Single-axle maxillary raking (Typhlopoidea)	- Rotation of maxilla about maxillary process of palatine - No contribution of mandible to feeding	- Elongate and rod-like maxillary process of palatine - Deep medial excavation or foramen in maxilla - Edentulous and inflexible mandible, including elongate splenial and reduced angular

		- Elongate and anteroventrally oriented quadrate
Snout-shifting (Uropeltoidea and Amerophidia)	- Minor unilateral movement of palatomaxillary arches - Flexion of mandibles	- "Ball-and-socket"-like maxilla-palatine joint - Loose palatine-pterygoid joint - Robust palatine, though lacking osseous contact with vomer - Moderate basipterygoid processes - Robust mandible with flexible intramandibular joint, including abutting splenial-angular contact - Stout and upright quadrate, bearing large suprastapedial process

Table 4. Key features of each morphotype of "microstomy", presented in taxon-character matrix format. Each morphotype comprises a distinct suite of character states, with many features being entirely unique to and consistent within each morphotype (indicated by ***). Scorings are based on the exemplar taxa in Figures 3–4 for non-snake lizards, Figure 7 for "anilioids", and Figures 9–11 for scolecophidians; see main text for variations within these broader groups, as well as for anatomical descriptions and additional synapomorphies.

	Axle-brace maxillary raking (Anomalepididae)	**Mandibular raking** (Leptotyphlopidae)	**Minimal-kinesis microstomy** (Non-snake lizards)	**Single-axle maxillary raking** (Typhlopoidea)	**Snout-shifting** (Uropeltoidea and Amerophidia)
Dentary teeth: present (0); absent (1).	0/1	0	0	1	0
***Dentary, tooth row, orientation**: roughly anteroposterior (0); transverse (1).	0	1	0	–	0
***Maxillary teeth**: present (0); absent (1).	0	1	0	0	0
Maxilla, tooth row, orientation: roughly anteroposterior (0); transverse (1).	1	–	0	1	0
Pterygoid teeth: absent (0); present (1).	0	0	0	0	1
Palatine teeth: absent (0); present (1).	0	0	0	0	1
***Premaxilla, articulation with maxilla, extent of integration**: broad osseous contact (0); loosely articulated (1); broadly separate (2).	2	1	0	2	1
***Frontal, articulation with prefrontal, complexity**: extensive, abutting or overlapping (0); reduced, clasping (1).	1	0	0	0	0
***Frontal, ventral facet accommodating palatine and pterygoid**: absent (0); present (1).	0	1	0	0	0

***Prefrontal, articulation with maxilla, configuration**: abutting or overlapping (0); interlocking along facial process of maxilla in "peg-and-socket"-like joint (1); forked/bifurcating (2); broadly swivelling (3).	2	0	0	3	1
***Palatine, articulation with pterygoid, configuration**: broadly abutting or overlapping (0); interlocking, complex but mobile (1); interlocking, simple forking (2); simple flap-overlap (3).	3	3	0/1	2	1
Palatine, medial (= choanal, vomerine) process, osseous contact with vomer: present (0); absent (1).	1	0	0	1	1
***Palatine, medial (= choanal, vomerine) process, form**: flat process extending horizontally (0); broad arch (1); narrow arch (2).	2	1	0	2	1
***Palatine, maxillary process**: present (0); highly reduced or absent (1).	1	0	0	0	0
***Palatine, maxillary process, articulation with maxilla, configuration**: broad osseous contact (0); articulating via "ball-and-socket"-like joint accommodating palatine process of maxilla (1); articulating with large medial excavation or foramen on maxilla (2); articulation minimal (3).	–	3	0	2	1
Pterygoid, posterior process (= quadrate ramus), form: robust (0); simple, rod-like (1).	1	1	0	1	0
Ectopterygoid: present (0); absent (1).	0	1	0	1	0
***Ectopterygoid, form**: robust (0); distinctly reduced, rod-like (1).	1	–	0	–	0
Quadrate, orientation in lateral view: roughly vertical (0); slanted clearly anteriorly, nearly horizontal (1).	1	1	0	1	0
***Quadrate, shaft, length:** short/stout (0); elongate (1); extremely elongate (2).	1	2	0	1	0
Supratemporal: present (0); highly reduced or absent (1).	1	1	0	1	0
Squamosal: present (0); absent (1).	1	1	0	1	1
Parabasisphenoid, basipterygoid processes: present (0); absent (1).	1	1	0	1	0
***Parabasisphenoid, basipterygoid processes, size:** large, forming distinct projections (0); moderate, forming low ridges (1).	–	–	0	–	1
***Dentary, dental concha**: absent (0); present (1).	0	1	0	0	0
***Dentary, symphysis, articular facet**: present (0); absent (1).	1	1	0	1	1
***Dentary, symphysis, symphyseal process**: absent (0); present (1).	0	1	0	0	0
Dentary, symphysis, cartilaginous inter-ramal nodule: absent (0); present (1).	?	1	0	1	0
Angular, form: robust (0); simple, rod-like (1).	1	0	0	1	0
Splenial: present (0); absent (1).	1	0	0	0	0
Splenial, articulation with angular, configuration: overlapping (0); abutting (1).	–	1	0	0	1

***Splenial, length relative to dentary**: shorter than (0); subequal to or longer than (1).	–	0	0	1	0
Surangular-articular, fusion: unfused (0); fused to form compound bone (1).	1	1	0	1	1
***Compound bone, surangular and prearticular laminae, fusion**: fully fused (0); briefly separate (1); fully separate (2).	1	2	–	0	0
***Compound bone / surangular, anterior terminus, orientation**: not downcurved (0); distinctly downcurved (1); slightly downcurved, resulting in gentle sinusoidal shape (2).	2	0	0	1	0
***Surangular, supracotylar process**: absent (0); present (1).	0	1	0	0	0

#NEXUS

BEGIN TAXA;

TITLE Taxa;

DIMENSIONS ntax = 80;

TAXLABELS Acrochordus_arafurae Acrochordus_granulatus Acutotyphlops_infralabialis Acutotyphlops_kunuaensis Acutotyphlops_solomonis Acutotyphlops_subocularis Afronatrix_anoscopus Afrotyphlops_angolensis Afrotyphlops_schlegelii Agamodon_anguliceps Amerotyphlops_paucisquamus Amphisbaena_alba Amphisbaena_fuliginosa Anelytropsis_papillosus Anilios_australis Anilios_bicolor Anilius_scytale Anomalepis_aspinosus Anomalepis_mexicanus Anomochilus_leonardi Antillotyphlops_monastus Atractaspis_irregularis Bipes_biporus Bipes_canaliculatus Boa_constrictor Boaedon_fuliginosus Bothrops_asper Calabaria_reinhardtii Casarea_dussumieri Cubatyphlops_paradoxus Cylindrophis_ruffus Dibamus_leucurus Dibamus_novaeguineae Dipsosaurus_dorsalis Epictia_albifrons Eryx_colubrinus Gerrhopilus_ater Gerrhopilus_beddomii Gerrhopilus_persephone Helminthophis_praeocularis Homalopsis_buccata Indotyphlops_braminus Lanthanotus_borneensis Liotyphlops_albirostris Liotyphlops_argaleus Liotyphlops_beui Loxocemus_bicolor Lycophidion_capense Myriopholis_longicauda Myriopholis_macrorhyncha Myriopholis_tanae Naja_naja Namibiana_occidentalis Natrix_natrix Pareas_hamptoni Physignathus_cocincinus Python_molurus Python_regius Ramphotyphlops_depressus Ramphotyphlops_lineatus Rena_dulcis Rena_myopica Rhineura_floridana Sauromalus_ater Thamnophis_radix Tricheilostoma_bicolor Trilepida_dimidiata Trogonophis_wiegmanni Typhlophis_squamosus Typhlops_jamaicensis Typhlops_titanops Ungaliophis_continentalis Uranoscodon_superciliosus Uropeltis_melanogaster Uropeltis_woodmasoni Varanus_exanthematicus Xenopeltis_unicolor Xenotyphlops_grandidieri Xerotyphlops_vermicularis Sphenodontidae;

END;

BEGIN TREES;

TITLE SquamatePhyloSpecies;

LINK TAXA = Taxa;

TREE SquamateTreeSpecies = (((((((((((((Afronatrix_anoscopus:27.29,(Thamnophis_radix:18.76,Natrix_natrix:18.76):8.53):19.94,((Atractaspis_irregularis:36.58,(Boaedon_fuliginosus:24.07,Lycophidion_capense:24.07):12.51):2.81,Naja_naja:39.39):7.84):2.75,Homalopsis_buccata:49.98):9.52,Bothrops_asper:59.5):3.98,Pareas_hamptoni:63.48):23.84,(Acrochordus_arafurae:0.83,Acrochordus_granulatus:0.83):86.49):11.3,(((((Boa_constrictor:58.0,Eryx_colubrinus:58.0):2.43,Ungaliophis_continentalis:60.43):11.71,Calabaria_reinhardtii:72.14):24.92,((((Python_molurus:30.13,Python_regius:30.13):31.93,Loxocemus_bicolor:62.06):26.3,Xenopeltis_unicolor:88.36):7.36,Casarea_dussumieri:95.72):1.34):0.97,((Cylindrophis_ruffus:27.27,Anomochilus_leonardi:27.27):48.67,(Uropeltis_melanogaster:55.34,Uropeltis_woodmasoni:55.34):20.6):22.09):0.59):3.68,Anilius

_scytale:102.3):25.27,(Anomalepis_aspinosus:57.73,Anomalepis_mexicanus:57.73,Helminthophis_praeocularis:57.73,Liotyphlops_argaleus:57.73,Liotyphlops_albirostris:57.73,Liotyphlops_beui:57.73,Typhlophis_squamosus:57.73):69.84):2.23,((((((Afrotyphlops_angolensis:1.9,Afrotyphlops_schlegelii:1.9):48.4,((((Typhlops_titanops:8.2,Typhlops_jamaicensis:8.2):8.2,Antillotyphlops_monastus:16.4):6.9,Cubatyphlops_paradoxus:23.3):6.9,Amerotyphlops_paucisquamus:30.2):20.1):12.7,(((((Anilios_australis:16.3,Anilios_bicolor:16.3):24.1,(Acutotyphlops_solomonis:39.3,Acutotyphlops_infralabialis:39.3,Acutotyphlops_kunuaensis:39.3,Acutotyphlops_subocularis:39.3):1.1):1.1,(Ramphotyphlops_depressus:37.0,Ramphotyphlops_lineatus:37.0):4.5):3.3,Indotyphlops_braminus:44.8):8.2,Xerotyphlops_vermicularis:53.0):10.0):17.6,Xenotyphlops_grandidieri:80.6):9.8,(Gerrhopilus_persephone:10.41,Gerrhopilus_beddomii:10.41,Gerrhopilus_ater:10.41):79.99):34.07,((Namibiana_occidentalis:30.4,(Myriopholis_macrorhyncha:15.2,Myriopholis_tanae:15.2,Myriopholis_longicauda:15.2):15.2):30.4,((((Rena_myopica:17.37,Rena_dulcis:17.37):17.37,Trilepida_dimidiata:34.74):8.68,Epictia_albifrons:43.42):8.68,Tricheilostoma_bicolor:52.1):8.68):63.67):5.33):45.35,((Varanus_exanthematicus:58.42,Lanthanotus_borneensis:58.42):115.24,((Uranoscodon_superciliosus:95.77,(Sauromalus_ater:56.86,Dipsosaurus_dorsalis:56.86):38.91):62.03,Physignathus_cocincinus:157.8):15.86):1.49):4.04,((((Amphisbaena_alba:34.86,Amphisbaena_fuliginosa:34.86):12.76,(Agamodon_anguliceps:23.81,Trogonophis_wiegmanni:23.81):23.81):29.78,(Bipes_biporus:13.38,Bipes_canaliculatus:13.38):64.02):29.29,Rhineura_floridana:107.19):72):14.04,((Dibamus_novaeguineae:35.0,Anelytropsis_papillosus:35.0):35.0,Dibamus_leucurus:70.0):123.23):48.27,Sphenodontidae:241.5);

END;

BEGIN CHARACTERS;

TITLE Character_Matrix;

DIMENSIONS nchar=3;

FORMAT DATATYPE = standard GAP = - MISSING = N SYMBOLS = " 1 2 3 4 5 6 7";

CHARSTATELABELS

1 FeedingMorphotype_Basic / [1]micro [2]macro,

2 FeedingMorphotype_DetailedMicro / [1]microMinKin [2]microSnoutShift [3]microAxleBrace [4]microMandRak [5]microSingleAxle [6]macro,

3 FeedingMorphotype_DetailedMicroMacro / [1]microMinKin [2]microSnoutShift [3]microAxleBrace [4]microMandRak [5]microSingleAxle [6]macroBooid [7]macroCaeno ;

MATRIX

Sphenodontidae ---

Acrochordus_arafurae 267

Acrochordus_granulatus 267

Acutotyphlops_infralabialis	155
Acutotyphlops_kunuaensis	155
Acutotyphlops_solomonis	155
Acutotyphlops_subocularis	155
Afronatrix_anoscopus	267
Afrotyphlops_angolensis	155
Afrotyphlops_schlegelii	155
Agamodon_anguliceps	111
Amerotyphlops_paucisquamus	155
Amphisbaena_alba	111
Amphisbaena_fuliginosa	111
Anelytropsis_papillosus	111
Anilios_australis	155
Anilios_bicolor	155
Anilius_scytale	122
Anomalepis_aspinosus	133
Anomalepis_mexicanus	133
Anomochilus_leonardi	122
Antillotyphlops_monastus	155
Atractaspis_irregularis	267
Bipes_biporus	111
Bipes_canaliculatus	111
Boa_constrictor	266
Boaedon_fuliginosus	267
Bothrops_asper	267
Calabaria_reinhardtii	266
Casarea_dussumieri	266
Cubatyphlops_paradoxus	155
Cylindrophis_ruffus	122

Dibamus_leucurus	111
Dibamus_novaeguineae	111
Dipsosaurus_dorsalis	111
Epictia_albifrons	144
Eryx_colubrinus	266
Gerrhopilus_ater	155
Gerrhopilus_beddomii	155
Gerrhopilus_persephone	155
Helminthophis_praeocularis	133
Homalopsis_buccata	267
Indotyphlops_braminus	155
Lanthanotus_borneensis	111
Liotyphlops_albirostris	133
Liotyphlops_argaleus	133
Liotyphlops_beui	133
Loxocemus_bicolor	266
Lycophidion_capense	267
Myriopholis_longicauda	144
Myriopholis_macrorhyncha	144
Myriopholis_tanae	144
Naja_naja	267
Namibiana_occidentalis	144
Natrix_natrix	267
Pareas_hamptoni	267
Physignathus_cocincinus	111
Python_molurus	266
Python_regius	266
Ramphotyphlops_depressus	155
Ramphotyphlops_lineatus	155

```
                Rena_dulcis                 144
                Rena_myopica                144
                Rhineura_floridana          111
                Sauromalus_ater             111
                Thamnophis_radix            267
                Tricheilostoma_bicolor      144
                Trilepida_dimidiata         144
                Trogonophis_wiegmanni       111
                Typhlophis_squamosus        133
                Typhlops_jamaicensis        155
                Typhlops_titanops           155
                Ungaliophis_continentalis   266
                Uranoscodon_superciliosus   111
                Uropeltis_melanogaster      122
                Uropeltis_woodmasoni        122
                Varanus_exanthematicus      111
                Xenopeltis_unicolor         266
                Xenotyphlops_grandidieri    155
                Xerotyphlops_vermicularis   155
        ;
END;
```